AD-A163 814 AFRRI (ARMED FORCES RADIOBIOLOGY RESEARCH INSTITUTE) 1/1
REPORTS APRIL-JUNE 1985(U) ARMED FORCES RADIOBIOLOGY
RESEARCH INST BETHESDA MD 1985

UNCLASSIFIED F/G 6/18 NL

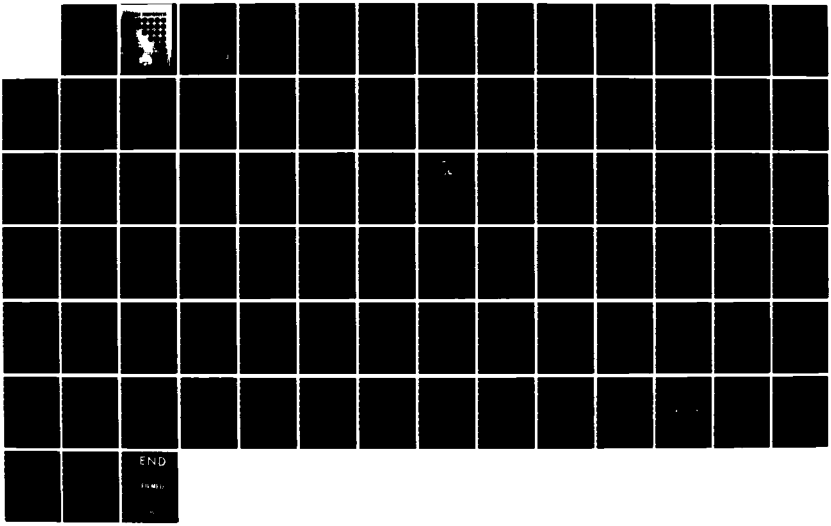

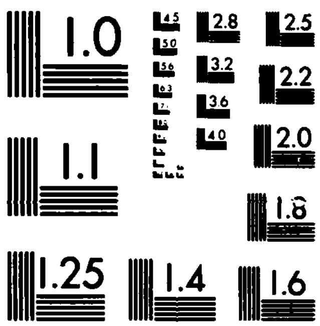

MICROCOPY RESOLUTION TEST CHART
NATIONAL BUREAU OF STANDARDS-1963-A

AFRRI REPORTS

APRIL
MAY
JUNE
1985

DEFENSE NUCLEAR AGENCY
ARMED FORCES RADIOBIOLOGY RESEARCH INSTITUTE
BETHESDA, MD 20814-5145

(2)

UNCLASSIFIED
SECURITY CLASSIFICATION OF THIS PAGE

AD-A163 814

REPORT DOCUMENTATION PAGE

1a. REPORT SECURITY CLASSIFICATION UNCLASSIFIED	1b. RESTRICTIVE MARKINGS
2a. SECURITY CLASSIFICATION AUTHORITY	3. DISTRIBUTION/AVAILABILITY OF REPORT Approved for public release; distribution unlimited.
2b. DECLASSIFICATION/DOWNGRADING SCHEDULE	
4. PERFORMING ORGANIZATION REPORT NUMBER(S) AFRRI SR85-17 through 85-25	5. MONITORING ORGANIZATION REPORT NUMBER(S)
6a. NAME OF PERFORMING ORGANIZATION Armed Forces Radiobiology Research Institute 6b. OFFICE SYMBOL (If applicable) AFRRI	7a. NAME OF MONITORING ORGANIZATION
6c. ADDRESS (City, State and ZIP Code) Defense Nuclear Agency Bethesda, Maryland 20814-5145	7b. ADDRESS (City, State and ZIP Code)
8a. NAME OF FUNDING/SPONSORING ORGANIZATION Defense Nuclear Agency 8b. OFFICE SYMBOL (If applicable) DNA	9. PROCUREMENT INSTRUMENT IDENTIFICATION NUMBER
8c. ADDRESS (City, State and ZIP Code) Washington, DC 20305	10. SOURCE OF FUNDING NOS. PROGRAM ELEMENT NO.: NWED QAXM PROJECT NO.: TASK NO.: WORK UNIT NO.:
11. TITLE (Include Security Classification) AFRRI Reports, Apr-Jun 1985	
12. PERSONAL AUTHOR(S)	
13a. TYPE OF REPORT Reprints/Technical 13b. TIME COVERED FROM ______ TO ______	14. DATE OF REPORT (Yr., Mo., Day) 15. PAGE COUNT 85
16. SUPPLEMENTARY NOTATION	
17. COSATI CODES FIELD / GROUP / SUB. GR.	18. SUBJECT TERMS (Continue on reverse if necessary and identify by block number) N/A

19. ABSTRACT (Continue on reverse if necessary and identify by block number)

This volume contains AFRRI Scientific Reports SR85-17 through 85-25 for Apr-Jun 1985.

20. DISTRIBUTION/AVAILABILITY OF ABSTRACT UNCLASSIFIED/UNLIMITED ☒ SAME AS RPT. ☐ DTIC USERS ☐	21. ABSTRACT SECURITY CLASSIFICATION UNCLASSIFIED
22a. NAME OF RESPONSIBLE INDIVIDUAL Junith A. Van Deusen	22b. TELEPHONE NUMBER (Include Area Code) (202)295-3536 22c. OFFICE SYMBOL ADMG

DD FORM 1473, 83 APR   EDITION OF 1 JAN 73 IS OBSOLETE.

UNCLASSIFIED
SECURITY CLASSIFICATION OF THIS PAGE

86-2-7-322

CONTENTS

Scientific Reports

Biochem. J. (1985) **226**, 335–338
Printed in Great Britain

Presence of a high-affinity Ca^{2+}- and Mg^{2+}-dependent ATPase in rat peritoneal mast-cell membranes

Lynn M. AMENDE* and Mildred A. DONLON
Biochemistry Department, Armed Forces Radiobiology Research Institute, Bethesda, MD 20814-5145, U.S.A.

(*Received 6 November 1984/Accepted 17 December 1984*)

Purified perigranular and plasma membranes isolated from rat peritoneal mast cells were examined for Ca^{2+}- and Mg^{2+}-dependent ATPase activity. Isolated perigranular membranes contained only a low-affinity Ca^{2+}- or Mg^{2+}-dependent ATPase ($K_m > 0.5$ mM). The plasma membranes contained both a low-affinity Ca^{2+}- or Mg^{2+}-dependent ATPase ($K_m = 0.4$ mM, $V_{max.} = 20$ nmol of P_i/min per mg), as well as a high-affinity Ca^{2+}- and Mg^{2+}-dependent ATPase ($K_m = 0.2\,\mu$M, $V_{max.} = 6$ nmol of P_i/min per mg).

Although the release of histamine from mast cells may be elicited by a variety of secretagogues, an absolute requirement for Ca^{2+} exists. A rapid increase in intracellular Ca^{2+} concentration is required to trigger exocytosis of the histamine-containing granules from mast cells. Although a plasma-membrane Ca^{2+},Mg^{2+}-ATPase (or Ca^{2+} pump) has been demonstrated in a variety of cell types (reviewed by Penniston, 1983), a role for such a Ca^{2+} pump in the histamine release mechanism has only been postulated (Fewtrell & Gomperts, 1977*a,b*; Magro *et al.*, 1983). Pharmacological agents shown to inhibit the Ca^{2+},Mg^{2+}-ATPase found in muscle sarcoplasmic reticulum also inhibit mast-cell degranulation (Fewtrell & Gomperts, 1977*a,b*). Unlike the $Na^{+}+K^{+}$-dependent ATPase, which is specifically inhibited by ouabain, no inhibitor specific for the high-affinity Ca^{2+},Mg^{2+}-ATPase has been identified. Therefore studies measuring the direct effect of potential inhibitors on the mast-cell Ca^{2+},Mg^{2+}-ATPase could be useful for elucidating the role of various transport ATPases in the secretory process. To initiate these studies, rat peritoneal mast-cell membranes were examined for the high-affinity Ca^{2+},Mg^{2+}-ATPase. This paper reports evidence for such a high-affinity Ca^{2+},Mg^{2+}-ATPase in mast-cell plasma membranes.

Abbreviations used: Ca^{2+},Mg^{2+}-ATPase, Ca^{2+}- and Mg^{2+}-dependent ATPase; HEDTA, *N*-hydroxyethylethylenediaminetriacetic acid.

* To whom correspondence and reprint requests should be sent. Present address: NIADDK, Bldg. 10, Rm. 8D06, National Institutes of Health, Bethesda, MD 20205, U.S.A.

Ca^{2+} has been detected by ion-probe analysis in the membrane-bound histamine-containing granules (Chock *et al.*, 1982; Hein & Caulfield, 1982, 1983). The granules may form an intracellular Ca^{2+}-storage site, thereby serving as an integral component of the mechanism for the maintenance of low intracellular Ca^{2+} concentrations. Therefore the perigranular membrane may contain components of a Ca^{2+}-transport mechanism necessary for Ca^{2+} sequestration within the granule matrix. Accordingly, the perigranular membranes were also examined for high-affinity Ca^{2+},Mg^{2+}-ATPase activity.

Materials and methods

Membrane isolation and purification

Male Sprague Dawley rats (300–400 g) were killed by CO_2 inhalation and mast cells were obtained by peritoneal lavage. The mast cells were purified (>95% pure) by centrifugation through 38% (w/v) albumin (Sullivan *et al.*, 1975) and disrupted by repeating a cycle of single 0.5 s sonication pulses, followed by centrifugation to separate the released granules (Amende & Donlon, 1985). Plasma membranes were separated from intact granules by centrifuging the sonicated material through a self-generating Percoll gradient (Kruger *et al.*, 1980). The plasma membranes remained at the Percoll/buffer interface and were washed three times with 50 mM-Hepes/tetramethylammonium hydroxide, pH 7.5. Perigranular membranes were prepared by the osmotic lysis of intact granules (Percoll pellet) (Uvnas *et al.*, 1970). These membrane fractions

were examined by using membrane marker enzymes. The plasma-membrane fraction was enriched 4–6-fold in 5′-nucleotidase (a plasma-membrane marker) specific activity, and mitochondrial contamination as measured by succinate dehydrogenase total activity was 15% of the initial homogenate activity. The perigranular membranes contained 10% of the initial homogenate 5′-nucleotidase specific activity and 1% of the succinate dehydrogenase activity.

ATPase activity determination

ATPase assays were conducted as described previously (Amende *et al.*, 1983). The high-affinity Ca^{2+},Mg^{2+}-ATPase was assayed in the presence of 0.2mM-Tris/ATP, 80mM-KCl, 20mM-Hepes/tetramethylammonium hydroxide (pH 7.5), 1mM-NaN_3 and 0.8mM-ouabain, with 1mM-HEDTA as the Ca^{2+}-chelating agent, with various amounts of $CaCl_2$ added as needed for each Ca^{2+} concentration, determined as described by Amende *et al.* (1983). The Ca^{2+} concentration was varied from 0.11 to 57μM in the presence of 0 and 200μM-Mg^{2+}. Phosphate was determined by an automated assay (Raess & Vincenzi, 1980). Symbols and bars in Figures represent means ± S.E.M. for triplicate assays. Values for K_m and $V_{max.}$ were calculated from Lineweaver–Burk double-reciprocal plots of the data.

The assay media for the low-affinity Ca^{2+}- and Mg^{2+}-dependent ATPases contained 3mM-ATP, 20mM-Hepes/tetramethylammonium hydroxide, 80mM-KCl, 1mM-NaN_3, 3mM-ouabain, and $CaCl_2$ (Ca^{2+}-dependent ATPase), $MgCl_2$ (Mg^{2+}-dependent ATPase plus high-affinity Ca^{2+},Mg^{2+}-ATPase activated by the micromolar amounts of Ca^{2+} present in the assay system) or $MgCl_2$ and 1mM-EGTA (Mg^{2+}-dependent ATPase only), as indicated in the Figure legends.

Protein content was determined by a modification of the Lowry method (Peterson, 1977), with bovine serum albumin as standard.

Materials

Hepes, HEDTA, ouabain and bovine serum albumin were obtained from Sigma Chemical Co., St. Louis, MO, U.S.A.

Results and discussion

Fig. 1(*a*) shows the high-affinity Ca^{2+},Mg^{2+}-ATPase activity found in the enriched rat peritoneal mast-cell plasma-membrane fraction. In the absence of Mg^{2+}, only a Ca^{2+}-dependent ATPase is present, with a K_m for Ca^{2+} of approx. 3μM and $V_{max.}$ of around 12.3nmol of P_i/min per mg. When assayed in the presence of 200μM-Mg^{2+}, both high- and low-affinity components of the ATPase are

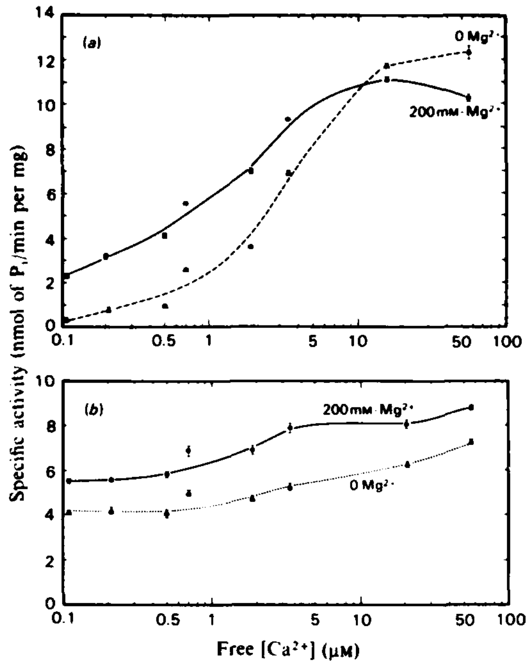

Fig. 1. *Effect of Ca^{2+} and Mg^{2+} on the ATPase activity of mast-cell (a) plasma and (b) perigranular membranes*
The isolated mast-cell membranes were assayed for ATPase activity as described in the Materials and methods section. The free Ca^{2+} concentration was varied from 0 to 60μM in the presence of (▲) 0 and (●) 200μM-Mg^{2+}.

apparent. The high-affinity component has a K_m for Ca^{2+} of approx. 0.2μM, with a $V_{max.}$ of 6–7nmol of P_i/min per mg, whereas the low-affinity ATPase shows an approx. K_m of 0.9μM and an estimated $V_{max.}$ of 11.5nmol of P_i/min per mg. The high-affinity component is activated by Mg^{2+}. This is the first report of a high-affinity Ca^{2+}, Mg^{2+}-ATPase in mast-cell plasma membranes. The low-affinity component was previously identified (Cooper & Stanworth, 1976; Magro, 1977; Chakravarty & Echetebu, 1978). The addition of 200μM-Mg^{2+} to the assay medium for perigranular-membrane ATPase activity caused a small increase in activity (Fig. 1*b*). This low Ca^{2+}, Mg^{2+}-ATPase activity may be due to the presence of plasma membranes in the final perigranular-membrane preparation. The 5′-nucleotidase activity (a plasma-membrane enzyme marker) of the perigranular membranes was 10% of that of the whole mast-cell sonicated preparation, indicating that some residual plasma-membrane contamination of the perigranular-membrane preparation had occurred (Amende & Donlon, 1985).

Another approach to detecting the Ca^{2+},Mg^{2+}-ATPase is shown in Fig. 2. Various low-affinity ATPases were assayed in the plasma-membrane fraction (Fig. 2*a*), with millimolar amounts of ATP, Mg^{2+}, Ca^{2+} and Mg^{2+}+1mM-EGTA (Amende *et al.*, 1983). The activity of the Mg^{2+}-dependent ATPase is greater than that of the Ca^{2+}-dependent ATPase. The addition of EGTA chelates the small amount of contaminating Ca^{2+} present in the assay buffer (1–2μM) and thereby eliminates the high-affinity Ca^{2+},Mg^{2+}-ATPase component. Thus, in the plasma membrane (Fig. 2*a*), EGTA addition decreases the activity of the Mg^{2+}-dependent ATPase. However, the Mg^{2+}-dependent ATPase of the perigranular membrane does not show a similar EGTA inhibition (Fig. 2*b*). The addition of EGTA to the perigranular Mg^{2+}-dependent ATPase has no effect. These results are consistent with those shown in Fig. 1(*b*) and indicate the absence of the high-affinity Ca^{2+},Mg^{2+}-ATPase from perigranular membranes. The perigranular membranes contain only the low-affinity ATPase. These data support the histochemical observations by Chakravarty & Nielson (1980), who showed the presence of a low-affinity ATPase in perigranular membranes as well as the plasma membranes. Our results show that the high-affinity ATPase is present in the plasma membrane, but not in the perigranular membranes. The mechanism by which Ca^{2+} accumulates in the mast-cell granule (Chock *et al.*, 1982; Hein & Caulfield, 1982, 1983) is still unknown, since no high-affinity ATPase could be demonstrated in the perigranular membranes.

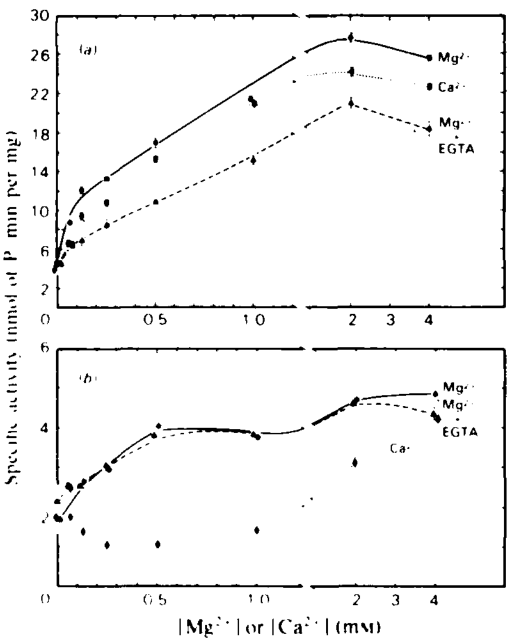

Fig. 2. *Variation in (a) plasma-membrane and (b) perigranular-membrane ATPase activity with concentration of bivalent cation at 3mM-Tris ATP*

Enzyme activity was determined for various concentrations of $CaCl_2$ (Ca^{2+}-dependent ATPase), $MgCl_2$ (both Mg^{2+}-dependent ATPase and high-affinity Ca^{2+},Mg^{2+}-ATPase) or $MgCl_2$ with 1mM-EGTA (Mg^{2+}-dependent ATPase only).

This demonstration of the high-affinity Ca^{2+},Mg^{2+}-ATPase in mast-cell plasma membranes provides a new experimental approach to the study of the mast-cell degranulation process. The high-affinity Ca^{2+},Mg^{2+}-ATPases so far described function to maintain the low intracellular Ca^{2+} concentrations that are found in resting mast cells. It is reasonable to hypothesize that inhibition of the mast-cell Ca^{2+},Mg^{2+}-ATPase would result in the following sequence: Ca^{2+} efflux would be blocked, thereby causing an increase in intracellular Ca^{2+}, which would lead to histamine release. Although several pharmacological inhibitors of similar ATPases have been applied to the mast cell and result in decreased histamine release (Fewtrell & Gomperts, 1977*a*,*b*; Chakravarty, 1980), none were specific inhibitors of the ATPase. Their effects on the mast-cell Ca^{2+},Mg^{2+}-ATPase are unknown.

L.M.A. was supported as a National Research Council Associate. This work was supported by the Armed Forces Radiobiology Research Institute, Defense Nuclear Agency, under Research Work Unit MJ 00068. Views presented in this paper are those of the authors; no endorsement by the Defense Nuclear Agency has been given or should be inferred. Research was conducted according to the principles enunciated in the 'Guide for Care and Use of Laboratory Animals' prepared by the Institute of Laboratory Animals Resources, National Research Council.

References

Amende, L. M. & Donlon, M. A. (1985) *Biochim. Biophys. Acta* in the press

Amende, L. M., Chock, S. P. & Albers, R. W. (1983) *J. Neurochem.* **40**, 1040–1047

Chakravarty, N. (1980) *Acta Pharmacol. Toxicol.* **47**, 223–235

Chakravarty, N. & Echetebu, Z. (1978) *Biochem. Pharmacol.* **27**, 1561–1569

Chakravarty, N. & Nielson, F. H. (1980) *Exp. Cell Res.* **130**, 175–184

Chock, E. S., Donlon, M. A., Fiori, C. E. & Catravas, G. N. (1982) *J. Cell Biol.* **95**, 409a

Cooper, P. H. & Stanworth, D. R. (1976) *Biochem. J.* **156**, 691–700

Fewtrell, C. M. S. & Gomperts, B. D. (1977*a*) *Biochim. Biophys. Acta* **469**, 52–60

Fewtrell, C. M. S. & Gomperts, B. D. (1977*b*) *Nature (London)* **265**, 635–636
Hein, A. & Caulfield, J. P. (1982) *J. Cell Biol.* **95**, 397a
Hein, A. & Caulfield, J. P. (1983) *J. Cell Biol.* **97**, 171a
Kruger, P. G., Lagunoff, D. & Wan, H. (1980) *Exp. Cell Res.* **129**, 83–93
Magro, A. M. (1977) *Clin. Exp. Immunol.* **30**, 160–167
Magro, A. M., Cragoe, E. J., Hurtado, I., & Rudofsky, U. H. (1983) *Int. Arch. Allergy Appl. Immunol.* **72**, 41–45
Penniston, J. T. (1983) *Ann. N.Y. Acad. Sci.* **402**, 296–303
Peterson, G. L. (1977) *Anal. Biochem.* **83**, 346–356
Raess, B. K. & Vincenzi, F. F. (1980) *J. Pharmacol. Methods* **4**, 273–283
Sullivan, T. J., Parker, K. L., Stenson, N. & Parker, C. J. (1975) *Immunology* **114**, 1473–1478
Uvnas, B., Aborg, C. H. & Bergendorff, A. (1970) *Acta Physiol. Scand.* **78**, *Suppl.* **336**, 3–26

1985

JOURNAL OF SURGICAL RESEARCH 38, 501–508 (1985)

Prostanoid Production by Lipopolysaccharide-Stimulated Kupffer Cells[1]

GARY J. BOWERS, M.D.,*‡ THOMAS J. MACVITTIE, PH.D.,* E. F. HIRSCH, M.D.,‡
JAMES C. CONKLIN, M.D.,* RONALD D. NELSON,† RUDOLPH J. ROETHEL, B.S.,†
AND MITCHELL P. FINK, M.D.†

*Armed Forces Radiobiology Research Institute, Defense Nuclear Agency, Bethesda, Maryland 20814-5145; †Naval Medical Research Institute, Bethesda, Maryland 20814-5055; ‡Boston University Medical Center, Department of Surgery, Boston, Massachusetts 02118

Presented at the Annual Meeting of the Association for Academic Surgery, San Antonio, Texas, October 31–November 3, 1984

Although some data suggest that macrophages in the reticuloendothelial system (RES) are important sources of thromboxane A_2 (TxA_2) and prostacyclin (PGI_2) during endotoxic shock, we are unaware of data documenting the ability of hepatic macrophages (Kupffer cells) to release either TxA_2 or PGI_2 when exposed to lipopolysaccharide (endotoxin, LPS). In this study, Kupffer cells were examined for their ability to release prostaglandin E_2 (PGE_2), TxA_2, and PGI_2 following stimulation with 0, 1.0, 50.0, and 100.0 μg/ml of *Escherichia coli* LPS. Kupffer cells were obtained from rat livers by enzymatic digestion with 0.05% collagenase followed by enrichment of the macrophage population on the basis of differences in density and adherence among the various cell populations isolated. Based on several criteria (phagocytosis of opsonized sheep erythrocytes, positive staining for esterase and peroxidase, failure to replicate), 95% of adherent cells were Kupffer cells. After 4 days of incubation, cells were stimulated with various doses of LPS for 4 and 8 hr. Prostanoid concentrations in culture supernatants were determined by radioimmunoassay. Increasing doses of LPS significantly ($P < 0.001$) increased the concentration of immunoreactive PGE_2 ($iPGE_2$) and $iTxB_2$ (the stable metabolite of TxA_2). The concentration of i6-keto-$PFG_{1\alpha}$ (stable metabolite of PGI_2) increased following stimulation with 1.0 μg/ml of LPS, but declined as the dose of LPS was increased. The results provide evidence that endotoxin-activated Kupffer cells, like other macrophage populations, release several metabolites of arachidonic acid. Kupffer cell-derived prostanoids, particularly TxA_2, may be important mediators of some of the pathophysiologic manifestations of acute endotoxemia. © 1985 Academic Press, Inc.

INTRODUCTION

Thromboxane (Tx) A_2 and prostacyclin (PGI_2) have been implicated as contributing to the pathophysiologic manifestations of endotoxic shock [13]. Thromboxane A_2 is a potent vasoconstrictor [29] and inducer of platelet [18] and leukocyte [33] aggregation. There is evidence that TxA_2 participates in the pathogenesis of endotoxin-induced pulmonary hypertension [8, 16], disseminated intravascular coagulation [1, 35], hepatocellular dysfunction [1, 35], and mortality [1, 35]. Prostacyclin is a vasodilator [2] and platelet antiaggregant [27]. This prostanoid may contribute to delayed hypotension in experimental endotoxic shock [7] and decreased systemic vascular resistance in human sepsis [31].

Several lines of evidence suggest that macrophages within the reticuloendothelial system (RES) are an important source of TxA_2 and PGI_2 in endotoxic shock. First, systemically administered endotoxin is primarily sequestered by fixed macrophages (Kupffer cells) within the liver [26]. Second, endotoxin stimulates TxA_2 and prostacyclin release from cultured peritoneal macrophages [9]. Third,

[1] The opinions and assertions contained herein are the private ones of the authors and are not to be construed as official or reflecting the views of the Navy Department, the naval service at large, or the Defense Nuclear Agency. The experiments contained here were conducted according to the principles set forth in the "Guide for the Care and Use of Laboratory Animals," Institutes of Laboratory Resources, National Research Council, DHEW, Publication (NIH) 78-23. Supported by Naval Medical Research Institute Work Unit M0095.001.1032, and Armed Forces Radiobiology Research Institute Task 4441-00082.

0022-4804/85 $1.50

stimulation of the RES sensitizes animals to the prostaglandin (PG)-releasing effects of endotoxin whereas RES depression has the opposite effect [10].

Although endotoxin stimulates Kupffer cells to release PGE_2 [4, 11] and a variety of other inflammatory mediators and lytic enzymes [3, 4, 11, 23, 24], we are unaware of data indicating that Kupffer cells synthesize TxA_2 or PGI_2 when challenged with endotoxin. The purpose of the present study was to determine the effects of the endotoxin *Escherichia coli* on *in vitro* TxA_2, PGI_2, and PGE_2 production by rat Kupffer cells.

MATERIALS AND METHODS

Materials. Halothane (Ayerest Laboratories, New York, N. Y.), Hanks' balanced salt solution (HBSS) with (+) and without (−) calcium and magnesium salts (GIBCO, Grand Island, N. Y.), collagenase (Millipore Corp., Freehold, N. J.), trypsin (DIFCO, Detroit, Mich.), *E. coli* lipopolysaccharide (055:B5; DIFCO), TxB_2 and 6-keto-$PGF_{1\alpha}$ (Upjohn, Kalamazoo, Mich.), activated charcoal (Sigma, St. Louis, Mo.), Dextran T-70 (Pharmacia Fine Chemicals AB, Upsala, Sweden), and lymphocyte separation medium (LSM; Litton Bionetics, Kensington, Md.) were purchased from the indicated suppliers. Assay kits for PGE_2, "Atomlight" scintillation fluid, $[^3H]TxB_2$, and $[^3H]$6-keto-$PGF_{1\alpha}$ were purchased from New England Nuclear (Boston, Mass.). Antibodies against TxB_2 (stable metabolite of TxA_2) and 6-keto-$PGF_{1\alpha}$ (stable metabolite of prostacyclin) were kindly provided by Dr. L. Levine (Boston, Mass.). These antibodies demonstrated less than 2% cross-reactivity with other prostanoids. Assay kits ("Bio-Rad") for protein determination were obtained from Bio-Rad Laboratories (Richmond, Calif.). Falcon 24-well plastic tissue culture plates were obtained from Beckton Dickinson Labware (Oxnard, Calif.). Male Sprague–Dawley rats (250–300 g) were purchased from Taconic Farms (Germantown, N. Y.).

In general, Kupffer cells were cultured in medium consisting of minimum essential medium (GIBCO) supplemented with 2% (w/v) glucose (Fisher Scientific, Fair Lawn, N. J.), 15% (v/v) fetal calf serum (FCS), penicillin (50 U/ml), streptomycin (50 μg/ml), and 0.2 m*M* glutamine (all obtained from GIBCO). The medium employed for studies of LPS-stimulated prostanoid release was identical to the above except that FCS was deleted.

The buffer for radioimmunoassay of TxB_2 and 6-keto-$PGF_{1\alpha}$ consisted of Trizma-7.0 (Sigma)-buffered saline containing 0.1% (w/v) gelatin (DIFCO), 2 m*M* $MgSO_4$ and 0.2 m*M* $CaCl_2$.

Cell isolation and maintenance. Under halothane anesthesia, the liver was exposed via a midline laparotomy. The portal vein was cannulated and the liver perfused with approximately 150 ml of warm (37°C) HBSS (−) until the organ blanched. The liver was then perfused with 10 ml of HBSS (+) containing 0.05% (w/v) collagenase, after which the organ was excised, stripped of adherent tissues, minced into small fragments, and digested in 0.05% collagenase in HBSS (+) for 60 min at 37°C with continual stirring. After filtering through nylon mesh to remove nondigested fragments and washing several times with iced HBSS (−), the resulting cell suspension was subjected to LSM density gradient centrifugation (400*g* for 45 min at 4°C). The nonparenchymal cell (NPC) fraction was collected from the interface and washed multiple times using HBSS (−). Viability was determined on the basis of trypan blue dye exclusion. The cells were suspended in enriched Kupffer cell culture medium (1.0–1.5×10^6 cells/ml) and transferred to multiwell tissue culture plates (1.0 ml/well). Cultures were maintained at 37°C in humidified air containing 5% CO_2. Following overnight incubation, the cultures were washed briefly once with HBSS (−) containing 0.1% trypsin (w/v) and followed by multiple washes with HBSS (−) to remove debris and loose or nonadherent cells. The cells were incubated

for 4 days with daily washings and media changes prior to use in studies of prostanoid production after endotoxin stimulation.

Cell identification. Adherent cells did not proliferate during the time course of the study. These cells showed positive staining for both esterase [22] and peroxidase [19] and phagocytized opsonized sheep erythrocytes. In general, greater than 95% of adherent cells met these accepted criteria [19] for identification as Kupffer cells.

Endotoxin stimulation. After 4 days of incubation, the cultured cells were washed several times with HBBS (−). The cells were then reincubated for 4 or 8 hr in serum-free medium (1.0 ml/well) containing 0, 1.0, 50.0, or 100.0 μg/ml of LPS. At the end of the specified time, the supernatants from each well were collected and stored individually at −60 to −80°C in polypropylene tubes. Viability of the cells following LPS stimulation was determined by trypan blue staining. The cells were then washed and stored frozen for subsequent protein determination.

Protein determinations. The protein content of the frozen cell monolayer was determined following three freeze–that cycles using the Bio-Rad microassay technique [6].

Radioimmunoassay. Immunoreactive PGE_2 ($iPGE_2$) was determined using the kit supplied by New England Nuclear, according to the procedure specified in the package insert for assays of $iPGE_2$ in urine. The lower limit of sensitivity for this assay was 2.5 pg/ml. With slight modifications, the assay for $iTxB_2$ and i6-keto-$PGF_{1\alpha}$ was as previously described [14]. Briefly, the assay was conducted in 12 × 75-mm plastic tubes, containing 100 μl of tissue culture medium or standard, 100 μl of tritiated antigen dissolved in assay buffer, 100 μl of appropriately diluted antibody in assay buffer, and 300 μl of assay buffer. Standards were prepared in assay buffer. After overnight incubation at 4°C, bound antigen was separated from free by centrifugation after the addition of 900 μl of assay buffer containing 0.03% (w/v) dextran and 0.3% (w/v) charcoal. Supernatants were decanted into scintillation vials containing 5 ml of scintillation fluid and counted for 10 min in a scintillation counter. Concentrations of $iPGE_2$, $iTxB_2$, and i6-keto $PGF_{1\alpha}$ in sample unknowns were determined by comparison with a standard curve after log-logit transformation of the data. Samples were always run in duplicate and the results averaged. Variations between duplicate samples was less than 10%.

Statistical analyses. In each experiment, each condition (defined by LPS dose and incubation time) was run in quadruplicate. All data are expressed as the arithmetic mean ± standard errors. Data for $iTxB_2$ were obtained in two replicate experiments (i.e., eight entries per data point). Other results were obtained in a single experiment. Data were analyzed by two-way analysis of variance, using a fully randomized design, with endotoxin dose and incubation time being the independent sources of variation. Differences with $P \leq 0.05$ were considered significant.

RESULTS

Only 25–30% of the origina. oopulation added to the cultures remained adherent to the plates after overnight incubation and washing as determined by cell counts of the removed nonadherent cells. This is consistent with estimates of the constituent proportion of Kupffer cells within the liver's nonparenchymal cell population [30]. It was not practical to count the total number of adhered cells within each well nor were we able to accurately estimate the number from representative fields as the cells generally did not assume a uniform distribution within the culture wells. Nonetheless, calculated estimates based on the original number of cells incubated would suggest that each well contained 10^5 cells. Protein content of the individual wells varied from 3 to 5 μg/well, suggesting minor variation in the number of adherent cells present among the wells. Variation in protein content did not correlate with variation in prostanoid production.

Viability was greater than 95% for freshly isolated Kupffer cells as well as those incubated for 4 days in the macrophage medium. Exposure of the cells for 4 to 8 hr to the highest concentration of LPS used in the study (100 μg/ml) decreased viability to 80–85%. Lower LPS concentrations did not affect viability.

The concentrations of $iTxB_2$, $iPGE_2$, and i6-keto-$PGF_{1\alpha}$ detected in the supernatants of Kupffer cells cultures are depicted in Figs. 1, 2, and 3, respectively. Supernatants from unstimulated cultures contained detectable levels of all three prostanoids. Lipopolysaccharide affected production of $iTxB_2$, $iPGE_2$, and i6-keto-$PGF_{1\alpha}$. Depending on the prostanoid, there were marked differences in the effects of increasing LPS dose and duration of incubation on measured prostanoid concentrations.

Resting Kupffer cells released 55.2 ± 6.6 and 72.8 ± 9.9 pg/ml of $iTXB_2$ into the media at 4 and 8 hr, respectively (Fig. 1). In the presence of 1 μg/ml LPS, the detectable concentration of $iTxB_2$ was essentially unchanged from control for both time periods. However, in the presence of 50 μg/ml LPS, 188.5 ± 38.7 pg/ml at 4 hr and 232.8 ± 70 pg/ml at 8 hr were detected in the supernatants. Stimulated macrophages released 235.2 ± 36.6 pg/ml and 256.0 ± 52.5 pg/ml at 4 and 8 hr, respectively, when incubated with 100 μg/ml LPS. Thus, dose of LPS ($F(3,88) = 25.38$; $P < 0.001$) but not incubation time ($F(1,88) = 1.01$) significantly affected TxA2 production.

The concentration of $iPGE_2$ also increased as a function of increasing LPS concentration ($F(3,40) = 85.91$; $P < 0.001$) (Fig. 2). At 8 hr a similar rise was noted in the presence of similarly increasing doses of LPS. The effect of incubation time was also significant ($F(1,40) = 34.08$; $P < 0.001$).

When stimulated with the lowest concentration of LPS (1 μg/ml), Kupffer cell production of i6-keto-$PGF_{1\alpha}$ rose from 79.2

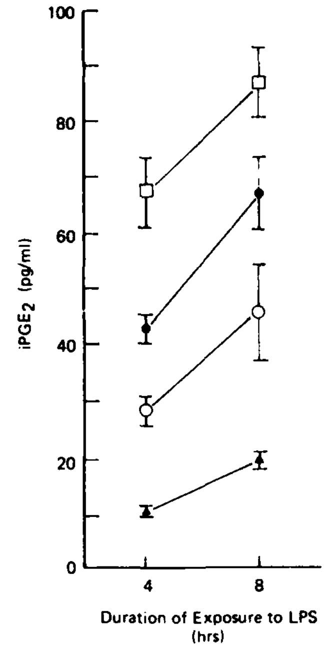

FIG. 2. Concentration of $iPGE_2$ in supernatants from LPS-stimulated Kupffer cells. Each point represents the mean ± SE of four separate measurements (one experiment). □, 100 μg LPS; ●, 50 μg LPS; ○, 1 μg LPS; ▲, 0 μg LPS.

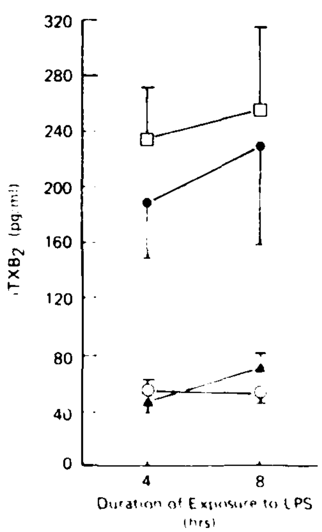

FIG. 1. Concentration of $iTxB_2$ in supernatants from LPS-stimulated Kupffer cells. Each point represents the mean ± SE of eight separate measurements obtained from two experiments. □, 100 μg LPS; ●, 50 μg LPS; ○, 1 μg LPS; ▲, 0 μg LPS.

± 18.2 pg/ml for nonstimulated cells to 156.0 ± 1.8 pg/ml (4 hr) and 81.2 ± 13.6 pg/ml to 147.5 ± 13.7 pg/ml (8 hr) (Fig. 3). However, unlike $iTxB_2$ and $iPGE_2$, with 50 μg/ml of LPS, the concentration of i6-keto-$PGF_{1\alpha}$ decreased. This decline was further pronounced in the presence of 100 μg/ml LPS. The dose effect was significant ($F(3,40) = 10.18$; $P < 0.001$); the effect of incubation time was not ($F(1,40) = 0.22$).

Table 1 presents, as a function of LPS concentration, the ratio of mean i6-keto $PGF_{1\alpha}$ concentration to mean $iTxB_2$ concentration. The addition of 1 μg/ml of LPS resulted in this ratio increasing from baseline values of 1.4 (4-hr cultures) and 1.1 (8-hr cultures) to 2.8 (both 4- and 8-hr cultures). Adding increasingly larger doses of LPS, however, caused the ratio to progressively and significantly ($F(3,3) = 232.4$, $P < 0.001$) decline to 0.2 at the highest LPS concentration tested (100 μg/ml).

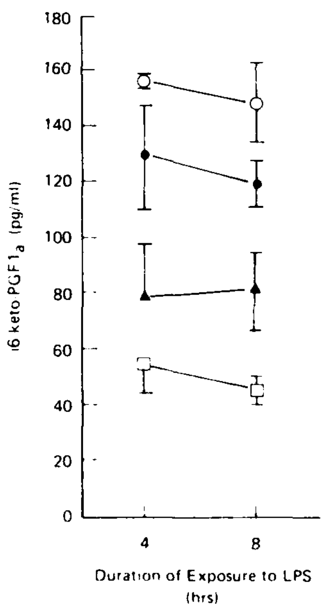

FIG. 3. Concentration of i6-keto-$PGF_{1\alpha}$ in supernatants from LPS-stimulated Kupffer cells. Each point represents the mean ± SE of four separate measurements (one experiment). □, 100 μg LPS; ●, 50 μg LPS; ○, 1 μg LPS; ▲, 0 μg LPS.

TABLE I

RATIO OF MEAN i6-KETO-$PGF_{1\alpha}$:$iTxB_2$ IN SUPERNATANTS FROM LPS-STIMULATED KUPFFER CELLS

Concentration of LPS (μg/ml)	Duration of exposure to LPS (hr) 4	8
0	1.4	1.1
1	2.8	2.8
50	0.7	0.5
100	0.2	0.2

DISCUSSION

Hepatic dysfunction, ranging from mild hyperbilirubunemia and serum transaminase elevations to overt organ failure, occurs in septic patients [5]. The mechanisms underlying this phenomenon are incompletely understood, although it is likely that endotoxins derived from gram-negative bacteria are involved [21,30]. Intravenously administered endotoxin localizes within the liver, being cleared from the circulation by Kupffer cells lining the sinusoids [26,30]. In the presence of endotoxin hepatocellular dysfunction occurs including altered carbohydrate, fat, and protein metabolism [21]. Although hepatocytes have receptors for endotoxins [30], high-resolution audioradiographic studies have failed to demonstrate the ability of these cells to internalize endotoxin [26]. Thus, it is not clear whether endotoxin is capable of causing direct toxicity to hepatocytes. On the other hand, there is convincing evidence that endotoxemia triggers an inflammatory response within the liver characterized by Kupffer cell activation, platelet aggregation, fibrin deposition, intravascular thrombosis, and polymorphonuclear leukocyte infiltration [21]. This inflammatory response may cause injury to hepatocytes, either because of relative ischemia secondary to intravascular thrombosis or because of extracellular release of potent inflammatory mediators by acti-

vated Kupffer cells [3, 4, 23–25] and/or infiltrating leukocytes [34].

It is well established that peritoneal macrophages synthesize a variety of arachidonic acid (AA) metabolites when stimulated with LPS [9, 10, 20]. Production of PGE_2 by endotoxin-stimulated hepatic macrophages (Kupffer cells) *in vitro* has been reported previously [4, 11]. In the present study, we have confirmed this observation and, in addition, have shown that (1) high LPS concentrations (50 and 100 μg/ml) trigger the release of TxA_2, and (2) whereas PGI_2 synthesis is increased by a low LPS dose (1 μg/ml), higher doses of LPS result in less detectable PGI_2.

Thromboxane A_2 induces vasoconstriction (hence low flow) and platelet aggregation [18, 29]. Within the liver, endotoxin-induced venous stasis and platelet aggregation may derive from TxA_2 released by activated Kupffer cells. The procoagulant activity (PCA) of Kupffer cells is stimulated by endotoxin in a dose–response relationship similar to that observed for LPS-stimulated TxA_2 release [23, 25]. This PCA peaks within 6–8 hr following exposure to LPS [25], a time course during which increased amounts of $iTxB_2$ were present in our Kupffer cell cultures (Fig. 1). Thus, LPS-activated Kupffer cells release two agents which can promote the intrahepatic intravascular thrombosis associated with endotoxins. Additionally, TxA_2 causes leukocyte aggregation [33]. Thus, Kupffer cell-derived TxA_2 may also contribute to the accumulation of inflammatory cells within the liver during endotoxemia.

Changes in Kupffer cell production of PGI_2 are more sensitive to LPS concentrations than TxA_2. A dose which had no discernable effect on TxA_2 synthesis (1 μg/ml) augmented PGI_2 release into the media. The physiologic properties of PGI_2 antagonize those of TxA_2 and therefore, PGI_2 released by low concentrations of LPS may minimize the effects of basal TxA_2 production. Conceivably, PGI_2 might also antagonize the thrombotic effects of PCA stimulated by low LPS concentrations [25].

Inhibition of prostacyclin synthetase by cyclo-oxygenase-derived products may explain why increasing doses of LPS decreased PGI_2 production. Fatty acid hydroperoxides inhibit prostacyclin synthetase [17, 32]. Such species are produced following the oxidation of AA [12]. Increased mobilization of AA triggered by LPS may lead to inactivation of prostacyclin synthetase and shunting of intermediates into PGE_2 and/or TxA_2 synthesis. In support of this, selective thromboxane synthetase inhibitors have been shown to increase the production of 6-keto-$PGF_{1\alpha}$ in human peritoneal macrophages [15].

We used doses of LPS that are high relative to presumed circulating concentrations of endotoxin in septic patients. Endotoxins, however, are highly concentrated within the liver [26]. In rabbits, following an intravenous infusion of 250 μg of ^{125}I-LPS, as much as 40–50% of the infused dose is detectable in the liver within 5 min [26]. This corresponds to a tissue concentration ranging from 0.7 to 2.0 μg/g of liver tissue. Within the liver, it is the Kupffer cell which accumulates endotoxin. Therefore, the concentration of endotoxin per gram of macrophage tissue, a small component of the total liver mass, would accordingly be much higher. In rats, a 250-μg dose of LPS is a small dose. In our laboratory, 15 mg/kg is an LD_{50} dose. Thus, in a 0.3-kg rat, 4.5 mg of LPS would result in a liver concentration of 2.25 mg/g liver tissue (assuming 50% uptake by a 10-g liver).

Endotoxin is toxic to Kupffer cells. Following the infusion of endotoxin into mice, swelling of Kupffer cells occurs within a short period of time [21]. In culture, exposure to endotoxin causes Kupffer cells to become vacuolated, rounded, and to leak various intracellular enzymes [24]. Our present observations substantiate the toxicity of endotoxin for Kupffer cells, but only at the highest dose (100 μg/ml) of LPS employed. In general, our data agree with previous reports [4, 24], although the toxicity observed in our study was not as severe, probably reflecting relatively shorter incubation times.

In summary, we showed that endotoxin

stimulates cultured rat Kupffer cells to produce TxA_2, PGI_2, and PGE_2. Dose and time effects appeared to be unique for each prostanoid. Whether Kupffer cell-derived prostanoids are important in the pathophysiology of experimental endotoxic shock or clinical sepsis remains to be established. Unpublished observations from our laboratory and results reported by other [1, 10], however, suggest that this may indeed be the case. Nonetheless, the data presented here substantiate that LPS-activated Kupffer cells release AA metabolites which have properties that can profoundly alter the microenvironment of the liver.

REFERENCES

1. Anderegg, K., Anzeveno, P., Cook, J. A., Halushka, P. V., McCarthy, J., Wagner, E., and Wise, W. C. Effects of a pyridine derivative thromboxane synthetase inhibitor and its inactive isomer in endotoxic shock in the rat. *Brit. J. Pharmacol.* **78:** 725, 1983.
2. Armstrong, J. M., Lattimier, N., Moncada, S., and Vane, J. R. Comparison of the vasodepressor effects of prostacyclin and 6-oxo-prostaglandin $F_{1\alpha}$ with those of prostaglandin E_2 in rats and rabbits. *Brit. J. Pharmacol.* **62:** 125, 1978.
3. Bhatnager, R., Schirmer, R., Ernst, M., and Decker, K. Superoxide release by zymosan-stimulated rat Kupffer cells *in vitro*. *Eur. J. Biochem.* **119:** 171, 1981.
4. Bhatnagar, R., Schade, U., Rietschel, E. Th., and Decker, K. Involvement of prostaglandin E and adenosine 3′, 5′-monophosphate in lipopolysaccharide-stimulated collagenase release by rat Kupffer cells. *Eur. J. Biochem.* **125:** 125, 1982.
5. Borzotta, A. P., and Polk, H. C. Multiple system organ failure. *Surg. Clin. North Amer.* **63:** 315, 1983.
6. Bradford, M. M. A rapid and sensitive method for the quantitation of microgram quantities of protein utilizing the principle of protein-dye binding. *Anal. Biochem.* **72:** 248, 1976.
7. Bult, H., Beetens, J., and Herman, A. G. Blood levels of 6-oxo-prostaglandin $F_{1\alpha}$ during endotoxin-induced hypotension in rabbits. *Eur. J. Pharmacol.* **63:** 47, 1980.
8. Casey, L. C., Fletcher, J. R., Zmudka, M. I., and Ramwell, P. W. Prevention of endotoxin-induced pulmonary hypertension in primates by the use of a selective thromboxane synthetase inhibitor, OKY 1581. *J. Pharmacol. Exp. Ther.* **222:** 441, 1982.
9. Cook, J. A., Wise, W. C., and Halushka, P. V. Thromboxane A_2 and prostacyclin by lipopolysaccharide-stimulated peritoneal macrophages. *J. Reticuloendothel. Soc.* **30:** 445, 1981.
10. Cook, J. A., Halushka, P. V., and Wise, W. C. Modulation of macrophage arachidonic acid metabolism: Potential role in the susceptibility of rats to endotoxic shock. *Circ. Shock* **9:** 605, 1982.
11. Decker, K., Birmelin, M., Bhatnagar, R., and Rieder, H. The role of Ca^{++} and prostaglandin in the response of rat Kupffer cells to external stimuli. *In* D. L. Knock and E. Wisse (Eds.), *Sinusoidal Liver Cells*. Amsterdam/New York: Elsevier, 1982. Pp. 361–368.
12. Egan, R. W., Paxton, J., and Kuehl, F. A. Mechanism for irreversible self-deactivation of prostaglandin synthetase. *J. Biol. Chem.* **251:** 7329, 1976.
13. Fink, M. P. The role of prostaglandins and related compounds in the pathophysiology of endotoxic and septic shock. *Semin. Respir. Med.*, in press.
14. Fink, M. P., MacVittie, T. J., and Casey, L. C. Inhibition of prostaglandin synthesis restores normal hemodynamics in canine hyperdynamic sepsis. *Ann. Surg.* **200:** 619, 1984.
15. Foegh, M., Maddox, Y. T., Winchester, J., Rabowski, T., Schrunes, G., and Ramwell, P. W. Prostacyclin and thromboxane release from human peritoneal macrophages. In B. Samuelsson, R., Paoletti, and P. Ramwell (Eds.), *Advances in Prostaglandin, Thromboxane, and Leukotuene Research*. Raven Press, New York, 1983, Vol. 12, pp. 45–49.
16. Hales, C. A., Sonne, L., Peterson, M., Kong, D., Miller, M., and Watkins, W. B. Role of thromboxane and prostacyclin in pulmonary vasomotor changes after endotoxin in dogs. *J. Clin. Invest.* **68:** 497, 1981.
17. Ham, E. A., Egan, R. W., Soderman, D. D., Gale, P. F., and Kuehl, F. A. Peroxidase-dependent deactivation of prostacyclin synthetase. *J. Biol. Chem.* **254:** 2191, 1979.
18. Hamberg, M., Svensson, J., and Samuelsson, B. Thromboxane: A new group of biologically active compounds derived from prostaglandin endoperoxides. *Proc. Natl. Acad. Sci. USA* **72:** 2994, 1975.
19. Knook, D. L., and Sleyster, E. Ch. Preparation and characterization of Kupffer cells from rat and mouse liver. In E. Wisse and D. L. Knook (Eds.), *Kupffer Cells and Other Liver Sinusoidal Cells*. Amsterdam/New York: Elsevier, 1977. Pp. 273–288.
20. Kurland, J. I., and Bockman, R. Prostaglandin E production by human blood monocytes and mouse peritoneal macrophages. *J. Exp. Med.* **147:** 952, 1978.
21. Levy, E., Path, F. C., and Ruebner, B. H. Hepatic changes produced by a single dose of endotoxin in the mouse. *Amer. J. Pathol.* **51:** 269, 1967.
22. Li, C. Y., Lam, K. W., and Yam, L. T. Esterases in human leukocytes. *J. Histochem. Cytochem.* **21:** 1, 1973.
23. Maier, R. V., and Ulevitch, R. J. The induction of a unique procoagulant activity in rabbit hepatic macrophages by bacterial lipopolysaccharide. *J. Immunol.* **127:** 1596, 1981.

24. Maier, R. V., and Ulevitch, R. J. The response of isolated rabbit hepatic macrophages (H-MØ) to lipopolysaccharide (LPS). *Circ. Shock* **8:** 165, 1981.

25. Maier, R. V., and Hahnel, G. B. Potential for endotoxin-activated Kupffer cells to induce microvascular thrombosis. *Arch. Surg.* **119:** 62, 1984.

26. Mathison, J. C., and Ulevitch, R. J. The clearance, tissue distribution and cellular localization of intravenously injected lipopolysaccharide in rabbits. *J. Immunol.* **123:** 2133, 1979.

27. Moncada, S., Gryalewski, R., Bunting, S., and Vane, J. R. An enzyme isolated from arteries transforms prostaglandin endoperoxides to an unstable substance that inhibits platelet aggregation. *Nature (London)* **263:** 663, 1976.

28. Munthe-Kaas, A. C., Berg, T., Seglen, P. O., and Seljelid, R. Mass isolation and culture of rat Kupffer cells. *J. Exp. Med.* **141:** 1, 1975.

29. Needleman, P., Minkes, M., and Rez, A. Thromboxanes: Selective biosynthesis and distinct biological properties. *Science (Washington, D. C.)* **193:** 163, 1976.

30. Nolan, J. P., and Camara, D. S. Endotoxin and liver disease. In D. L. Knook and E. Wisse (Eds.), *Sinusoidal Liver Cells*. Amsterdam/New York: Elsevier, 1982. Pp. 377–386.

31. Rie, M., Peterson, D., Kong, D., Quinn, D., and Watkins, D. Plasma prostacyclin increases during acute human sepsis. *Circ. Shock* **10:** 232, 1983.

32. Salmon, J. A., Smith, D. R., Flower, R. J., Moncada, S., and Vane, J. R. Further studies on the enzymatic conversion of prostaglandin endoperoxide into prostacyclin by porcine aorta microsomes. *Biochim. Biophys. Acta* **523:** 250, 1978.

33. Spagnulo, P. J., Ellner, J. J., Hassid, A., and Dunn, M. J. Thromboxane A_2 mediates augmented polymorphonuclear leukocytes adhesiveness. *J. Clin. Invest.* **66:** 406, 1980.

34. Weissman, G., Snolen, J. E., and Korchak, H. M. Release of inflammatory mediators from stimulated neutrophils. *N. Engl. J. Med.* **303:** 27, 1980.

35. Wise, W. C., Cook, J. A., Halushka, P. V., and Knapp, D. R. Protective effects of thromboxane synthetase inhibitors in rats in endotoxic shock. *Circ. Res.* **46:** 854, 1980.

ARMED FORCES RADIOBIOLOGY RESEARCH INSTITUTE
SCIENTIFIC REPORT
SR85-19

FUNDAMENTAL AND APPLIED TOXICOLOGY 5, 597–604 (1985)

Antihistamines Block Radiation-Induced Increased Intestinal Blood Flow in Canines[1]

LORRIS G. COCKERHAM, THOMAS F. DOYLE, MILDRED A. DONLON AND CRAIG J. GOSSETT-HAGERMAN

Physiology and Biochemistry Departments, Armed Forces Radiobiology Research Institute, Bethesda, Maryland 20814

Antihistamines Block Radiation-Induced Increased Intestinal Blood Flow in Canines. COCKERHAM, L. G., DOYLE, T. F., DONLON, M. A., AND GOSSETT-HAGERMAN, C. J. (1985). *Fundam. Appl. Toxicol.* 5, 597–604. Radiation-induced systemic hypotension is accompanied by increased intestinal blood flow (IBF) and an increased hematocrit (HCT) in dogs. Histamine infusion leads to increased IBF and intestinal edema with consequent secretion of fluid into the intestinal lumen. This study was performed to determine whether these effects could be diminished by prior administration of H_1 and H_2 histamine blockers. Dogs were given an iv infusion of mepyramine (0.5 mg/min) and cimetidine (0.25 mg/min) for 1 hr before and for 1 hr after radiation (H_1 and H_2 blockers, respectively). Mean systemic arterial blood pressure (MBP), IBF, and HCT were monitored for 2 hr. Systemic plasma histamine levels were determined simultaneously. Data obtained indicated that the H_1 and H_2 blockers, given simultaneously, were successful in blocking the increased IBF and the increased HCT seen after 100 Gy, whole-body, γ radiation. However, the postradiation hypotension was only somewhat affected, with the MBP falling to a level 28% below the preradiation level. Plasma histamine levels reached a sharp peak, as much as 20% above baseline, at 4 min postradiation. These findings implicate histamine in the radiation-induced increase in IBF and HCT but not for the gradual decrease in postradiation blood pressure.

Supralethal exposure to ionizing radiation such as γ photons results in postradiation hypotension, increased intestinal blood flow, and increased hematocrits in canine subjects (Cockerham *et al.*, 1984a). Studies have reported elevations of circulating blood histamine in humans undergoing radiation therapy (Lasser and Stenstrom, 1954), decreases in tissue histamine levels in rats (Eisen and Wilson, 1957), and increases in canine plasma histamine levels (Cockerham *et al.*, 1984b) following radiation. Histamine has been reported to cause intestinal vasodilation and increased gastrointestinal blood flow in dogs (Shehadeh *et al.*, 1969; Lee and Silverberg, 1976; Granger *et al.*, 1980; Meiners *et al.*, 1982) and rats (Timmermans and Gerber, 1980). Infusion of histamine into the small intestine not only causes an increase in intestinal blood flow but also produces a copious secretion of fluid following edema (Lee and Silverberg, 1976). This loss of fluid from the blood would result in the observed increased hematocrit and contribute to postradiation hypotension.

Histamine is stored in mast cells throughout the body (Metcalfe *et al.*, 1981) and is released under the stimulus of ionizing radiation (Doyle and Strike, 1977; Alter *et al.*, 1983) and may be implicated in radiation-induced hypotension accompanied by increased intestinal blood flow and increased hematocrits in dogs. This study was designed

[1] Supported by Armed Forces Radiobiology Research Institute, Defense Nuclear Agency, under Research Work Unit MJ 00081. The views presented in this paper are those of the authors. No endorsement by the Defense Nuclear Agency has been given or should be inferred.

0272-0590/85 $3.00

to determine whether these radiation-induced effects could be mitigated by preradiation administration of antihistamines. Since, in the dog, both endogenously released and exogenous histamine exert both peripheral and cardiac effects by activation of both H_1 and H_2 receptors (Dobbins *et al.*, 1981; Powell and Brody, 1976; Reinhardt *et al.*, 1980), the H_1 and H_2 histamine blockers mepyramine and cimetidine were selected to be given in combination.

MATERIALS AND METHODS

Eighteen male beagles (Hazelton Research Animals, Cumberland, Va.), 12 to 15 months old and weighing between 7.3 and 16.0 kg, were used in this study. After a physical examination performed by the staff veterinarians of the Armed Forces Radiobiology Research Institute, and 2 weeks of quarantine, the animals were divided randomly into three groups of six animals each. Food was withheld from all dogs overnight before the experiment, but water was available *ab libitum*. Research was conducted according to the principles enunciated in the *Guide for the Care and Use of Laboratory Animals* prepared by the Institute of Laboratory Animal Resources, National Research Council.

Sixty minutes before radiation, six of the subjects were started on an iv infusion of physiological saline containing mepyramine (0.5 mg/min) (Douglas, 1975; Powell and Brody, 1976) and cimetidine (0.25 mg/min) (Dobbins *et al.*, 1981) to block the effects of histamine. This infusion continued until 60 min after radiation. Another group of six animals was given a saline only, iv infusion for 60 min before and 60 min after radiation. The third, or control group of six subjects was also given saline for the 2 hr time but were only sham-radiated.

Approximately 3 hr before radiation or simulated radiation, the animals were weighed and a foreleg was shaved to facilitate administration of anesthetic by iv administration of 30 mg/kg sodium pentobarbital (Nembutal). Each dog was intubated with a cuffed endotracheal tube and respired using a forced volume respirator to maintain a stable blood pH and oxygen tension. After insertion of the endotracheal tube, each dog was placed in a supine position on a circulating water blanket to maintain body temperature. The water blanket and the dog were positioned in a wooden "V" tray to maintain the animal in a steady supine position. With the animals in this position, a rectal probe was inserted to monitor body temperature. A femoral arterial catheter was used to measure blood pressure, blood gas, and hematocrit and to withdraw blood for plasma histamine determinations, while a systemic venous catheter was used to administer the antihistamines, physiological saline, and maintenance doses of anesthetic. The blood pressure was measured using a Statham P23 Db pressure transducer.

For this experiment, the abdominal incision followed the linea alba from the umbilicus caudally to the pubic area. The incision was made with an electrocautery apparatus, additionally suturing any large bleeding vessels after clamping with hemostats. Once the midline incision was complete, a catheter was inserted into the hepatic portal vein via a splenic vein to obtain blood samples for plasma histamine determinations.

A section of the small intestine approximately 15 cm from the ileocecal junction was withdrawn from the abdomen for the insertion of four blood flow measuring electrodes (Teflon-coated wire, 90% platinum, 10% iridium, of 0.178-mm diameter, with a 3-mm uncoated tip) into the submucosa approximately 2 cm apart. After the electrodes were placed in the submucosa of the ileum and sewn in place with cotton sutures, they were connected to the hydrogen polarographic amplifier. The instrumented intestine was then returned to the peritoneal cavity and the abdominal wall sutured or clamped. A stainless-steel reference electrode was placed in nearby tissue.

Intestinal submucosal blood flow was measured by the hydrogen clearance technique for 60 min before radiation or sham radiation and for 60 min after (Aukland *et al.*, 1964; Young, 1980). This technique is essentially an amperometric method, which measures the current induced in a platinum electrode by the reduction of hydrogen. The current produced has a linear relationship with the concentration of hydrogen in the tissue (Hyman, 1961). Hydrogen was introduced into the blood via inhalation through the endotrachael tube at a rate of approximately 5% of the normal respiratory rate for 1 to 2 min for each flow measurement. Blood flow was measured by each of the four electrodes approximately every 5 min. The electrodes were maintained electrically at +600 mV with respect to the reference electrode to reduce possible oxygen and ascorbate interference. Four recording electrodes were used to compensate for transient regional variations due to intestinal contractions.

Measurements of currents from each electrode were fed through the polarographic amplifier and then to a recorder, which produced curves depicting the clearance of hydrogen from the tissues. The clearance curves were then analyzed by a PDP 11/70 computer equipped with a VT55 terminal and a versatex plotter (Digital Equipment Corp., Maynard, Mass.). The computer operates in either real time or off line mode, using a FORTRAN IV-plus program written by AFRRI's Computer Science Department. The first 60 sec after the peak of the curves was neglected to obviate contamination by arterial recirculation (Martins *et al.*, 1974). Data points were measured every second for 90 sec. The flow was calculated between

every two points and a linear regression performed over the 90-sec period. Measurements from the four electrodes were then averaged to compensate for transient regional variations.

After 60 min of recording, the animals were disconnected from the respirator and recording apparatus to facilitate radiation. After radiation, or sham radiation for controls, the animals were immediately reconnected to the respirator and recording apparatus, and measurements were continued for a minimum of 60 min. Approximately 10, 30, and 60 min pre- and postradiation, a blood sample was taken via the arterial catheter to determine pH and oxygen tension. Simultaneously, with blood gas determinations, hematocrit and temperature measurements were determined. At 60, 30, and 10 min preradiation or sham radiation and at 2, 4, 6, 30, and 60 min postradiation or sham radiation a blood sample was taken via both the arterial catheter and the hepatic portal vein to determine plasma histamine levels. After termination of the measurements, the electrodes were examined for verification of placement in the submucosa and then removed. The animals were then euthanized with an iv injection of saturated $MgSO_4$.

Blood samples for plasma histamine determinations were drawn from the arterial and venous catheters with plastic syringes and transferred to prelabelled, chilled collection tubes containing EDTA. The tubes were inverted gently and stored on ice until the termination of the experiment. The blood was then centrifuged (5°C) and the plasma transferred to polypropylene tubes, rapidly frozen, and maintained at −80°C until analyzed. Plasma histamine content was determined after treatment with 0.4 N perchloric acid (final concentration). The treated samples were centrifuged for 45 min (5°C) in an Eppendorf microfuge and the supernatant analyzed for histamine content using the Technicon II automated fluorometric technique developed by Siraganian (Siraganian, 1974, 1976).

Radiation was accomplished with a bilateral, whole-body, exposure to γ-ray photons from a cobalt-60 source located at AFRRI. Exposure was limited to a mean of 1.44 min at 73 Gy/min steady state, free-in-air. Dose rate measurements at depth were made with a tissue equivalent ionization chamber placed in a tube running along the midline of a beagle phantom. The measured midline intestinal dose rate was 66 Gy/min, producing a calculated total dose of 100 Gy.

Blood pressure and blood flow data were grouped into 10-min intervals, measured in relation to midtime of radiation, and plotted at the middle of the interval. The Wilcoxon rank sum test was used to analyze statistically the blood pressure, blood flow, hematocrit, and histamine data. A 95% level of confidence was employed to determine significance. Since the preradiation data for the control and test animals showed no significant difference, the preradiation data for the radiated and sham-radiated animals were combined and used as a base line.

RESULTS

To keep variables to a minimum, blood gases and blood pH were maintained at preradiation levels by regulation of the volume and rate of the respirator. Temperature was maintained at the preradiation level by using a circulating water blanket.

Intestinal blood flow (IBF) in the untreated, radiated group increased 100% within 10 min postradiation and then decreased to 24% above baseline level by 60 min postradiation (Fig. 1). A statistically significant difference ($p < 0.05$) exists between this group and the antihistamine-treated group for the first 20 min postradiation. When compared to the sham-radiated or control group, the significant difference lasted until 30 min postradiation. However, there was no significant difference between the antihistamine-treated group and the control, sham-radiated group.

Hematocrits (HCT) of the sham-radiated and untreated, radiated animals exhibited a significant difference at the 95% level of confidence at all three postradiation times of measurement (Fig. 2). The mean HCT noted for the untreated, radiated group was 8.5% higher than that for the control group at the 10-min postradiation measurement. By 60 min postradiation the difference had increased even more, with the untreated, radiated group now showing a HCT 14.5% higher than the control animals. The HCT of radiated animals pretreated with antihistamines was significantly different from the untreated, radiated animals at the 10-min measurement only and was not significantly different from the control animals at any of the three measurements.

Postradiation mean arterial blood pressure (MAP) for the control animals, after an initial decrease, remained stable for the remainder of the experiment (Fig. 3). However, within 10 min postradiation, the untreated, radiated

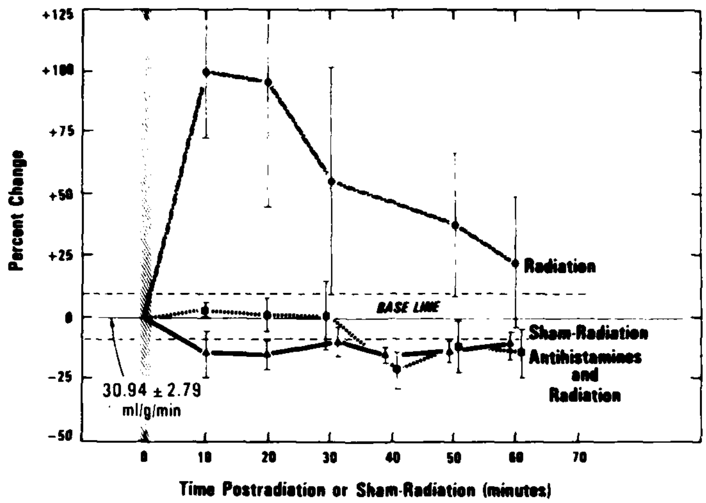

FIG. 1. Percentage change in postradiation intestinal blood flow (±SE) compared to a preradiation mean of 30.94 ± 2.79 ml/g of tissue/min. Animals in the first group were given physiological saline for 60 min before and after sham radiation. The second group also received saline but were exposed to 100 Gy γ radiation. The third group was also exposed to 100 Gy γ radiation but received saline containing antihistamines both before and after radiation.

animals showed an initial increase followed by a steady, rapid decrease in MAP. The drop in pressure reached its lowest point at 60 min postradiation, a level 47% below the preradiation baseline. When the data are examined statistically, a significant difference is noted between the two groups, beginning at 40 min postradiation. The MAP of the pretreated, radiated group did not display the

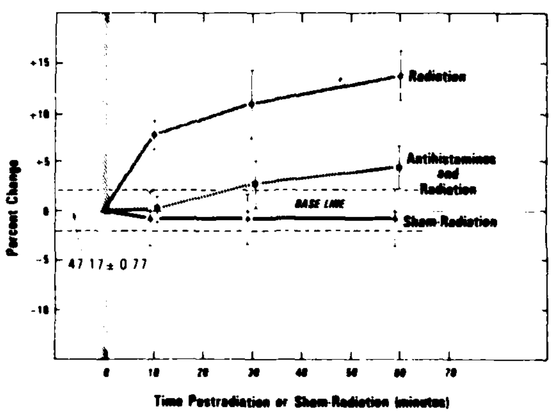

FIG. 2. Percentage change in postradiation hematocrit (±SE) compared to a preradiation mean of 42.17 ± 0.77. Animals in the first group were given physiological saline for 60 min before and after sham radiation. The second group also received saline but were exposed to 100 Gy γ radiation. The third group was alo exposed to 100 Gy γ radiation but received saline containing antihistamines both before and after radiation.

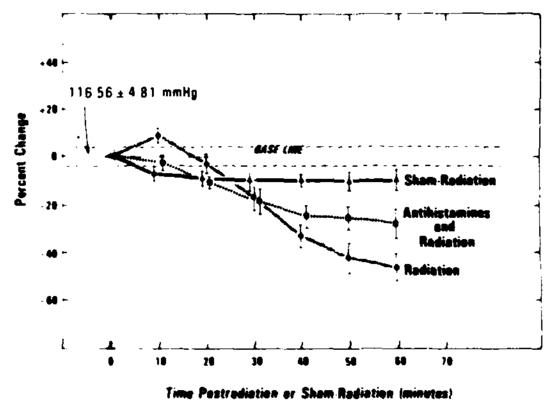

FIG. 3. Percentage change in postradiation mean arterial blood pressure (±SE) compared to a preradiation mean of 116.56 ± 4.81 mm Hg. Animals in the first group were given physiological saline for 60 min before and after sham radiation. The second group also received saline but were exposed to 100 Gy γ radiation. The third group was also exposed to 100 Gy γ radiation but received saline containing antihistamines both before and after radiation.

initial increase seen with the untreated, radiated group, nor did it show the rapid decrease seen with the latter group. In addition, the pretreated, radiated group reached a low MAP level of 28% below the baseline level at 60 min postradiation. However, the only significant difference seen between the pretreated, radiated group and the other two group was at the 50-min postradiation point when it was statistically different from the untreated, radiated group.

When the aortic plasma histamine levels from the three groups were compared, no significant differences were seen at the 95% level of confidence (Fig. 4). However, if Fig. 4 is examined closely at the 4-min postradiation time, a peak in aortic histamine levels may be seen in both radiated groups but not in the control group.

At the 95% level of confidence, the only point at which there was a significant difference between the hepatic portal vein histamine levels of the untreated, radiated group and the control group was at the 4-min postradiation measurement (Fig. 5). The plasma histamine level in the untreated, radiated animals at this point reached a peak that was 20.4% above the baseline level. The antihistamine-pretreated, radiated group displayed a plasma histamine level that climbed to over 19% above baseline at the 60-min measurement, the only point that showed a significant difference from the other groups.

DISCUSSION

Radiation-induced hypotension accompanied by increased intestinal blood flow and hematocrit has been reported previously in the beagle (Cockerham *et al.*, 1984a) and is repeated in this experiment. In addition, this experiment demonstrated changes in these physiological parameters in animals treated with antihistamines both before and after supralethal radiation exposure. This study also shows postradiation variations of histamine levels in animals treated with antihistamines.

Lasser and Stenstrom (1954) showed a 33% increase in blood histamine levels in

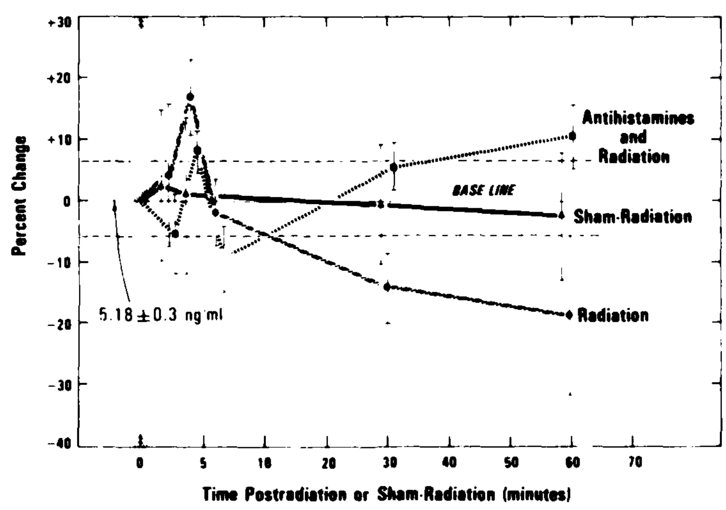

FIG. 4. Percentage change in postradiation aortic plasma histamine concentration (±SE) compared to a preradiation mean of 5.18 ± 0.3 ng/ml. Animals in the first group were given physiological saline for 60 min before and after sham radiation. The second group also received saline but were exposed to 100 Gy γ radiation. The third group was also exposed to 100 Gy γ radiation but received saline containing antihistamines both before and after radiation.

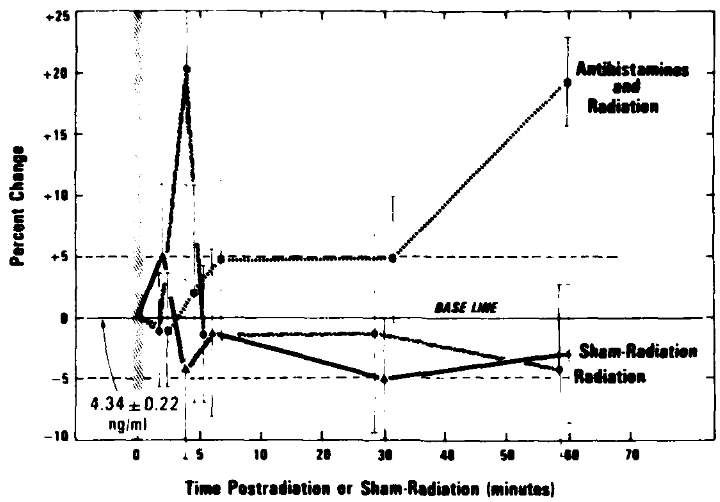

FIG. 5. Percentage change in postradiation hepatic portal vein histamine concentration (±SE) compared to a preradiation mean of 5.34 ± 0.22 ng/ml. Animals in the first group were given physiological saline for 60 min before and after sham radiation. The second group also received saline but were exposed to 100 Gy γ radiation. The third group was also exposed to 100 Gy γ radiation but received saline containing antihistamines both before and after radiation.

patients undergoing deep radiation therapy while Doyle and Strike (1977) showed a 100% increase in plasma histamine levels in monkeys exposed to 40 Gy of mixed neutron–γ radiation. In contrast, one group of investigators (Alter *et al.*, 1983) reported over a 2000% increase in plasma histamine-like activity in monkeys exposed to 40 Gy of γ radiation. The postradiation histamine levels found in this experiment do not corroborate these results reported on subhuman primates even though the peak levels with primates and canines did occur within the first 5 min postradiation. These differences could be attributed to species variations since other radiation effects have been reported to be species specific (Chaput *et al.*, 1972; Miletich and Strike, 1970; Pitchford, 1968).

The postradiation hypotension found in this experiment and in a previous report (Cockerham *et al.*, 1984a) was different from that reported in primates (Alter *et al.*, 1983). The primate report showed a 50% decrease in blood pressure within 2 min postradiation, followed by a partial recovery and a subsequent, gradual hypotensive response. Monkeys pretreated with the histamine receptor antagonists diphenhydramine and cimetidine did not show the immediate decrease in blood pressure seen in untreated monkeys, with the pressure experiencing a gradual decline which temporally coincided with the subsequent hypotensive response of untreated monkeys. The initial hypertension seen in this canine experiment is abolished by antihistamine pretreatment, resulting in a hypotensive response resembling that seen in the antihistamine-treated monkeys. However, the hypotensive response in pretreated canines was only half as great as in untreated canines. The results of this experiment support the hypothesis that histamine, in dogs, is responsible for the immediate increase in systemic blood pressure and only partially involved in the subsequent hypotensive response as contrasted to the monkey where it seems to be involved in only the immediate hypotensive response.

The significant differences seen in hematocrits further suggests the involvement of histamine in postradiation effects since Lee and Silverberg (1976) have shown that infu-

sion of histamine into the small intestine produces a copious secretion of fluid following edema. This loss of fluid from the blood would result in the observed increased postradiation hematocrits. Diminution of the radiation-induced increase in hematocrits by pretreatment with antihistamines strongly supports the hypothesis of histamine involvement.

Lee and Silverberg (1976) have also shown that infusion of histamine into the small intestine causes an increase in intestinal blood flow, and several investigators (Alter *et al.*, 1983; Cockerham *et al.*, 1984b; Doyle and Strike, 1977) have reported a radiation-induced increase in plasma histamine. A previous report (Cockerham *et al.*, 1984a) was the first report known to these authors to show an immediate postradiation increase in intestinal blood flow. Likewise, this experiment is the first known to the authors to abolish that immediate radiation-induced increase in intestinal blood flow through the use of antihistamines. These reports and the results of this experiment support the hypothesis that the radiation-induced histamine release is involved in the immediate increase in intestinal blood flow and that this increase can be prevented through the administration of antihistamines.

The aparent ability of a combination of mepyramine and cimetidine to ameliorate some of the effects of radiation implicate histamine as the chemical mediator at least partially responsible for the postradiation increased intestinal blood flow, hypotension, increased hematocrit, and, ultimately, diarrhea, performance decrement, and incapacitation. Understanding the physiological basis for these radiation effects is essential to providing protection against them and for the treatment of casualties resulting from radiation exposure.

ACKNOWLEDGMENTS

The authors thank E. A. Helgeson for technical assistance and Mrs. M. H. Owens for preparation of the manuscript.

REFERENCES

ALTER, W. A., III, HAWKINS, R. N., CATRAVAS, G. N., DOYLE, T. F., AND TAKENAGA, J. K. (1983). Possible role of histamine in radiation induced hypotension in the rhesus monkey. In *Proceedings, 31st Annual Meeting of the Radiation Research Society, San Antonio, Tex.*

AUKLAND, K., BOWER, B. R., AND BERLINER, R. W. (1964). Measurement of local blood flow with hydrogen gas. *Circ. Res.* **14**, 164–287.

CHAPUT, R. L., KOVACIC, R. T., AND BARRON, E. L. (1972). *Performance of Trained Beagles after Supralethal Doses of Radiation*, Scientific Report SR72-1. Armed Forces Radiobiology Research Institute, Bethesda, Md.

COCKERHAM, L. G., DOYLE, T. F., TRUMBO, R. B., AND NOLD, J. B. (1984a). Acute postradiation canine intestinal blood flow. *Int. J. Radiat. Biol.* **45**(1), 65–72.

COCKERHAM, L. G., DOYLE, T. F., DONLON, M. A., AND HELGESON, E. A. (1984b). Canine postradiation histamine levels and subsequent response to compound 48/80. *Aviat. Space Environ. Med.* **55**(11), 1041–1045.

DOBBINS, D. E., SWINDALL, B. T., HADDY, F. J., AND DABNEY, J. M. (1981). Blockade of histamine-mediated increases in microvascular permeability by H_1- and H_2-receptor antagonists. *Microvasc. Res.* **21**, 343–350.

DOUGLAS, W. W. (1975). Histamines and antihistamines: 5-Hydroxytryptamine and antagonists. In *The Pharmacological Basis of Therapeutics* (L. S. Goodman and A. Gilman, eds.), 5th ed. Macmillan, New York.

DOYLE, T. F., AND STRIKE, T. A. (1977). Radiation-released histamine in the rhesus monkey as modified by mast-cell depletion and antihistamine. *Sep. Experientia* **33**, 1047–1048.

EISEN, V. D., AND WILSON, C. W. M. (1957). The effect of β-irradiation on skin histamine and vascular responses in the rat. *J. Physiol.* **136**, 122–130.

GRANGER, D. N., RICHARDSON, P. D. I., KVIETYS, P. R., AND MORTILLARO, N. A. (1980). Intestinal blood flow. *Gastroenterology* **78**, 837–863.

HYMAN, E. S. (1961). Linear system for quantitating hydrogen at a platinum electrode. *Circ. Res.* **9**, 1093–1097.

LASSER, E. C., AND STENSTROM, K. W. (1954). Elevation of circulating blood histamine in patients undergoing deep roentgen therapy. *Amer. J. Roentgenol.* **72**, 985–988.

LEE, J. S., AND SILVERBERG, J. W. (1976). Effect of histamine on intestinal fluid secretion in the dog. *Amer. J. Physiol.* **231**, 793–798.

MARTINS, A. N., KOBRINE, A. I., DOYLE, T. F., AND RAMIREZ, A. (1974). Total cerebral blood flow in the monkey measured by hydrogen clearance. *Stroke* **5**, 512–517.

MEINERS, D. J., DESHPANDE, Y. G., AND KAMINSKI, D. L. (1982). The role of histamine in control of gastric mucosal blood flow in dogs. *J. Surg. Res.* **32**, 608–616.

METCALFE, D. D., KALINER, M., AND DONLON, M. A. (1981). The mast cell. In *CRC Critical Reviews in Immunology* (M. Z. Atassi, ed.). CRC Press, Boca Raton, Fla.

MILETICH, D. J., AND STRIKE, T. A. (1970). *Alteration of Postirradiation Hypotension and Incapacitation in the Monkey by Administration of Vasopressor Drugs.* Scientific Report SR70-1. Armed Forces Radiobiology Research Institute, Bethesda, Md.

PITCHFORD, T. L. (1968). *The Acute Mortality Response of Beagles to Pulsed, Mixed Gamma-Neutron Radiations.* Scientific Report SR68-15. Armed Forces Radiobiology Research Institute, Bethesda, Md.

POWELL, J. R., AND BRODY, M. J. (1976). Identification and blockade of vascular H_2 receptors. *Fed. Proc.* **35**(8), 1935–1941.

REINHARDT, D., WALKENHORST, R., AND ARNOLD, G. (1980). Identification of histamine H_1- and H_2-receptors by means of mepyramine, cimetidine and theophylline in the cardiovascular system of the dog. *Agents Actions* **10**(1/2), 152–156.

SHEHADEH, Z., PRICE, W. E., AND JACOBSON, E. D. (1969). Effects of vasoactive agents on intestinal blood flow and motility in the dog. *Amer. J. Physiol.* **216**, 386–392.

SIRAGANIAN, R. P. (1974). An automated continuous-flow system fr the extraction and fluorometric analysis of histamine. *Anal. Biochem.* **57**, 383–394.

SIRAGANIAN, R. P. (1976). Histamine release and assay methods for the study of human allergy. In *Manual of Clinical Immunology* (N. R. Rose and H. Friedman, eds.). Amer. Soc. Microbiol., Washington, D.C.

TIMMERMANS, R., AND GERBER, G. B. (1980). Reaction of blood pressure and mesenteric blood flow to infusion of biogenic amines in normal and supralethally X-irradiated rats. *Radiat. Res.* **82**, 81–92.

YOUNG, W. (1980). H_2 clearance measurement of blood flow: A review of technique and polarographic principles. *Stroke* **11**, 552–564.

INT. J. RADIAT. BIOL., 1985, VOL. 47, NO. 2, 205–212

WR-2721 inhibition of radiation-induced prostaglandin excretion in rats

M. DONLON, L. STEEL, E. A. HELGESON, W. W. WOLFE and G. N. CATRAVAS

Biochemistry Department, Armed Forces Radiobiology Research Institute, Bethesda, Maryland 20814, U.S.A.

(Received 6 March 1984; revision received 20 August 1984; accepted 29 August 1984)

Pre-irradiation administration of the radioprotectant drug WR-2721 to rats resulted in a significant reduction in radiation-induced increases in excretion rates of prostaglandins (PGE and $PGF_{2\alpha}$) and thromboxane (TxB_2). In animals not irradiated, WR-2721 did not significantly alter these excretion rates. Dramatic reductions in the levels of urinary PGE and TxB_2 were observed following exposure to 9·0 Gy of whole-body, unilateral γ-radiation in WR-2721-treated animals, whereas changes in $PGF_{2\alpha}$ levels were less pronounced. Radiation-induced diuresis was also significantly depressed in animals given WR-2721 before irradiation. Reduced prostaglandin excretion rates may reflect the general radioprotective capacity of the chemoprotector WR-2721 on the release of prostaglandins from radiation-damaged tissue. The decrease in diuresis may be related to the observed prostaglandin decreases.

Indexing terms: prostaglandins, WR-2721, radioprotection.

1. Introduction

Exposure to ionizing radiation can initiate the production and/or release of potent biochemicals within specific organs, tissues or cell types, resulting in a wide range of harmful effects (Altman *et al.* 1970). One such class of biologically active agents is the prostaglandins. The biosynthesis of prostaglandins from their fatty acid precursors, arachidonic acid and dihomo-γ-linoleic acid, can be stimulated by either specific cell surface membrane receptors or non-specific cell injury. In experimental animals, ionizing radiation has been shown to produce changes in the levels of prostaglandins in a variety of tissues. Significant increases in PGE, $PGF_{2\alpha}$ and TxB_2 levels were observed within 1–3 h in guinea pig lung tissue following 3·0 Gy whole-body γ-radiation (Steel and Catravas 1982). Transient increases were reported in rat liver and spleen at 3–6 h after exposure to 10·0 Gy γ-radiation (Trocha and Catravas 1980). Significant increases in PGI_2 formation in the irradiated rabbit abdominal aorta have also been reported (Sinzinger *et al.* 1982). Mouse liver and spleen were similarly affected following exposure to 9·0 Gy γ-radiation (Pyranishnikova *et al.* 1978). Eisen and Walker (1976) demonstrated prostaglandin changes in the lung and spleen of X-irradiated (7·0 Gy) mice. These data strongly suggest significant early alterations in prostaglandin levels resulting from exposure to moderate doses of radiation. While the precise role of prostaglandins in the biological response to ionizing radiation has not been fully explained, these changes may be related to subsequent pathophysiological responses (Mennie *et al.* 1975).

Various chemicals have been explored as protectants against the harmful action of ionizing radiation. Chemical radioprotection of normal tissues was first demonstrated with cysteine as a sulphydryl donor in rats and mice (Patt *et al.* 1949). Since then, a series of radioprotectants, analogues of cysteamine, have been synthesized. Of these drugs, WR-2721 has emerged as one of the most effective (Yuhas and Phillips 1983). WR-2721 is an organic thiophosphate [*S*-2-(3-aminopropylamino)-ethyl phosphorothioic acid] that in irradiated mice improves bone marrow tolerance by a factor of 1·3–3·0 (Denekamp *et al.* 1983), lung and kidney tolerance by 1·3, and skin clone tolerance by 2·2 (Denekamp *et al.* 1982). In addition, since this radioprotectant drug is more readily absorbed by normal tissues than by solid tumour cells (Washbrun *et al.* 1974), under certain circumstances WR-2721 may provide selective protection of normal human tissues against the toxicity of radiation therapy. Although the precise mechanism of action of this drug has not yet been defined *in vivo*, a protective mechanism proposed by Eldjarn *et al.* (1956) is related to the protection by WR-2721 of cellular proteins from radiation-induced free radicals produced in the tissues.

It has been previously reported that whole-body irradiation results in elevations in urinary levels of $PGF_{2\alpha}$, PGE and TxB_2 (Donlon *et al.* 1983) and PGI (Schneidkraut *et al.* 1983). This suggests the potential use of these eicosanoids as indicators of radiation damage. In this study, we have examined the prostaglandin and thromboxane excretion rates in rat urine following 1·0 and 9·0 Gy whole-body, unilateral γ-radiation with and without the prior administration of WR-2721 in order to assess the efficacy of WR-2721 in eliminating radiation-induced increases in excretion rates.

2. Materials and methods

Male Sprague Dawley rats (Taconic Farms Inc., Germantown MD) were maintained in individual lucite metabolic cages for a period of 7 days in order to acclimatize them to their new environment before initiating urine collection. The animals were fed once daily with a standard rat diet (Wayne Lab Blox, Continental Grain Co., Chicago IL) prepared in the form of hydrated food balls (20–30 g wet weight) and were allowed water *ad libitum*. Twenty-four hours before the first urine collection, a preservative of 50 μl of 10 N HCl was added to the collection vessel. The urine was collected at 24 h intervals and the volume recorded for 3 days (−48 h, −24 h and 0 h) before radiation exposure. The collection intervals represented are −72 h to −48 h, −48 h to −24 h and −24 h to 0 h. The third control sample (−24 h to 0 h) was taken just before irradiation; thus the zero time point represents both the endpoint of the collection interval and the time of irradiation. Immediately after collection, 475 μl aliquots of urine were added to 25 μl perchloric acid (PCA) (final concentration 0·04 N PCA), mixed immediately and stored at −90°C for subsequent analysis. All urine samples, pre- and post-irradiation, were treated in an identical manner.

The drug-treated animals received WR-2721 (200 mg/kg) intraperitoneally, 20–30 min before irradiation. This dose represents two-thirds of the toxic LD_{50} in rats. The drug (NSC 296961-R) received from the National Cancer Institute (Drug Synthesis and Chemistry Branch, Division of Cancer Treatment) was dissolved as 100 mg/ml of Hanks' Balanced Salt Solution, pH 7·2, immediately before injection. Control animals received Hanks' solution only.

On the day of irradiation, both drug-treated and non-treated animals were placed in individual lucite boxes and were unilaterally irradiated in groups of 10 with 1·0 or 9·0 Gy of γ-radiation derived from a Theratron 80 ^{60}Co source (1·17 and 1·33 MeV gamma). The dose rate was 0·402–0·410 Gy/min with a tissue/air ratio of 0·89 and a target distance of 112–115 cm. A wax phantom with an ion chamber placed at midline was used to determine absorbed dose.

Following irradiation, the animals were returned to the metabolic cages and the amount of HCl added to the collection vessel was varied from 5 to 50 μl to compensate for the expected changes in urine volume depending on the collection time interval. (Prior experience in this laboratory with radiation-induced increases in volume allowed for a reasonable estimate of post-irradiation urine volume.) Post-irradiation collections were made and urine volume measured at the end of the following time intervals: 0–1 h, 1–3 h and 3–6 h for animals that received 1·0 Gy exposure, 0–6 h and 6–12 h for those that received 9·0 Gy and thereafter at 12 h intervals for both exposure doses. Experiments were terminated at 4 days (1·0 Gy) and 5 days (9·0 Gy).

On the day of analysis, the samples were thawed and the PCA-precipitated protein was removed by centrifugation (13 000 **g**) at 4°C for 15 min. The supernatants were assayed for prostaglandins and thromboxane by radioimmunoassay as previously described (Donlon *et al.* 1983). The specificity of the antisera employed in the radioimmunoassay for prostaglandins was characterized, and the ratio of PG concentration to the cross-reacting substance concentration at 50 per cent inhibition of maximum binding was determined. TxB_2 antiserum demonstrated less than 2 per cent cross-reactivity with other prostaglandins ($PGF_{2\alpha}$, PGE_1, PGD_2 and 6-keto $PGF_{1\alpha}$). Specificity of the commercially prepared antiserum to $PGF_{2\alpha}$ demonstrated only minor cross-reactivity with 6-keto $PGF_{1\alpha}$ (< 12 per cent), whereas anti-PGE_2 did not distinguish between PGE_1 and PGE_2 (0·1–2·0 per cent cross-reactivity with $PGF_{2\alpha}$, PGD_2, 6-keto $PGF_{1\alpha}$ and TxB_2). Therefore, the data are expressed as PGE to indicate the cross-reactivity of anti-PGE_2 with PGE_1.

2.1. *Statistical analysis and data presentation*

Experimental data from each animal at each collection time were recorded as urinary prostaglandin concentration (pg/ml) and urinary excretion rate (ml/h). Prostaglandin levels were subsequently converted to pg/h. These values, rate of prostaglandin accumulation and rate of urinary output were determined for all sampling intervals pre- and post-irradiation.

Each animal served as its own control for conversion of the raw data to a percentage value. For each animal, the three 24 h preirradiation values were averaged for prostaglandins and urine volume, and this value was defined as the mean control for that animal. Each pre- and post-irradiation value was then expressed as a percentage of its mean control value. By using this conversion, animal to animal variation was reduced.

The prostaglandin data presented are geometric means ($n = 10$) expressed as the per cent of mean control values. The distribution of the PG excretion data was determined to be log normal; thus, the percentage values calculated for individual animals were log transformed for statistical analysis. Student's t test for unpaired samples was applied to the log transformed data to determine the significance between post-irradiation values of prostaglandin levels from WR-2721-treated

animals compared to levels in non-treated animals. A Behrens–Fisher test replaced the t test for those comparisons in which variation between treatments was not homogeneous (Snedecor and Cochran 1980). The antilog of each geometric mean was then calculated for graphic presentation.

Urine volume is expressed as the arithmetic mean of individual percentage values; no data transformations were necessary. Treatment comparisons were made as indicated above.

In figures 1–3 the data are shown as the geometric mean plus and minus one standard error of the mean (s.e.m.). The error bars in these figures were calculated using these formulae: [antilog (X + s.e.m.)] and [antilog (X − s.e.m.)], where X and s.e.m. represent the mean and standard error of the log-transformed data. Figure 4 shows the arithmetic mean plus and minus one standard error. To simplify graphic presentation of the data, the time noted on the figures represents the end of the time interval of collection; i.e. 0–1 (1 h), 1–3 (3 h), etc.

3. Results

Patterns of PGE excretion following whole-body γ-radiation (1·0 and 9·0 Gy) with and without prior administration of WR-2721 are shown in figure 1. Highly significant ($P < 0{\cdot}01$) differences in urinary PGE levels were observed between the drug-treated and non-treated rats at 3, 6 and 12 h following 1·0 Gy, whereas reduced significance ($P < 0{\cdot}05$) was observed at 36 and 60 h. These differences were transient and PGE levels in the urine did not differ significantly at 24 h post-irradiation from

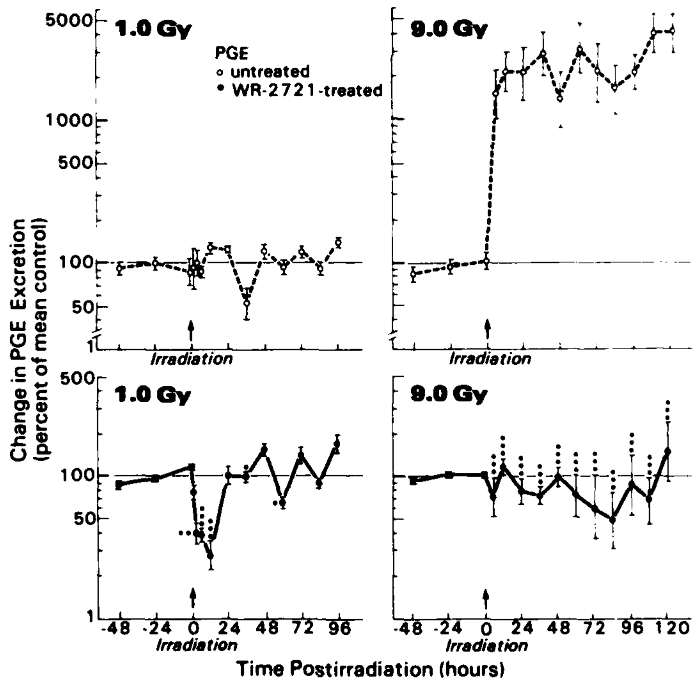

Figure 1. Effect of WR-2721 on urinary levels of PGE following γ-radiation. Values represent the geometric means ($n = 10$) in pre- and post-irradiated urine samples (see text). Error bars express the geometric mean ± s.e.m. * $= 0{\cdot}05 > P > 0{\cdot}01$; ** $= 0{\cdot}01 > P > 0{\cdot}001$; *** $= 0{\cdot}001 > P$. The range of control values for PGE (pg/ml) were: untreated, 39·0–3719·3, and WR-2721 treated, 387·4–8929·6.

those for animals not injected with WR-2721. Approximately 20-fold increases in excretion rates of urinary PGE were detected in non-treated animals following exposure to 9·0 Gy. These increases persisted for the duration of the experiment (5 days). These dramatic increases were inhibited by injection of WR-2721 before irradiation.

Alterations in excretion rates of urinary $PGF_{2\alpha}$ with and without prior administration of WR-2721 are shown in figure 2. 'Significant' reduction of $PGF_{2\alpha}$ was observed in animals treated with WR-2721 at 3 and 96 h post-irradiation (1·0 Gy) and at 36, 72 and 84 h following 9·0 Gy. While 'statistically significant' differences were found at isolated points where between-group variation was minimal, WR-2721 did not appear to appreciably affect excretion levels of $PGF_{2\alpha}$.

Urinary thromboxane excretion following a single exposure to γ-radiation (1·0 Gy) was significantly reduced at 6 and 84 h in animals that received WR-2721 before whole-body irradiation (figure 3). Inhibition of radiation-induced increases were observed in pre-treated animals that received 9·0 Gy of γ-radiation, detectable at 6 h post-exposure, and persisting for the duration of the experiment (120 h).

Changes in urine volume following 1·0 and 9·0 Gy radiation exposure, with and without prior WR-2721 treatment, are shown in figure 4. A significant reduction in urine volume was observed at 3, 36, 48, 60 and 84 h (1·0 Gy) with prior drug treatment. Urine volume was also reduced by WR-2721 pre-treatment following 9·0 Gy at 6, 12 and 24 h; no significant differences in urine volume were detected between treated and non-treated groups in all subsequent collection intervals.

In WR-2721 treated, non-irradiated animals ($n = 7$), no significant alterations in either prostaglandin and thromboxane excretion levels or urine volume were detected.

4. Discussion

The present study demonstrates that injection of WR-2721 before irradiation reduces (*a*) increased urinary excretion rates of $PGF_{2\alpha}$, PGE and TxB_2 after

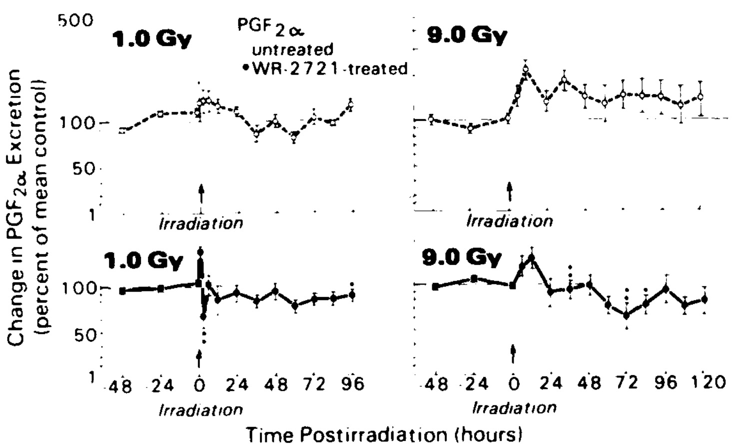

Figure 2. Effect of WR-2721 on urinary levels of $PGF_{2\alpha}$ following γ-radiation. Values represent the geometric means ($n = 10$) in pre- and post-irradiated urine samples (see text). Error bars express the geometric mean ± s.e.m. * = $0·05 > p > 0·01$; ** = $0·01 > p > 0·001$. The range of control values for $PGF_{2\alpha}$ (pg ml) were: untreated, 63·0 2472·5, and WR-2721 treated, 1213·0 6218·7.

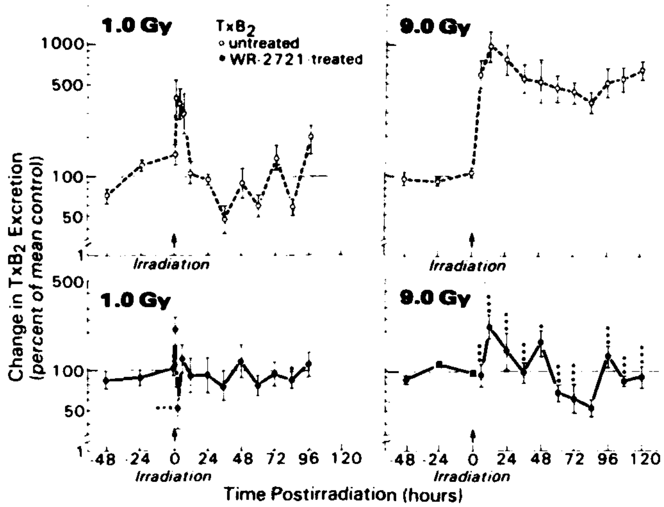

Figure 3. Effect of WR-2721 on urinary levels of TxB_2 following gamma radiation. Values represent the geometric means ($n=10$) in pre- and post-irradiated urine samples (see text). Error bars express the geometric mean ± s.e.m. * = 0·05 > P > 0·01; ** = 0·01 > P > 0·001; *** = 0·001 > P. The range of control values for TxB_2 (pg/ml) were: untreated, 10·0–4425·0, and WR-2721 treated, 656·6–5175·0.

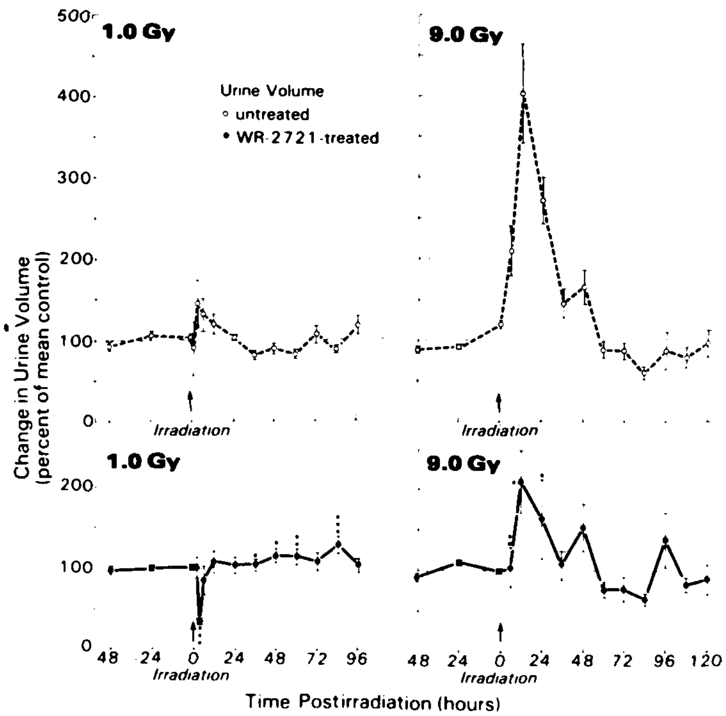

Figure 4. Changes in urine volume following γ-radiation. Values represent the arithmetic means ($n=10$) pre- and post-irradiation. Error bars express the mean ± s.e.m. * = 0·05 > P > 0·01; ** = 0·01 > P > 0·001; *** = 0·001 > P.

irradiation, and (*b*) radiation-induced diuresis. The effect on prostaglandin excretion in the irradiated animal may be the result of specific effects of WR-2721 on kidney prostaglandin production, the generalized effect on prostaglandin metabolism, or a combination of both. The decreased diuresis may reflect either a diminished supply of prostaglandin to the kidney or a decreased synthesis of kidney prostaglandins.

In the non-irradiated animal, the lung is the major site for the catabolism of circulating prostaglandins (Piper *et al.* 1970). Ferreira and Vane (1967) first demonstrated that up to 95 per cent of PGE_1, PGE_2 and $PGF_{2\alpha}$ was removed in one passage through the pulmonary circulation. This observation was subsequently confirmed in a variety of experimental animals (McGiff *et al.* 1969, Horton and Jones 1969). In the irradiated animal, however, the lung generates substantial quantities of prostaglandin (Steel and Catravas 1982). As a result, circulating levels of prostaglandins in the irradiated animal may exceed and/or impair the lung's capacity for clearance, thereby causing increased levels to remain in the blood stream. Rats secrete albumin into their urine and the degree of albuminuria is dependent on age (Berg 1965). Prostaglandins are known to bind to serum proteins, primarily albumin (Raz 1972). In the irradiated animal, increased diuresis, accompanied by significant increases in proteinuria as early as 1 h following 9·0 Gy whole-body γ-radiation may partially account for the observed elevated prostaglandin levels (Amende *et al.* 1982). Prostaglandins bound to circulating albumin may pass through the radiation-altered glomerulus and also may contribute to increased urinary prostaglandin levels.

Considerable evidence supports the concept that in the non-irradiated animal the kidney may be the main source of prostaglandins and their metabolites that appear in the urine (Frölich *et al.* 1975, Gulner *et al.* 1980). Furthermore, prostaglandin administered through the renal artery results in biochemical and functional alterations within the kidney tubule. Most pronounced is the diuretic effect of PGE, which is thought to affect volume regulation by counteracting vasopressin action (Omachi *et al.* 1974).

Increased urine volume in the irradiated animal is transient (figure 4). In this study, peak increases after 9·0 Gy were observed at 12 h and returned to control levels by 36 h. However, the PGE excretion rates after 9·0 Gy (figure 1) continue for the duration of the experiment. If the increases of PGE are related to the increases in urine volume induced by radiation, it is necessary to postulate that the cellular components of the kidney tissue become refractory to these high levels of PGE following radiation, thus resulting in a return of the urine volume to pre-irradiation levels.

The observed increases in urine prostaglandin excretion may arise from the loss of the normal integrity of clearance mechanisms and/or from increased prostaglandin production in the kidney. The inhibition of the urine prostaglandin excretion rates by WR-2721 in the irradiated animal suggests that the radioprotectant may act at either of these levels.

The decreased radiation-induced excretion of prostaglandin and the diuresis caused by prior administration of WR-2721 may also be the result of the protective effect of WR-2721 on a variety of tissues other than kidney (Yuhas *et al.* 1980). WR-2721 inhibition of cellular destruction resulting from whole-body irradiation, in the skin and/or bone marrow for example, may reduce prostaglandin release or decrease the release of mediators which may affect diuresis secondarily.

Although precise definition of the origin of urinary prostaglandin and thromboxane is limited in this study, little doubt exists that the radioprotectant WR-2721

profoundly affects the excretion patterns of PGE and TxB_2, but minimally affects the excretion of $PGF_{2\alpha}$ in the whole-body irradiated animal. Additional studies are in progress to examine the metabolism of prostaglandins in the irradiated kidney.

Acknowledgments

Supported by the Armed Forces Radiobiology Research Institute, Defense Nuclear Agency, under Research Work Unit MJ00068 and MJ00064. The views presented in this paper are those of the authors; no endorsement by the Defense Nuclear Agency has been given or should be inferred. The authors gratefully acknowledge Allan Shipp for his help with the various assays used in the study, William E. Jackson for his advice concerning the statistical analysis of our data and Dr John Christopher for discussing and proofreading several drafts of this paper.

References

ALTMAN, K. I., GERBER, G. B., and OKADA, S., 1970, *Radiation Biochemistry*, Vol. II: *Tissues and Body Fluids* (New York, London: Academic Press).
AMENDE, L. M., KELLEHER, D. L., and DONLON, M. A., 1983, *Fedn. Proc.*, **42,** 1124.
BERT, B. N., 1956, *Proc. Soc. expl. Biol. Med.*, **119,** 417.
DENEKAMP, J., MICHAEL, B. D., ROJAS, A., and STEWART, F. A., 1982, *Int. J. Radiat. Oncol. Biol. Phys.*, **8,** 531.
DENEKAMP, J., ROJAS, A., and STEWART, F. A., 1983, *Radioprotectors and Anticarcinogens*, edited by O. F. Nygaard and M. G. Simic (New York, London: Academic Press), p. 655.
DONLON, M., STEEL, L., HELGESON, E. A., SHIPP, A., and CATRAVAS, G. N., 1983, *Life Sci.*, **32,** 2631.
EISEN, V., and WALKER, D. I., 1976, *Br. J. Pharmac.*, **57,** 527.
ELDJARN, L., and PIHL, A., 1956, *J. biol. Chem.*, **224,** 341.
FERREIRA, S. H., and VANE, J. R., 1967, *Nature, Lond.*, **216,** 868.
FROLICH, J. C., WILSON, T. W., SWEETMAN, B. J., SMIGEL, M., NIES, A. S., CARR, K., THROCK-WATSON, J., and OATES, J. A., 1975, *J. clin. Invest.*, **55,** 763.
GULLNER, H.-G., SMITH, J. B., and BARTTER, F. C., 1980, *Adv. Prostaglandin Thromboxane Res.*, **7,** 1185.
HORTON, E. W., and JONES, R. L., 1969, *Br. J. Pharmac.*, **37,** 705.
MCGIFF, J. C., TERRAGNO, N. A., STRAND, J. C., LEE, J. B., LONGIGRO, A. J., and NG, K. K. F., 1969, *Nature, Lond.*, **223,** 742.
MENNIE, A. T., DALLEY, V. M., DINNEEN, L. C., and COLLIER, H. O. J., 1975, *Lancet*, **2,** 942.
OMACHI, R., ROBBIE, D., and HANDLER, J., 1974, *Am. J. Physiol.*, **226,** 1152.
PATT, H. M., TYREE, E. B., and STRAUBE, R. L., 1949, *Science, N.Y.*, **110,** 213.
PIPER, P. J., VANE, J. R., and WYLLIE, J. H., 1970, *Nature, Lond.*, **225,** 600.
PYRANISHNIKOVA, E. N., ZHULANOVA, Z. I., and ROMANTSEV, E. F., 1978, *Radiobiologiya*, **18,** 124.
RAZ, A., 1972, *Biochem. J.*, **130,** 631.
SCHNEIDKRAUT, M. J., KOT, P. A., RAMWELL, P. W., and ROSE, J. C., 1983, *Adv. Prostaglandin Thromboxane Leukotriene Res.*, **12,** 107.
SINZINGER, H. FIRBAS, W., and CROMWELL, M., 1982, *Prostaglandins*, **24,** 323.
SNEDECOR, G. W., and COCHRAN, W. G., 1980, *Statistical Methods* (Ames, Iowa: Iowa State University Press), p. 96.
STEEL, L. K., and CATRAVAS, G. N., 1982, *Int. J. Radiat. Biol.*, **42,** 517.
TROCHA, P. J., and CATRAVAS, G. N., 1980, *Int. J. Radiat. Biol.*, **38,** 503.
WASHBURN, L. C., HAYES, R. L., YUHAS J. M., and CARLSON, J., 1974, *Radiat. Res.*, **59,** 475.
YUHAS, J. M., and PHILLIPS, T. L., 1983, *Radioprotectors and Anticarcinogens*, edited by O. F. Nygaard and M. G. Simic (New York, London: Academic Press), p. 639.
YUHAS, J. M., SPELLMAN, J. M., and CULO, F., 1980, *Cancer Clin. Trials*, **3,** 211.

RADIATION RESEARCH **101**, 434–441 (1985)

Effects of Mixed Neutron-γ Total-Body Irradiation on Physical Activity Performance of Rhesus Monkeys[1]

CAROL G. FRANZ

Behavioral Sciences Department, Armed Forces Radiobiology Research Institute, Bethesda, Maryland 20814

FRANZ, C. G. Effects of Mixed Neutron-γ Total-Body Irradiation on Physical Activity Performance of Rhesus Monkeys. *Radiat. Res.* **101**, 434–441 (1985).

Behavioral incapacitation for a physical activity task and its relationship to emesis and survival time following exposure to ionizing radiation were evaluated in 39 male rhesus monkeys (*Macaca mulatta*). Subjects were trained to perform a shock avoidance activity task for 6 hr on a 10-min work/5-min rest schedule in a nonmotorized physical activity wheel. Following stabilization of performance, each subject received a single, pulsed dose of mixed neutron-γ, whole-body radiation ($n/\gamma = 3.0$) ranging between 1274 and 4862 rad. Performance testing was started 45 sec after exposure. A dose-response function for early transient incapacitation (ETI) during the first 2 hr after irradiation was fitted, and the median effective dose (ED_{50}) was calculated to be 1982 rad. More subjects experienced both incapacitation and emesis in this study than has been reported for other behavioral tasks in similar radiation fields. Analysis done on the relationship of dose to ETI, emesis, and survival time found (a) a significant relationship between the radiation dose and the number and duration of ETIs; (b) no correlation between emesis and dose, survival time, or ETI; (c) no relation between survival time and ETI at any dose; and (d) no significant difference in survival time for dose groups between 1766 ± 9 (SEM) and 2308 ± 23 rad.

INTRODUCTION

Behavioral incapacitation following high doses of ionizing radiation has been observed in several animal species performing a variety of learned tasks. Miniature swine exhibit transient periods of inability to traverse a two-chamber shuttlebox almost immediately after receiving doses greater than 2400 rad of mixed neutron-γ radiation (*1*). Rats trained to a shock-avoidance jump box (*2, 3*) or a swimming task (*4*) were temporarily incapacitated immediately after mixed fission spectra irradiation. Thorp and Young (*5*) and Turbyfill *et al.* (*6*) reported incapacitations in monkeys performing a visual discrimination task, and similar effects were observed for the delayed match-to-sample task (*7*) and primate equilibrium platform task (*8*).

Most animal species tested showed two distinct phases of behavioral incapacitation

[1] Research was conducted according to the principles enunciated in the *Guide for the Care and Use of Laboratory Animals* prepared by the Institute of Laboratory Animal Resources, National Research Council. Supported by the Armed Forces Radiobiology Research Institute, Defense Nuclear Agency under research Work Unit MH 20201. The views presented in this paper are those of the author; no endorsement by the Defense Nuclear Agency has been given or should be inferred.

0033-7587/85 $3.00

in response to supralethal doses of ionizing radiation. In monkeys, for example, the first phase, early transient incapacitation (ETI), begins within 3–8 min after irradiation. It usually lasts approximately 5–20 min and is followed by recovery to a level approximating the preirradiation performance.

Occasionally, subjects have other ETIs within the first 2 hr after irradiation. Seigneur and Brennan (*9*) differentiated these ETIs from permanent complete incapacitation (PCI). PCI occurs shortly before death and is characterized by total cessation of performance and increasing physical debility, terminating in death.

Several studies investigating primate behavior following exposure to mixed neutron–γ radiations have used subjects confined to restraint chairs and trained to perform a learned task requiring little physical movement (*5–8, 10*). Three studies at this laboratory evaluating the effects of ionizing radiation on the performance of unrestrained subjects showed that performance on a task requiring greater physical activity (traversing a chamber) was more severely degraded after irradiation (*11–13*). Another experiment in which locomotor activity was a separate task also showed that performance of the more physically demanding task was more severely affected (*14*).

Although data suggest that the performance of a physical activity task is affected more by ionizing radiation than is a cognitive task, previous studies in primates have neither specifically tested for locomotor ETI immediately after irradiation nor established a dose–response relationship for this phenomenon. This study was designed to establish a dose–response curve and ED_{50} for ETI in a physical activity wheel (PAW) and to define the relationship of incapacitation to death and emesis.

MATERIALS AND METHODS

Subjects. Thirty-nine naive male rhesus monkeys (*Macaca mulatta*) were used. Subjects were individually housed in stainless-steel cages in a restricted access primate colony with a 12/12-hr light/dark cycle. Mean age was 44.9 ± 1.7 (SEM) months (range 26 to 72 months), and mean weight was 5.5 ± 0.2 kg (range 3.0 to 7.1 kg). Subjects were maintained on Purina monkey chow and fruit; water was available *ad libitum.* Subjects were not fed for 14 hr prior to irradiation.

Apparatus. Training and testing were done in a nonmotorized activity wheel consisting of a 24-in.-wide, 4-ft-diameter cylindrical treadmill that rotated freely on four ball bearings between two $\frac{5}{8}$-in. Plexiglas walls (Fig. 1).

The wheel was constructed of $\frac{1}{2}$-in. Plexiglas and $\frac{3}{8}$-in.-diameter aluminum bars (*15*). A $\frac{1}{2}$-pound pull on the tangent was sufficient to initiate wheel rotation. A microswitch recorded the number of wheel rotations and a tachometer measured the speed in miles per hour (mph). One mile per hour equals 7.3 RPM. The 120 aluminum bars that created the running surface were connected to a constant-current shock generator. A motor-driven brake was used to stop the wheel for rest periods and to reduce excessive speed.

Mounted on the support wall opposite the entrance door were two visual displays for presentation of color cues, and a $2\frac{1}{4}$-in., 3.2-ohm speaker for presentation of auditory cues consisting of a high-frequency tone interrupted by a pulse generator to vary the number of beats per minute (bpm). A Plexiglas restraint box used to transport the subjects was mounted against the door. When the door was remotely opened, it allowed subjects to enter the wheel. A shock grid on the floor of the box ensured that the subjects left the box and also prevented them from reentering.

Performance measure. Performance was controlled by a shock-motivated, free-operant reinforcement schedule (*16*) with visual and auditory cues (Table I). Subjects could indefinitely avoid a 5-mA shock by rotating the wheel at or above 1 mph. After incapacitation had been established by 1 min of 0-mph performance, shock frequency was changed to one per minute until recovery occurred. To ensure that this did not lead to extended periods of inactivity shock intensity was increased to 10 mA. The 3 mph safe zone represents a smooth, natural four-beat gait for monkeys of the size range used in this study.

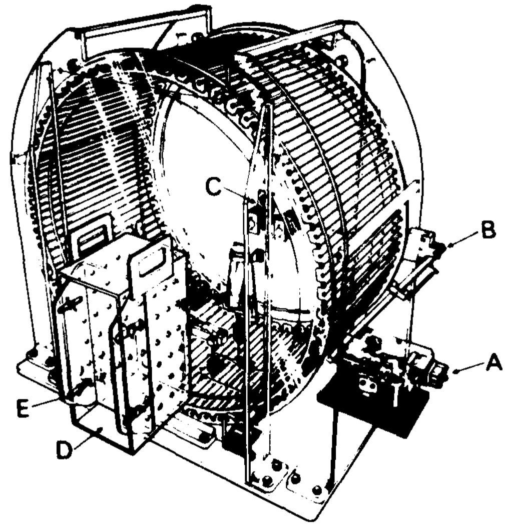

FIG. 1. Monkey physical activity wheel with restraint box. Components include (A) electronic connector for shock scrambler and generator, (B) motor-driven brake, (C) digital lights and speaker, (D) monkey restraint and exposure box, and (E) tachometer.

Since preliminary work indicated that subjects might be injured at excessive speeds, the brake automatically increased the drag on the wheel to reduce the speed if the subject exceeded 5 mph. Thirty seconds before the start of a work period, the wheel brake was gradually released, and the 90-bpm tone and green light were turned on to indicate the beginning of a 10-min performance period. Rotation rate and the number of revolutions were recorded on a strip chart. The shock was disabled until the brake was completely off. During rest periods the brake held the wheel in a fixed position, and there were no auditory or visual cues.

Subjects were trained for at least 9 weeks (2 hr per day, 5 days per week) until the work/rest regimen could be maintained for 6 continuous hr. Performance was measured as the mean running speed for each 10-min work period. When performance did not vary more than ±20% across the 6 hr, the subjects were sham-irradiated, performing for 2 hr in the radiation exposure room. The normal training schedule was resumed for 5 days after sham irradiation. On the radiation day, the subjects were transported to the exposure room and given a 10-min pretest. If the pretest performance was ±20% of that achieved during

TABLE I

Task Control Parameters

	mph	*Tone (bpm)*	*Lights*	*Shock*
Shock zone	0–1	90	green	0.4-sec 5-mA pulse every 1.3 sec[a]
Shock avoidance danger zone	1–3	90	green	none
Shock avoidance safe zone	3–5	60	white	none
Overspeed zone	5 and up	30	red	none[b]

[a] 0.4-sec 10-mA pulse once every minute during incapacitation.

[b] Brake moves to on position.

the first 10 min of the sham irradiation, the subjects were placed in the box and irradiated. If the subject failed the pretest, training was resumed for an additional 8 days before a second sham irradiation.

After radiation exposure, subjects were released from the box, and testing began within 45 seconds. Postirradiation testing was continued for 2 hr in the exposure room. The subjects were tested for 2 hr per day for 3 days. Subjects were monitored by closed-circuit television for changes in gross performance and for emesis.

Performance was videotaped after irradiation. Performance was analyzed for each 10-min work session to determine the number and duration of incapacitations. Subjects were considered incapacitated if no rotations of the wheel occurred for at least 1 min. The subjects were considered recovered when they continuously rotated the wheel at any speed for 1 min.

Radiation exposure and dosimetry. Subjects were exposed to mixed neutron-γ radiation from the AFRRI TRIGA reactor (*17*). The reactor was operated in the 10-msec pulsed mode. A 5-cm-thick lead shield was positioned between the reactor and the subject to produce a free-in-air neutron-to-γ kerma ratio of 3.

Neutron and γ spectrum average energies were 1.0 and 1.4 MeV, respectively. Subjects were exposed while restrained in a Plexiglas box attached to the PAW (Fig. 1). The box was positioned so that each subject's vertical midline was 90 cm from the centerline of the reactor core, while the animal was facing away from the reactor.

Dosimetry measurements were made using paired 0.5-cm^3 ionization chambers, described in ICRU Report 27 (*18*), positioned at the midline of a monkey phantom inside the restraining box. In these measurements, one chamber had A-150 plastic walls and was filled with tissue-equivalent (TE) gas. The other had magnesium walls and was filled with argon. The phantom trunk was a Plexiglas cylinder (10-cm diameter by 33 cm tall) filled with TE liquid. The head section consisted of four 3-cm-thick disks of TE plastic with diameters of 9, 10, 10, and 8 cm, respectively, from top to bottom. Each leg of the phantom consisted of one Plexiglas cylinder 5 cm in diameter and one 3 cm in diameter, each 18 cm long. They were positioned to model the monkey in the restraint box.

Results of dose measurements are shown in Table II; the total neutron plus γ dose at the midline thorax position was the defined dose for all subjects. To provide corrections for variations, actual animal irradiations were monitored with ionization chambers and sulfhur foils mounted at fixed positions near the reactor core and on the Plexiglas restraining box. Propagation of error analysis indicated uncertainties of 8% on total dose and 18% on neutron-γ ratio, besides the uncertainties associated with individual animal size/weight variation.

Analysis. The range of doses for the initial estimate of the ED_{50} was determined by a modified up-down sensitivity procedure (*19*). For example, if a subject was not incapacitated during the first 2 hr after irradiation, the next subject was irradiated at a higher dose. Conversely, if a dose produced incapacitation within 2 hr, the next subject received a lower dose. After the ED_{50} had been estimated, subjects were irradiated at doses between 1766 and 2312 rad to improve the confidence limits of the dose-response function.

TABLE II

Summary of Monkey Phantom Dosimetry

	% of total[a]	*Neutron/γ*
Free-in-air kerma		
Thorax	132	3:1
Head	113	3:1
Midline tissue		
Thorax	100	1.4:1
Head	80	1.6:1

[a] Defined dose = midline tissue thorax dose.

Using the technique described by Finney (*20*), a probit fit was made to establish the ED_{50} for ETI. Further analysis was done of the duration of incapacitation, frequency of emesis, and survival time. For this analysis, subjects were grouped so that the dose range in any group was ±5% of the median dose for the group. The result was that four dose groups were created with means and SEMs as follows: 1766 ± 9, 2037 ± 22, 2308 ± 23, and 4610 ± 22, hereafter called the 1800-, 2000-, 2300-, and 4600-rad dose groups, respectively. Doses for six subjects fell outside the group criteria range, and they were excluded from the group analysis. The Kruskal–Wallis test was used to compare group differences in ETI, emesis, and survival time. Significant group differences were further analyzed with a multiple comparisons test (*21*). The Wilcoxon signed rank test was used to test for difference in the time lost between the first and second hours.

RESULTS

The results of the probit analysis for ETI are plotted in Fig. 2. As shown in this figure, the slope (4.57) for the function is quite steep. Based on the probit, the ETI ED_{50} for physical activity performance 2 hr after radiation exposure was 1982 rad. In a more detailed group analysis, no particular time of ETI manifestation was found for the 2-hr assessment interval.

Analysis of the percentage of performance time lost to incapacitation revealed that although the 2000- and 2300-rad dose groups lost more time in the first hour after exposure (Table III), these differences were not significant. The total percentage time lost to incapacitation revealed a monotonic increase as a function of radiation dose. However, only the 1800-rad dose group differed significantly from the two highest dose groups. The data on emesis for each dose group are also shown in Table III. None of the 13 subjects that received less than 2050 rad vomited, whereas 9 of the 20 animals that received more than that dose vomited one to seven times. Aside from this dichotomy, no relationship existed between groups for emesis. Most vomiting episodes occurred during the rest periods between 20 and 60 min after irradiation; however, 4 animals vomited during a period of incapacitation, and 2 while performing.

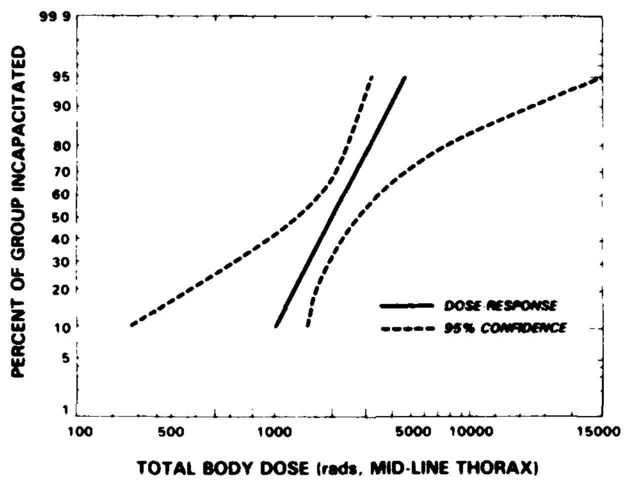

FIG. 2. Dose–response curve and 95% confidence limits for ETI for monkeys performing on a physical activity wheel. ED_{50} is 1982 rad following TBI to mixed neutron-γ (n/γ = 3.0) ionizing radiation.

TABLE III

ETI, Emesis, and Survival Time

Dose group (rad)	*N*	*Number showing ETI*	*Mean % of performance time lost during ETI*			*Subjects with emesis*	*Mean survival time (hr)*
			1st hr	*2nd hr*	*Mean*		
1800	9	1	3.0	0.0	1.5[a]	0/9	96.3
2000	8	5	28.0	11.0	19.5	3/8	118.3
2300	7	6	39.0	19.0	29.0	3/7	121.6
4600	9	8	44.0	45.0	44.5	3/9	38.0[b]

[a] Significant difference in time lost in the 1800-rad group compared to the 2300- and 4600-rad groups, $P < 0.05$.

[b] Significant difference in survival time between the highest and all other dose groups, $P < 0.05$.

Survival time after irradiation was not significantly different below the 2300-rad dose group (Table III). Time of survival was significantly shorter for animals exposed to more than 4500 rad. Although time between the onset of PCI and death ranged from 4 to 180 hr, task performance ceased for most subjects at about 1 or 2 days before death. Duration of PCI was not related to dose.

DISCUSSION

This study established an ED_{50} of 1982 rad for incapacitation for primate locomotor activity. By comparison, the ED_{50} in the same field is 2729 for a primate visual discrimination task.[2] This suggests that the performance of a physical task is more affected by total-body irradiation than are tasks not requiring gross motor activity, which is an observation previously made by Young and Kessler (*11*) and Curran *et al.* (*12*). Two other observations from this study also support these conclusions.

First, incapacitations during the first 2 hr occurred more frequently and resulted in greater time lost to ETI than has been reported for monkeys performing nonphysical tasks. Bruner *et al.* (*7*), Thorp and Young (*5*), and Yochomowitz and Brown (*10*) have reported that ETI for chaired monkeys occurs predominantly as a single episode within the first 30 min after exposure. Although these authors report subjects having multiple ETI episodes, it was not the rule. Consistent with these findings, most incapacitations in the present study occurred during the first hour after exposure but, unlike previous reports, most subjects were incapacitated more than once. As a result, nonperformance time during the second hour after irradiation was greater for the PAW than for other tasks, and overall nonperformance time increased monotonically with dose. Thus no significant differences were seen in nonperformance time between the first and second hour at any dose, and at 4600 rad, as much time was lost to incapacitation during the second hour as during the first.

[2] R. W. Young, S. G. Levin, C. G. Franz, and W. E. Jackson, *Analysis of Monkey Incapacitation Data for Military Application* Defense Nuclear Agency Report, in press.

The second observation from this study suggesting that gross motor performance is more significantly affected by radiation than is nonmotor performance concerns the duration of PCI. Typically, monkey PCI is short, since animals perform with little or no decrement until just before death (*9*). On the other hand, PCI occurred 1 or 2 days before death for the PAW-irradiated subjects. Since Seigneur and Brennan (*9*) describe PCI as a condition of increasing physical debility terminating in death, the earlier onset of PCI for monkeys performing a gross motor-activity task suggests that they become too debilitated to perform motor functions before losing the ability to perform a nonphysical function, or before losing the ability to exhibit a useful aggressive or evasive response (the performance criterion used in that study).

The occurrence of emesis did not appear related to either dose or incapacitation. While some animals vomited in each dose group above 2000 rad, no significant difference existed between the groups as a function of dose. Since all but seven vomiting episodes occurred during the rest periods between 20 and 60 min after irradiation, emesis did not contribute to the ETIs that began 3–7 min after the pulse. In fact, 11 of 20 subjects that were incapacitated did not vomit; 2 that vomited were not incapacitated. Surprisingly, however, 4 subjects vomited during a period of incapacitation, an effect not reported in other primate studies (*7*, *22*). This apparent discrepancy may be accounted for by the fact that incapacitation was defined as nonperformance on tasks that measured fundamentally different end points.

The observation that no significant differences existed in survival for animals irradiated with less than 2400 rad was not surprising, since these doses are supralethal and the dose range below 2400 is small. While survival was significantly less for subjects irradiated with more than 4500 rad, there did not appear to be any relationship between survival time and the number or duration of ETIs. Although PCI tended to be somewhat shorter for the highest dose group, this probably reflects merely the decreased survival, since no significant differences existed in duration of PCI for the grouped data.

ACKNOWLEDGMENTS

The author expresses her appreciation to Mr. Leonard Clark for his technical assistance, to members of the AFRRI Logistics Department for construction of the activity wheels, to Mr. William Jackson and Mr. Sheldon Levin for their statistical analyses of the data, and to Mr. Victor Bogo, Dr. Robert Young, and Dr. Robert Cartledge for their editorial contributions.

RECEIVED: April 27, 1984; REVISED: September 28, 1984

REFERENCES

1. R. L. CHAPUT and D. WISE, Miniature pig incapacitation and performance decrement after mixed gamma–neutron irradiation. *Aerosp. Med.* **41**, 290–295 (1970).

2. A. P. CASARETT and C. L. COMAR, Incapacitation and performance decrement in rats following split doses of fission spectrum radiation. *Radiat. Res.* **53**, 455–461 (1973).

3. G. A. MICKLEY and H. TEITELBAUM, Persistence of lateral hypothalamic-mediated behaviors after a supralethal dose of ionizing radiation. *Aviat. Space Environ. Med.* **49**, 868–873 (1978).

4. A. P. CASARETT, Swim-tank measurement of radiation induced behavioral incapacitation. *Psychol. Rep.* **33**, 731–736 (1973).
5. J. W. THORP and R. W. YOUNG, Monkey performance after partial body irradiation. *Aerosp. Med.* **42**, 503–507 (1971).
6. C. L. TURBYFILL, R. M. ROUDON, and V. A. KIEFFER, Behavior and physiology of the monkey (*Macaca mulatta*) following 2500 rads of mixed gamma-neutron radiation. *Aerosp. Med.* **43**, 41–45 (1972).
7. A. BRUNER, V. BOGO, and R. K. JONES, Delayed match-to-sample early performance decrement in monkeys after 60 Co irradiation. *Radiat. Res.* **63**, 83–96 (1975).
8. D. J. BARNES, *An Initial Investigation of the Effects of Pulsed Ionizing Radiation on the Primate Equilibrium Function.* Report TR66-106, U. S. Air Force School of Aerospace Medicine, Brooks AFB, TX, 1966.
9. L. J. SEIGNEUR and J. T. BRENNAN, *Incapacitation in the Monkey following Exposure to a Pulse of Reactor Radiations.* Report SR66-2, Armed Forces Radiobiology Research Institute, Bethesda, MD, 1966.
10. M. G. YOCHMOWITZ and G. C. BROWN, Performance in a 12-hr 300-rad profile. *Aviat. Space Environ. Med.* **48**, 241–247 (1977).
11. R. W. YOUNG and D. A. KESSLER, *Performance of Sequential Tasks by Unrestrained Monkeys following a 4200-rad Pulse of Mixed Gamma-Neutron Radiation.* Report SR69-14, Armed Forces Radiobiology Research Institute, Bethesda, MD, 1969.
12. C. R. CURRAN, D. W. CONRAD, and R. W. YOUNG, *The Effects of 2000 rads of Pulsed Gamma-Neutron Radiation upon the Performance of Unfettered Monkeys.* Report SR71-3, Armed Forces Radiobiology Research Institute, Bethesda, MD, 1971.
13. S. J. KAPLAN and E. M. GRESCO, *The Effects of Pulsed Gamma-Neutron Radiation upon the Performance of the Unfettered Monkey.* Report 69-6, Armed Forces Radiobiology Research Institute, Bethesda, MD, 1969.
14. C. R. CURRAN and C. G. FRANZ, *Primate Physical Activity following Exposure to a Single 2000-rad Pulsed Dose of Mixed Gamma-Neutron Radiation.* Report SR74-29, Armed Forces Radiobiology Research Institute, Bethesda, MD, 1974.
15. C. R. CURRAN, W. R. WIEGEL, and D. N. STEVENS, *Design and Operation of an Exercise Device for Subhuman Primates.* Report SR73-9, Armed Forces Radiobiology Research Institute, Bethesda, MD, 1973.
16. C. G. FRANZ, L. CLARK, and J. W. CABLE, *Primate Physical Activity following Exposure to a Single 4600-rad Pulsed Dose of Mixed Gamma-Neutron Radiation.* Report SR76-42, Armed Forces Radiobiology Research Institute, Bethesda, MD, 1976.
17. J. A. SHOLTIS, JR., and M. L. MOORE, *Reactor Facility, Armed Forces Radiobiology Research Institute.* Report TR81-2, Armed Forces Radiobiology Research Institute, Bethesda, MD, 1981.
18. ICRU, *An International Neutron Dosimetry Intercomparison.* Report No. 27, International Commission of Radiation Units and Measurements, Washington, DC, 1978.
19. W. J. DIXON, and F. J. MASSEY, JR., THE "up-and-down" method. In *Introduction to Statistical Analysis* (W. J. Dixon and F. J. Massey, Jr.), pp. 380–382. McGraw-Hill, New York, 1969.
20. D. J. FINNEY, Quantal responses and the tolerance distribution. In *Statistical Methods of Biological Assay* (D. J. Finney), pp. 349–369. Mcmillan, New York, 1978.
21. W. J. CONOVER, Some methods based on ranks. In *Practical Nonparametric Statistics* (W. J. Conover, Ed.), pp. 213–338. Wiley, New York, 1980.
22. G. R. MIDDLETON and R. W. YOUNG, Emesis in monkeys following exposure to ionizing radiation. *Aviat. Space Environ. Med.* **46**, 170–172 (1975).

ARMED FORCES RADIOBIOLOGY
RESEARCH INSTITUTE
SCIENTIFIC REPORT
SR85-22

Immunologic and Hematologic Perturbations in Models of Combined Injury

D. F. Gruber, PhD; T. J. MacVittie, PhD; O. R. Pavlovskis, PhD; R. I. Walker, PhD; J. J. Conklin, MD
Armed Forces Radiobiology Research Institute and Naval Medical Research Institute, Bethesda

Many aspects of the reports in the literature describing anergic conditions that exist post trauma are confirmed by data gathered by the Armed Forces Radiobiology Research Institute in a comprehensive program to study combined-injury effects. Dealing with one aspect of this study, this article discusses the synergism of trauma and illness coincident with such stressors as whole-body irradiation, thermal injury, and sepsis. Experimentally produced sepsis depresses and delays both cellular and humoral response patterns in canine and murine modeling systems. Lymphoid populations, dependent on the time of collection post trauma and the organ source, may present an initially augmented response pattern, which within 48 hours becomes depressed to below-normal levels. In addition, immunologic anergy can be induced by the presence of bacterial products such as exotoxin-A. Further mechanisms and regimens of prophylactic immunomodulation are under investigation.

Civilian disasters, technologic advances, and military confrontations during the past century have defined a whole new set of problems in the treatment of pathophysiologic conditions. Crush (renal failure) and shock syndromes exemplify clinical syndromes described during the World War I period. Similarly, World War II saw the development of transplantation techniques devised primarily as a means to help severely burned (and expensively trained) pilots.[1] In fact, many of the trauma guidelines of the American College of Surgeons are based on the educational experiences and lessons received in battlefield situations.[2]

Singular injuries often prove to be difficult cases for the medical practitioner, but when two or more sublethal traumas are combined, a truly lethal synergism can result. Combined injury has been defined by Schildt and Thoren[3] as "a complex injury caused by a simultaneous exposure of a recipient to two (or more) forms of energy or traumata." Combined injuries and trauma are the principal cause of death in North Americans under age 39. In 1982 alone, there were 165,000 trauma-associated deaths.[4]

Our group at the Armed Forces Radiobiology Research Institute has been primarily interested in investigating the medical effects of combined injury when one of the stressors is radiation. The increasing use of radioisotopes and radiation devices in industry, science, and medicine requires that they be moved via publicly accessible transportation systems. An accident within any of these systems could result in casualties, with radiation trauma as one element of combined-injury trauma.

Combined Injury and Whole-Body Irradiation

Whole-body irradiation is a stressor that, when combined with injury or trauma, can lead to death. The effect of such irradiation in various experimentally burned animals is shown in Table 1. In animals in nature, it has been reported that sheep, when exposed to a mixed radiation dose of 400 rads and one hour later subjected to an abrupt overpressure, had a 100% increase in mortality.[5] On the basis of research conducted on mice, Messerschmidt[6] has recommended early closure of open wounds. In his study, murine mortality from radiation rose from 26% to 90% when combined with open wounds. In contrast, if wounds were closed immediately, mortality fell to 18%. Radiation has also been reported to affect the outcome of murine surgical procedures. Laparotomy or splenectomy alone results in a mortality of 5%. The mortality of mice receiving 510 rads of radiation alone was 27%. When a surgical procedure, in this case splenectomy, was performed two, four, or eight days after radiation insult, the mortality increased to levels that were 12-, 15-, and 17-fold, respectively.

When thermal injuries occur along with sublethal levels of radiation, synergistic increases in mortality are seen. Mortality of mice receiving a contact burn alone was 30%,[7] and mortality re-

Dr Gruber, Dr MacVittie, and Dr Conklin are with the Armed Forces Radiobiology Research Institute. Dr Pavlovskis and Dr Walker are with the Naval Medical Research Institute.

Reprint requests to D. F. Gruber, PhD, Armed Forces Radiobiology Research Institute, Bethesda, MD 20814.

Table 1. Combined Effect of Whole-Body Irradiation and Approximately Simultaneous Burns in Various Animal Models

	LETHALITY (percent)
DOGS	
(Brooks, Evans, Ham, and Reid)	
20% burns	12
100 R	0
20% burns + 100 R	73
PIGS	
(Baxter, Drummond, Stephens-Newsham and Randall)	
10–15% burns	0
400 R	20
10–15% burns + 400 R	90
RATS	
(Alpen and Sheline)	
31–35% burns	50
250 R	0
500 R	20
31–35% burns + 100 R	65
31–35% burns + 250 R	95
31–35% burns + 500 R	100
GUINEA PIGS	
(Korlof)	
1.5% burns	9
250 R	11
1.5% burns + 250 R	38

sulting from a 510-rad irradiation was 30%. Combined, these traumas produced a mortality of 90%. Similarly, canine mortality due to a 20%-body-surface thermal injury alone was 12%. Combined with a sublethal radiation dose of 100 rads, the mortality rose to 73%.[8]

As mortality is affected by radiation, so too are the healing processes. Messerschmidt[8] has determined that healing times lengthen by as much as 50% when combined-injury includes radiation (519 rads, LD_{26}) and wounding. In other studies, callus formation was followed radiographically in rabbits. Control animals healed over a 32-day period,[7] but the healing period of rabbits receiving a radiation dose of 800 rads ($LD_{20/30}$) was almost twice as high.

Early closure of soft-tissue injuries is desirable but not always possible as in the case of extensive thermal injury. Open wounds provide an environment easily colonized by microbes, which in turn may enhance immunosuppression. Similarly, radiation and other forms of trauma suppress host immunologic surveillance to the point where the recipient is susceptible to endogenous/exogenous microorganisms and associated toxins.

The hematopoietic system is very sensitive to radiation. Sublethal doses of radiation are known to cause significant reductions in both hematopoietic stem cell and progenitor cell populations. Within the first week to 10 days after a radiation incident, the number of mature functional cells decrease, eg, neutrophils, monocytes, platelets, and lymphocytes. These cells have finite life spans, and in the presence of radiation-depleted stem cell and/or progenitor cell populations, the recipient is at enhanced risk. These end cells are responsible and necessary for the initiation of (1) a whole set of integrated responses to opportunistic pathogens, and/or (2) the healing processes. Reduced by trauma(s) to cellularly ineffectual levels or states, the recipient is at greatest risk for infectious complications. In the leukopenia that exists after radiation insult, it is vitally important that available circulating and tissue-bound granulocytes and monocytes be nonperfunctory and able to phagocytose, kill, and/or release mediators important to the overall revival of immunologic and hematologic competency.

Thermal Injuries

Annually in the United States, about 300,000 people sustain burns of one sort or another; of those injured, some 12,000 die.[10] In addition to the trauma itself, the burn causes suppression of vital immune systems, rendering the recipient extremely susceptible to bacterial and fungal infections.[11] The literature is replete with reports identifying various infectious organisms in burn injuries; one of the most frequently mentioned microbes, *Pseudomonas aeruginosa*, has been associated with infections bearing the highest mortality.[12-14]

Healthy laboratory animals are normally quite resistant to *P. aeruginosa*. To overcome problems of natural resistance, investigators have developed a number of artificial steps to induce experimental infection. Some of these have included use of unrealistically high doses of bacteria; use of cytostatic drugs; addition of virulence-enhancing factors, eg, mucin; and treatment with agents that disrupt the integrity of a host system (or organ), thereby permitting colonization opportunities for microorganisms. The Stieritz and Holder[15] thermally injured murine model, to be described, abrogates many of the aforementioned problems.

Murine experimental strains thus far examined in our laboratory have been BALB/C and C3H/HeN female mice, 18–22 gm in weight. One day before use, the backs of the mice were shaved. Before burn, mice were anesthe-

tized with methoxyflurane. A template with a 2.5-sq cm opening (corresponding to about 15% of total body surface area [TBSA] was placed on the shaved spot, bathed with 0.5 ml of 95% ethanol, and ignited for 11 seconds. Immediately postburn, 0.5 ml of an appropriate bacterial suspension was injected subcutaneously into the burned area. Control animals received an equivalent volume of saline. Wretlind and Pavlovskis[15] have reported that white blood cell counts of burned, noninfected mice did not differ significantly from normal values, whereas mice inflicted with trauma and given bacterial doses (1 LD_{50}) showed significant decreases in white blood cell counts only 22 to 28 hours postinfection. Interestingly, the 22- to 28-hour low point in the white blood cell count often corresponds temporally to maxima noted in the splenic and thymic lymphoid populations at 20 and 24 hours after trauma and also to low points noted in humoral response patterns.

Burned mice show susceptibility to infection with *P. aeruginosa*, which decreases eight to 18 hours postburn. Different strains of *P. aeruginosa* may vary markedly in virulence, as defined by measures of mean lethal dose. For that reason, most of our research efforts have been conducted with strain PA-220 (LD_{50} <10), the most virulent strain available in our laboratory.

Although it is not clear what components of *P. aeruginosa* are ultimately responsible for its virulence, one very important factor is the exotoxin (A) that is produced. Passive immunization with formaldehyde or glutaraldehyde toxoids of exotoxin-A increases the survival rates of burned, infected mice by 50% to 85%. If exotoxins were combined with gentamicin, 100% survival could be effected.[16] Enhanced survival rates have also been shown in human patients, who possess high levels of antibodies to exotoxin-A.[17]

Purified *P. aeruginosa* exotoxin-A has been reported to inhibit protein synthesis in cultured mammalian cells[18] and in mouse organs.[18] Murine protein synthesis is inhibited by more than 85% in the liver and 20% to 50% in other organs.[19] We have determined that the LD_{50-7} of mice to purified exotoxin falls within a range of 50 to 60 ng. Because immunologic response patterns in septic conditions were of interest, we evaluated the effects of exotoxin by adding it to in vitro cultures of ficoll-separated murine lymphocytes. To determine whether exotoxin abrogated a specific cellular-responding population, blastogenically induced mitogenesis patterns were evaluated. Mitogens used for assessment were concanavalin A (Con-A), pokeweed mitogen (PWM), phytohemagglutinin (PHA), and lipopolysaccharide (LPS). At the highest experimental concentration (50 ng) investigated, Con-A response patterns showed the greatest sensitivity to exotoxin and decreased to 15% of normal values (Figure 1, A). Response patterns to PHA (similar to Con-A in that it is primarily a T cell mitogen) decreased to 27% of normal values (Figure 1, B). Response patterns of cells capable of responding to B cell mitogens (LPS, PWM) showed somewhat less sensitivity to exotoxin and decreased to 35% and 38% of control values (Figure 1, C and D). PHA values were the first to return to normal levels and did so in the presence of 0.1 ng or less of exotoxin. Cellular responses to LPS and PWM reached normal levels in the presence of 0.01 ng of exotoxin. The pattern of Con-A–responsive cells again showed great sensitivity to exotoxin and did not reach normal levels until 0.0001 ng or less of exotoxin was present. Further experiments have shown that exotoxin, on the basis of Trypan Blue viability, is not cytotoxic. Also, it

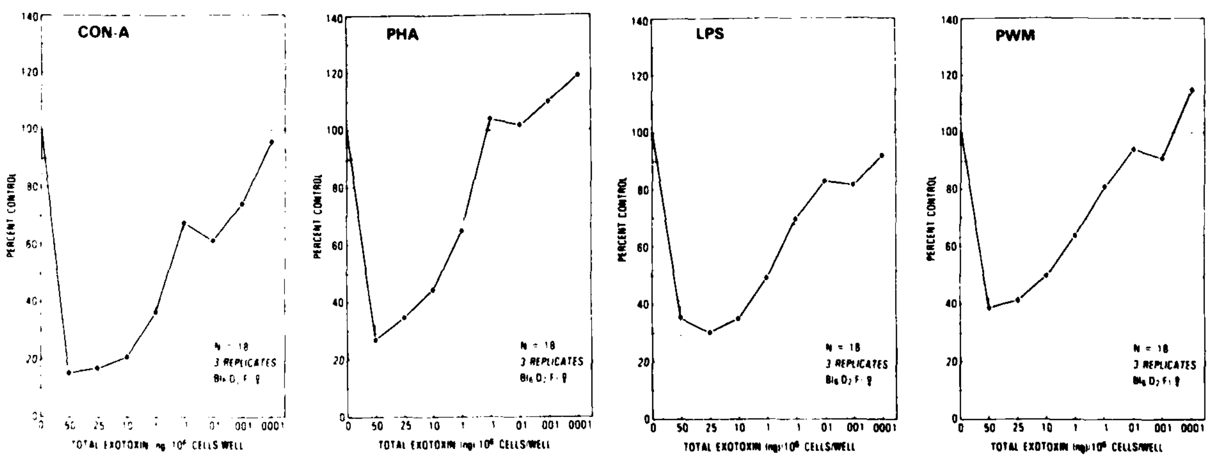

Fig 1. A–D. thymidine (1 μCi, 18 hours) uptake patterns in ficoll-separated murine splenic lymphocytes when co-cultured with mitogen (*CON-A, PHA, LPS, PWM*) and concentrations of purified *Pseudomonas* exotoxin-A. Data expressed as percent control + SEM (N = 18). Lymphocyte source: $B_6D_2F_1$ female mice.

has been determined that whatever effects are caused by exotoxin occur within the first 60 minutes of incubation and cannot be abrogated by washing one to three times.

Cellular response patterns of ficoll-Hypaque–separated murine splenic or thymic mononuclear cell populations were studied (Tables 2 through 5). Thymidine (1 μCi, 18 hours) uptake patterns were demonstrated by lymphocytic cellular populations one to 72 hours posttreatment to mitogenic stimulation. PHA (0.5 μg/10^6 cells/well) was used to assess T lymphocytes, and LPS (5 μg/10^6 cells/well) to assess B cells. Experimental treatment(s) were performed before tissue extirpation in five groups: (1) burns (*B*)—15% TBSA full-thickness contact burn; (2) Bacterial challenge ("Bug")—subcutaneous administration of an LD_{50-7} dose of *P. aeruginosa* (3–17 × 10^5); (3) exotoxin (*XO*)—intravenous administration of an LD dose of *Pseudomonas* exotoxin-A (53–65 ng); and (4) and (5) their combinations. Data are expressed as percent of normal control collected over three replicates (N = 36) in C_3H/HeN mice.

As shown in Tables 2 through 5, thermal injury appears to stimulate PHA T cell responses of ficoll-separated splenic monocytes for periods up to 24 hours (see Tables 2 and 3). At some time between 24 and 44 hours postinjury, splenic responses decreased significantly to levels below normal. Lower numbers of seed cells have shown similar response patterns, which seems to rule out hypermetabolic or nutritional constraints. It is interesting that the pattern of increased responsiveness for 24 hours, followed by a significant decline at 44 hours, apparently holds for almost all experimental treatments. Splenic B cell responses to LPS (lipopolysaccharide) were markedly different from overall splenic PHA responses and were significantly depressed throughout all time frames evaluated for all experimental treatments.

Table 2. Murine Spleen Cells (PHA Responses Expressed as Percent of Control)

	hours						
	1	4	20	24	44	48	72
Burn	95	121	153	182	63	47	42
Bug	72	170	270	338	95	84	60
Exotoxin	89	90	93	117	88	68	ND
B + XO	113	125	136	140	91	78	ND
B + Bug	245	316	434	402	219	186	92

Table 3. Murine Spleen Cells (LPS Responses Expressed as Percent of Control)

	hours						
	1	4	20	24	44	48	72
Burn	7	8	43	47	67	49	22
Bug	30	25	41	38	15	17	11
Exotoxin	81	52	16	20	13	11	ND
B + XO	35	22	19	18	32	51	ND
B + Bug	8	5	25	29	9	7	8

Table 4. Murine Thymus Cells (PHA Responses Expressed as Percent of Control)

	hours						
	1	4	20	24	44	48	72
Burn	279	294	827	1026	147	133	67
Bug	1140	487	145	2431	434	762	217
Exotoxin	288	250	112	160	563	512	ND
B + XO	1145	2312	2560	3216	1626	2027	ND
B + Bug	133	197	817	1035	211	197	84

Table 5. Murine Thymus Cells (LPS Responses Expressed as Percent of Control)

	hours						
	1	4	20	24	44	48	72
Burn	186	151	277	280	117	159	85
Bug	219	349	714	803	766	862	211
Exotoxin	249	237	119	128	245	167	ND
B + XO	4546	4127	ND	5225	1264	2560	ND
B + Bug	159	122	138	141	157	163	111

Thymic cells (see Tables 4 and 5), although reacting in a manner qualitatively similar to that of T cells, differed quantitatively. As in the case of splenic responses to PHA, thymic responses were elevated through 24 hours before decreasing at 44 hours. One common feature in the two thymic-responsive (PHA, LPS) populations was their trends. There appear to be parallel increases in both thymic (PHA, LPS) populations in the presence of experimental trauma(s). The thymic, LPS-responsive group (*B* + *Bug*) tended to mimic damage induced by burns alone.

Sepsis

A common outcome of an immunosuppressive event is infection caused by an opportunistic pathogen. In spite of the proliferation of antibiotics, sepsis is second only to head injury as the most frequent cause of death in trauma victims surviving more than three to four days.[20] Opportunistic pathogens, with their selective mechanisms of invasion combined with impaired host immune mechanisms, lend themselves to the development of lethal bacteremias. Despite the availability of more than 24 antimicrobial agents (with the exception of third-generation cephalosporins), the incidence of infection has not significantly decreased,[21] and in the United States alone, 200,000 to 400,000 septic-associated deaths occur annually.[22]

Factors that may predispose a person to infection include the degree of injury, magnitude of external contamination, organism invasiveness, and host immunologic and nonspecific resistance. Another factor that increases the incidence of infection is the presence of foreign bodies in crushed muscle. For example, clostridial myonecrosis (gas gangrene) occurs when *Clostridium perfringens* is injected into guinea pigs. In normal animals, 10^6 spores were required to establish the infection; in the presence of crushed muscle, only 10^3 spores were needed. When sterile dirt was applied to the crushed muscle, only one spore was needed to establish a similar pathologic condition.[23] Human beings have shown corresponding effects: use of silk sutures caused a 10^3–10^4 increase in susceptibility to *Staphylococcus* infection.[24]

Another element in infection is the time lag between injury and definitive treatment. The frequency of clostridial myonecrosis was almost seven-fold higher in prisoners of war whose opportunity for definitive surgery came three to four times later than that for our own service personnel.[25] Other factors that may contribute to infection include the number, location, and extent of wounds, eg, during World War II, buttock wounds accounted for only 5% of wounds but over 50% of cases of gas gangrene.[26]

Gram-negative bacilli have become the predominant etiologic agents of trauma and nosocomial infections during the past three decades, and there is no evidence that the incidence of these infections is abating.[12,27] A recent meeting of Army and Navy research and development communities concerned with opportunistic infections cited *Escherichia coli*, *P. aeruginosa*, and *Klebsiella pneumoniae* as the major gram-negative threats, although some anaerobes (*Bacteriodes*, *Staphylococcus*, *Candida*) were also implicated.

Normal mucosal surfaces show a certain resistance to pathogenic colonization. Human volunteers who gargled a challenge of 10^8 cells of *E. coli* or *K. pneumoniae* had less than 1% of the original number of organisms present when examined three hours later.[28] Immunologic, mucosal-related defense mechanisms are augmented by physical defense mechanisms, ie, peristalsis and mucociliary action. These mechanisms plus the presence of indigenous flora combine to regulate pathogenic colonization.

When normal mucosal defense systems are compromised (as is most likely the case in trauma), opportunistic pathogens gain access to binding sites heretofore inaccessible and initiate the disease processes. Desquamating cells of murine tracheas, traumatized by influenza virus or endotracheal intubation, bound *Pseudomonas* more readily than did those of normal animals.[29] Microulcerative lesions produced by hexamethylphosphoramide also enhanced *Pseudomonas* colonization.[30]

Intestinal colonization patterns may also change as a consequence of trauma. It has been reported that rats receiving 500 or 1,000 rads of radiation show a decrease in the number of bacteria per gram of intestine shortly after exposure (23.9×10^5, normal; 11.7×10^4, at 500 rads; 39.4×10^4, at 1,000 rads). Numbers of bacteria in the animals irradiated with 500 rads began to return toward normal levels by seven days postirradiation and were about normal by 11 days postirradiation. In contrast, animals that received higher doses of radiation had bacterial levels three times normal.[31,32] Changes in populations of intestinal bacteria may be altered by the mucous environment, such as that occurring after burn shock.[33] Lesions are purported to exist in intestinal tight junctional barriers (zonula occludens) associated with mucus-producing cells following radiation,[34] full-thickness dermal wounds,[32] or endotoxin shock.[35]

Experimental Studies

There is general agreement that the two major pathogens involved in opportunistic infections are *E. coli* and *P. aeruginosa*. We have therefore attempted to assess the immunologic impact of these pathogens in the combined-injury models that we have established. The canine, because of its size and similarity to the human being, was used as a model for *E. coli* sepsis. In this model, each canine received either a sterile

fibrin clot or a clot containing 10^9 *E. coli*/kg of body weight. Clots were placed surgically into the peritoneal cavity adjacent to the liver. Peripheral blood samples, drawn in heparin, were used as a source of lymphocytes and/or plasma for analysis. Lymphocyte-rich fractions were separated from whole blood using ficoll-Hypaque procedures. Lymphocyte fractions were examined in vitro for mitogenic response patterns. Concanavalin A was used to assess T lymphocyte response patterns, and pokeweed mitogen (PWM) was used to assess T cell-mediated B cell responses. Responses were quantified on the basis of 18-hour tritiated thymidine uptake.

Comparison of lymphocyte functional response patterns showed that the cellular aspects responsive to PWM stimulation (Figure 2, left) were much more susceptible overall to insult (radiation and sepsis) than were the Con-A–responsive elements (see Figure 2, right). In some cases, Con-A–responsive cells showed augmented response patterns. In the presence of 10^9 *E. coli*/kg of body weight, Con-A cellular response patterns were both depressed and delayed. The presence of sepsis depressed Con-A responses from the 50% of control values, shown by the sterile clot, to values only slightly higher than 10%. The radiation-augmented (hormetic) response seen with administration of 1.5 Gy of ^{60}Co irradiation was similarly depressed by the presence of *E. coli* for a period of 30 days. Definitive response patterns are much more difficult to characterize for PWM-responsive cells. However, *E. coli*, as in the case of Con-A–responsive cells, suppressed PWM cellular response patterns. The nadir reached by animals given the *sterile clot* amounted to about 40% of control values reached on day 7. The introduction of sepsis postponed the appearance of the nadir until about day 13, when it was quantitatively 20% of control values.

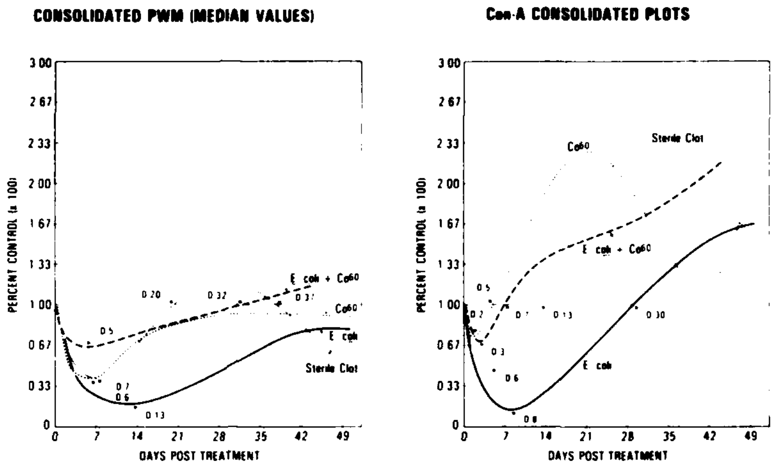

Fig 2. Thymidine uptake (2µCi, six hours) of ficoll-separated canine peripheral blood monocytes. Cells (10^5/well) were incubated with 1 µg of Con-A (*left*) or 10 µg of PWM (*right*). Median levels expressed as percent control, four contributors per data point (*D*). Treatment groups include sterile fibrin clot, clot-containing 10^9 *E. coli*/kg-body weight, or ^{60}Co irradiation (1.5 Gy midline, 0.1 Gy/minute).

Canine humoral responses were evaluated on the basis of plasma immunoglobulin levels determined by radial immunodiffusion (RID) techniques. Experimental implantation of a sterile clot resulted in increased levels of IgG, IgA, and IgM during 48 days of investigation. Interesting to note was the temporal pattern shown by all classes of immunoglobulins investigated. Immunoglobulins (IgG, IgA, IgM) immediately began to increase, reached maximal levels between days 10 and 14, and fell off to low levels (days 21–28) before showing a secondary but lower increase at about day 35 (Figure 3). The presence of *E. coli* in the clot depressed all humoral responses (Figures 4 and 5). In the case of

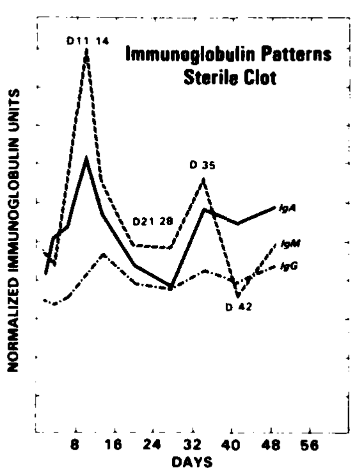

Fig 3. Periodicity of normalized canine immunoglobulins (IgG, IgM, IgA) as determined by radial immunodiffusion techniques in experimental insertion of sterile fibrin clot.

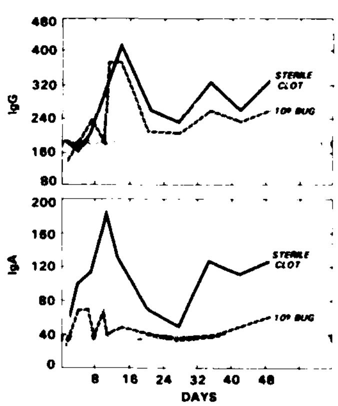

Fig 4. Radial immunodiffusion-determined levels of IgG (× 10^{-1}) or IgA expressed as milligrams per deciliter in canines receiving either a sterile fibrin clot or one containing 10^9 *E. coli*/kg of body weight. Each data point represents a minimum of five separate observations.

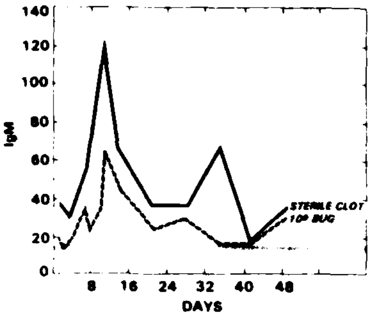

Fig 5. IgM ($\times 10^{-1}$) levels as per Figure 4.

IgG and IgM, although dampened somewhat by sepsis, the same pattern could be identified. In contrast, IgA levels were, in the presence of sepsis, near normal levels.

The effects of radiation on canine humoral response patterns are shown in Figures 6 through 8. Levels of IgA, IgG, and IgM are undoubtedly augmented by experimental surgery and the implantation of a sterile clot (IgA, IgM) that contains foreign proteins. Augmented levels are depressed by the imposition of 150 rads of ^{60}Co irradiation. IgA and IgM, but not IgG, levels were depressed further by the addition of *E. coli* to the radiation treatment protocol.

The number of white blood cells in the peripheral blood was decreased by one day after radiation and did not reach normal levels until day 49 (Figure 9). The hematopoietic cellular aspects responsible for homeostatic control include both stem cells and progenitor cells. In vitro soft-agar techniques are available that allow enumeration of progenitor cells. The hematopoietic progenitor cells responsible for the proliferation of granulocytes and macrophages have been termed granulocyte-macrophage colony-forming cells (GM-CFC). A requirement for GM-CFC proliferation is the presence of colony-stimulating activity (CSA). Analysis of CSA concentration in peripheral blood (Figure 10) showed significantly increased levels within three hours (2.65 times normal) of bacterial implantation. Over time, CSA levels slowly decreased. However, at day 10 postinfection, CSA levels were still 100% above normal levels. GM-CFC numbers in the peripheral blood (Figure 11, left) were increased between days 1 and 10 postsepsis, approached normal levels on day 14, and reached normal levels on or around day 28. The GM-CFC picture in the bone marrow was

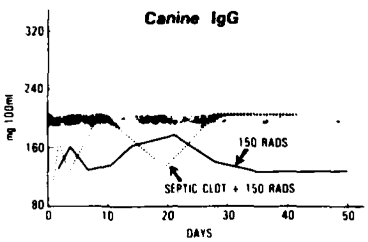

Fig 6. IgG ($\times 10^{-1}$) levels in canines receiving either bilateral (1.5 Gy at 0.1 Gy/minute) ^{60}Co radiation alone or in combination with septic (10^9 *E. coli*/kg of body weight) clot.

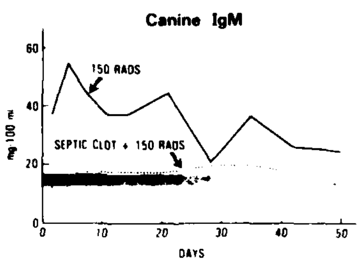

Fig 7. IgM ($\times 10^{-1}$) levels in canines receiving either bilateral (1.5 Gy at 0.1 Gy/minute) ^{60}Co radiation alone, or in combination with septic (10^9 *E. coli*/kg body weight) fibrin clot.

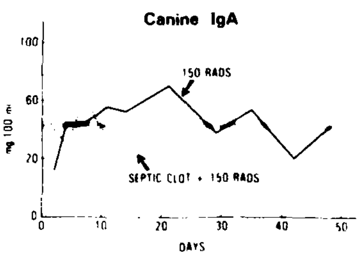

Fig 8. IgA levels ($\times 10^{-1}$ levels in canines receiving either bilateral (1.5 Gy at 0.1 Gy/minute) ^{60}Co radiation alone, or in combination with septic (10^9 *E. coli*/kg of body weight) fibrin clot.

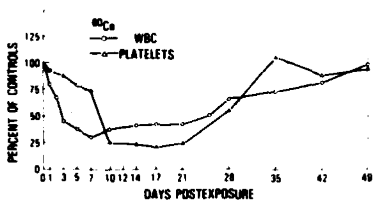

Fig 9. Percentage of white blood cells and platelets in samples of canine peripheral blood post ^{60}Co irradiation (1.5 Gy at 0.1 Gy/minute).

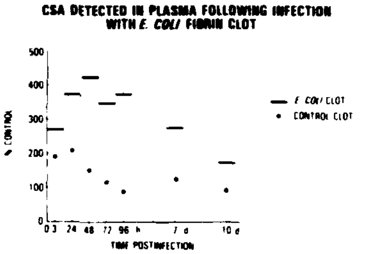

Fig 10. Temporal examination of colony-stimulating activity (CSA) present in canine plasma samples after induction of experimental sepsis. Quantitation of CSA (7.5% total culture volume) levels is made by comparison with colony-forming performance of normal dog serum. Data expressed as mean values from minimum of six animals per data point.

somewhat similar (Figure 11, right). On day 2 postinfection, GM-CFC demonstrated large-order increases (90 times) on or around experimental day 2, decreasing sharply to levels 7.5 times normal on day 4, and finally reaching normal levels around day 28. It appears, from at least a proliferative point of view, that granulocyte-macrophage progenitor cells are able to respond to experimentally induced septic lesions.

Comments and Conclusions

It is unfortunate that the very technologies that enrich our everyday lives also intensify incurred trauma. Our data substantiate numerous reports in the literature on the state of anergy that exists post trauma. Unfor-

tunately, the fibrin clot model, developed to mimic peritonitis, induces immunologic artifacts. Foreign proteins within the clot matrix enhance the humoral response pattern of canine prototypes. Addition of *E. coli* to the fibrin clot suppresses both cell-mediated and humoral response patterns over a period of seven weeks. The presence of *P. aeruginosa* or one of its virulence-enhancing factors, exotoxin-A, also induces immunoparalysis in in vitro lymphocyte cultures. Trauma-induced immunoparalysis, coupled with the presence of opportunistic pathogens and environments favorable to their proliferation, often leads to lethal results.

Our research demonstrates that early, aggressive immunomodulatory steps are very important and must be implemented as soon after trauma as practicable.

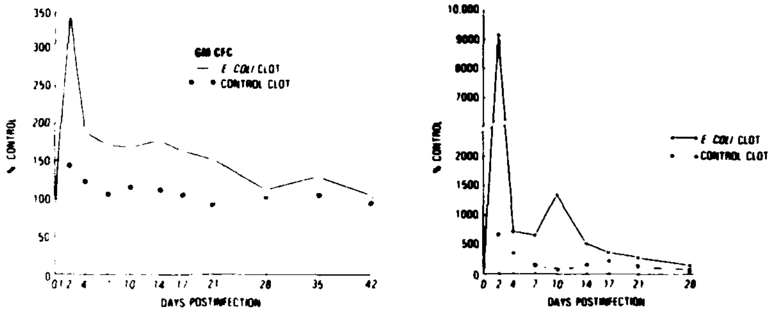

Fig 11. Peripheral blood and bone marrow concentrations of granulocyte-macrophage colony-forming cells (GM-CFC). Peripheral blood (10^6 cells culture, *left*) and bone marrow cells (2×10^5 cells culture, *right*) were plated with standard levels of CSA (7.5% by volume normal dog sera). Data expressed as percent of control, minimum of six representatives per data point.

References

1. Moore FD: Background: The pressing need for new knowledge on radiation injury with physical trauma. in Walker RI, Gruber DF, MacVittie TJ, et al (eds): *Proceedings of the First International Symposium on the Pathophysiology of Combined Injury and Trauma*. Kaman-Tempo, Santa Barbara, 1984, pp 11–19.
2. Conklin JJ, MacVittie TJ, Walker RI: Pathophysiology of combined injury and trauma: An overview. in Walker RI, Gruber DF, MacVittie TJ, et al (eds): *Proceedings of the First International Symposium on the Pathophysiology of Combined Injury and Trauma*. Kaman-Tempo, Santa Barbara, 1984, pp 20–35.
3. Schildt B, Thoren L: Experimental and clinical aspects of combined injuries. in Schildt B, Thoren L (eds): *Combined Injuries and Shock*. Stockholm, Forsvarets Forskningsanstalt, 1968, pp 3–15.
4. Trunkey DD: Trauma. *Sci Am* 249: 28–35, 1983.
5. Jones RK, Chiffele TL, Richmond DR: A study of effects of combined blast and radiation injury in sheep. in Schildt B, Thoren L (eds): *Combined Injuries and Shock*. Stockholm, Forsvarets Forskningsanstalt, 1968, pp 57–66.
6. Messerschmidt OE: Strahlanbelastung und offene Hautwunde. *Arch Klin Exp Dermatol* 227:329–335, 1966.
7. Messerschmidt OE: Untersuchungen uber Kombinationsschaden uber die Legenserwartung von Mausen, die mit Gans Korpei Bestrahlungen in Kombination mit offnen oder Geschlossenen Haut verletzunger Bauchoperationen oder Kompressionsschaden belastet Wurden. *Strahlentherapie* 131:298–311, 1966.
8. Messerschmidt OE, Birkenmay E, Bomes H, et al: Radiation sickness combined with burns. *Int'l Atomic Energy Ass'n Sci Manual*-119 173–179, 1970.
9. Zemljanoj AG: Heilring geschlosserer Frakturen der langen Rohrenknuchen ober Strahlenskrankheit an Versuchstreren. *Med Radiol* 5:72–80, 1956
10. Baycar RS, Aker F, Serowski A: Burn casualties in combat: A need for protective garments. *Milit Med* 148:281–282, 1983.
11. Pruitt BA: Infections of burns and other wounds caused by Pseudomonas aeruginosa. in Sabath LD (ed): *Pseudomonas aeruginosa the Organism, Diseases It Causes, and Their Treatment*. Berne, Hans Huber Publishers, 1980, pp 55–70.
12. McCabe WR, Jackson GG: Gram-negative bacteremia: I. Etiology and ecology. *Arch Intern Med* 110: 845–855, 1962.
13. Pruitt BA, Lindberg RB: Pseudomonas aeruginosa infections in burn patients. in Doggett RG (ed): *Pseudomonas aeruginosa. Clinical Manifestations of Infection and Current Therapy*. New York, Academic Press, 1979, pp 339–366.
14. Stieritz DD, Holder IA: Experimental studies of the pathogenesis of infections due to Pseudomonas aeruginosa: Description of a burned mouse model. *J Infect Dis* 131:688–691, 1975.
15. Wretlind B, Pavlovskis OR: Experimental Pseudomonas aeruginosa burn infection model in mice. in Zak O, Sande MA (eds): *Animal Models in the Evaluation of Chemotherapy of Infectious Diseases*. London, Academic Press (in press).
16. Pavlovskis OR, Yaffee LJ, Wretlind B, et al: Experimental Pseudomonas aeruginosa burn infections. in Walker RI, Gruber DF, MacVittie TJ (eds): *Proceedings of the First International Symposium on the Pathophysiology of Combined Injury and Trauma*. Kaman-Tempo, Santa Barbara, 1984, pp 380–390.
17. Pollack M, Young LS: Protective activity of antibodies to exotoxin A and lipopolysaccharide at the onset of Pseudomonas aeruginosa septicemia in man. *J Clin Invest* 63:276–286, 1979.
18. Middlebrook JL, Dorland RB: Response of cultured mammalian cells to exotoxins of Pseudomonas aeruginosa and Corynebacterium diphtheriae: Differential cytotoxicity. *Can J Microbiol* 23:189–198, 1977.
19. Pavlovskis OR, Shackelford AH: Pseudomonas aeruginosa exotoxin in mice: Localization and effects on protein synthesis. *Infect Immun* 9:540–546, 1974.
20. Caplan ES, Hoyt N: Infection sur-

veillance and control in the severely traumatized patient. *Am J Med* 70:638–640, 1981.
21. Sanford JP: Battlefield wound infection, in Walker RI, Gruber DF, MacVittie TJ, et al (eds): *Proceedings of the First International Symposium on the Pathophysiology of Combined Injury and Trauma*. Kaman-Tempo, Santa Barbara, 1984, pp 404–412.
22. Fletcher JR: Pharmacologic management of sepsis, in Walker RI, Gruber DF, MacVittie TJ, et al (eds): *Proceedings of the First International Symposium on the Pathophysiology of Combined Injury and Trauma*. Kaman-Tempo, Santa Barbara, 1984, pp 391–403.
23. Altemeir WA, Furste WL: Studies in the virulence of Clostridium welchii. *Surgery* 25:12–19, 1949.
24. Elek SD, Coren PE: The virulence of Staphylococcus pyogenes for man. A study of the problems of wound infection. *Br J Exp Pathol* 38:573–586, 1957.
25. Langley FH, Winkelstein LB: Gas gangrene. *JAMA* 128:783–792, 1945.
26. Conway H: Anaerobic infection and gangrene of war wounds in casualties from the Philippine Islands. *Surgery* 19:553–561, 1946.
27. Kreger EG, Craven DE, Carling PC, et al: Gram-negative bacteremia. III. Reassessment of etiology, epidemiology, and ecology in 612 patients. *Am J Med* 68:332–343, 1980.
28. Laforce MF, Hopkins J, Trow R, et al: Human oral defenses against gram-negative rods. *Am Rev Resp Dis* 114:929–935, 1976.
29. Ramphal R, Small PM, Shands J Jr, et al: Adherence of Pseudomonas aeruginosa to tracheal cells injured by influenza infection or by endotracheal intubation. *Infect Immun* 27:614–619, 1980.
30. Boyd RL, Ramphal R, Rice RW, et al: Chronic colonization of rat airways with pseudomonas aeruginosa. *Inf and Immun* 39 1403–1410, 1983.
31. Porvaznik M, Walker RI, Gillmore JD: Reduction of the indigenous filamentous microorganisms in the rat ileum following X-radiation. *Scan Electron Microsc* 3:15–22, 1979.
32. Walker RI, Porvaznik M: Association of bacteria and endotoxin with posttrauma events, in Ninnemann JL (ed): *Infection and Other Immunologic Sequelae*. Baltimore, University Park Press, 1983, pp 1–15.
33. Kaen RI, Mullakandov SM: Functional and morphological changes in gastrointestinal tract in experimental burn shock. *Bull Eksp Biol Med* 92:624–626, 1982.
34. Walker RI, Porvaznik M: Association of leukopenia and intestinal permeability with radiation-induced sensitivity to endotoxin. *Life Sci* 23:2135–2322, 1978.
35. Walker RI, Porvaznik M: Disruption of the permeability barrier (zonula occludens) between intestinal epithelial cells by lethal doses of endotoxin. *Infect Immun* 21:655–658, 1978.

ARMED FORCES RADIOBIOLOGY RESEARCH INSTITUTE
SCIENTIFIC REPORT
SR85-23

Germfree Research: Microflora Control and Its Application to the Biomedical Sciences, pages 139–143

Hematopoiesis in Conventional Mice After Wound Trauma[1]

G.D. Ledney, L.K. Steel, H.M. Gelston, Jr., W.E. Jackson, III, and E.D. Exum, Departments of Experimental Hematology and Biochemistry, Armed Forces Radiobiology Research Institute, Bethesda, Maryland 20814-5145

Macrophages, granulocytes, and platelets serve in wound debridement, bacterial neutralization, and homeostasis. Replacement of such cells may involve perturbations in the clonogenic cell populations responsible for replenishing specific adult cell populations. For example, the human blood granulocyte progenitor cell compartment is increased following abdominal hysterectomy (Philip et al, 1980). In mice, skin wound trauma produced changes in the proliferative cell compartments of the hematopoietic tissues 24 hrs after injury (Ledney et al, 1980). In this study we report (1) some of our findings on the hematopoietic clonogenic cell changes in conventional mice after trauma and (2) circulating substances which may mediate these changes.

Materials and Methods

Animals: Groups of 10-20 week old female B6CBF1 Cum BR mice were wounded under Metafane anaesthesia between the hours of 10AM and 2PM. A non-lethal 2.5 cm^2 circular wound (4% skin surface) was cut in the anterior-dorsal skin fold

1. Supported by the Armed Forces Radiobiology Research Institute, Defense Nuclear Agency (work unit 4421-00129). Views presented are those of the authors, and no endorsement by the Defense Nuclear Agency has been given nor should be inferred. Research was conducted according to the principles enunciated in the "Guide for the Care and Use of Laboratory Animals" prepared by the Institute of Laboratory Animal Resources, National Research Council.

and underlying panniculus carnosus muscle (between the shoulder blades) with a steel punch. The punch was cleaned after the wounding of each animal by immersion in 70% ethanol. Wounds were untreated and left open to the environment. After injury, all mice were placed in sanitized cages with autoclaved hardwood chip bedding. Control mice were anaesthetized and handled in the same manner as the wounded animals except for the wounding procedure.

Clonogenic Cell Assays: Colony forming unit-spleen assays (CFU-s) were used to determine the pluripotent cell numbers in hematopoietic tissues. Experimental groups (6-8 mice) were exposed to 10 Gy ^{60}Co radiation (dose rate 0.4 Gy/min). Within 4 hrs of irradiation, each mouse was injected i.v. with either 25 x 10^4 spleen or 25 x 10^3 marrow cells derived from control (C) or wounded (W; 3,7,10 or 14 days post-wounding) donors. Additional irradiated mice received 1,2, or 5 x 10^5 isolated peripheral blood cells from C or W (day 3) donors. Spleens were removed at 8 days, fixed in Bouin's solution (2-4 hr) and surface colonies counted.

Endogenous CFU (E-CFU) studies were performed on groups of mice wounded 24 hr prior to radiation (7 or 9 Gy) exposure. Spleen colonies were counted at 5,7,10 and 12 days after irradiation.

Tissues containing granulocyte-macrophage colony forming cells (GM-CFC) and macrophage colony forming cells (M-CFC), were taken from C or W mice (days 3,7,10 or 14 post-wound). 10^6 spleen, 25 x 10^3 marrow, and 0.5, 1 or 2 x 10^5 nucleated peripheral blood cells were grown in triplicate double-layer agar cultures with 5% growth stimulator (pregnant mouse uterine extract). Colonies (>50 cells) were counted at day 10 (GM-CFC) and day 25 (M-CFC).

All clonogenic data are quantitated on the basis of 10^6 nucleated cells.

Circulating Mediators: Serum from C or W mice (days 2 & 3) was examined for colony stimulating activity (CSA) via M-CFC and GM-CFC assays. C-reactive protein (C-RP) was measured nephelometrically using human C-RP antisera and standards. Plasma prostaglandin E_2 (PGE_2) levels were determined by ^{125}I-radioimmunoassay of samples previously subjected to organic extraction and purification on C-18 columns. C-RP and PGE_2 samples were obtained from C and W mice days 1-7,9,11,14,17 and 21.

Results

Clonogenic Cells After Wound Trauma: Splenic CFU-s in W mice were increased 2-fold on day 3 after injury. Also at this time, peripheral blood of W mice contained 4-fold more CFU-s (71 ± 4) than C mice (16 ± 4). No significant changes were seen in femoral marrow CFU-s.

The splenic GM-CFC concentration was increased 5-fold 3 days after trauma (80 ± 4 vs 16 ± 2). Thereafter, a 1.5-2-fold increase in splenic GM-CFC was observed during the remainder of the 2-week wound healing period. In the femoral marrow, the GM-CFC concentration was increased only on day 3 after trauma (1870 ± 139 vs 1328 ± 116). Also on day 3, an 8-fold increase in the GM-CFC concentration in the peripheral blood (48 ± 11 vs 6 ± 2) was seen.

The splenic M-CFC compartment of W mice was reduced 30-70% from that of C mice (153 ± 9) during the 2-week healing period. After injury, the femoral marrow concentration of M-CFC was increased on day 14 only (3224 ± 403 vs 2136 ± 157). The peripheral blood concentration of M-CFC was similar in both W and C mice (130-160) on day 3.

Wounding 24 hr prior to 7 Gy resulted in 3-fold more E-CFU at 5,7, and 10 days after irradiation than that formed after 7 Gy only (control E-CFU were 0.8, 1.7, and 6.4 respectively). A 10-fold increase in E-CFU at 5, 7, and 10 days was seen when wounding preceded 9 Gy by 24 hr (control E-CFU were 0.2, 0.4, and 2.7 respectively. Thus wounding had a greater effect at 9 Gy ($p<.05$) than at 7 Gy. The doubling time for E-CFU was 1.2 days and was independent of the radiation dose or the combined injury.

Circulating Mediators: CSA was detected in the serum of mice 2-3 days after trauma. About 250 GM-CFC and 20 M-CFC normal marrow cells cloned in 0.1 ml of serum from W mice. No colonies were formed in the serum from C mice while approx. 1200 and 200 GM-CFC and M-CFC respectively, cloned in enhancing medium.

Serum C-RP concentration increased 50-300% 2-4 days after wound trauma. One week after wounding the C-RP level returned to the control level of 4.0 ug/ml.

Plasma PGE_2 concentration increased immediately after trauma and was increased 10-20-fold 2-3 days after injury. By one week, PGE_2 returned to control values of about 50 pg/ml.

Discussion

In conventional mice, the pathophysiological stimulus of skin wounding and subsequent healing results in significant perturbation in clonogenic cell populations and circulating substances that may mediate hematopoiesis. Our findings suggest that tissue injury provokes cellular and humoral responses in the host's attempt to maintain homeostasis. The utilization of granulocytes to clear cellular debris and bacteria from the wound site may result in the mobilization of proliferative cells from the bone marrow and spleen. These cells produce mature elements to assist in repair. As the mature cells are consumed, the demand for more mature cells is met by proliferation and amplification of progenitor cell compartments (GM-CFC and M-CFC), the less differentiated E-CFU compartment, and the pluripotent CFU-S compartment.

One focus of our work is to identify mediators which may regulate clonogenic cells after trauma. PGE_2 is a known modulator of hematopoiesis (Kurland and Moore, 1977) and cells in resting stage (G_o) are known to undergo proliferation when exposed to higher levels of PGE_2 (Williams, 1979) and this could explain the reduced splenic M-CFC seen after trauma. Additionally, there is _in vitro_ evidence that C-RP inhibits M-CFC expression (Marcelletti et al, 1982). The finding of a serum substance (CSA) capable of promoting GM-CFC growth suggests negative feedback regulation (consumption of granulocytes) evoked by trauma. But, _in vitro_ demonstration of a CSA effect does not mean that it is active _in vivo_.

The hematopoietic proliferation and attending mediator release may be the result of host responses to infection or endotoxins. However, abscesses, pus formation, lymph node involvement, and histologic organ involvement with bacteria were never seen. Also, a secondary peak in C-RP, indicative of infection (Rowe et al, 1984) was never found. However, all wounds were contaminated with one to three naturally occurring skin or alimentary tract bacteria. Wound colonization with specific bacteria may enhance healing (Levenson et al, 1983) and/or inhibit colonization with more desirable organisms (Papageorgiou et al, 1976).

Bacterial endotoxin is a known modifier of hematopoietic responses. This substance could be released by bacteria into circulation at the wound site or through disrupted intestinal cell tight junction barriers after injury (Walker and Porvaznik, 1983). Germ-free animals may

provide a clue to understanding the clonogenic and mediator substances released after trauma. In germ-free rats, the intensity of the inflammatory reaction is less than that of rats with a "normal" flora (Dorati et al, 1971). Future experiments measuring hematopoietic proliferation and mediator substance release in germ-free animals are planned.

References

1. Dorati RM, Frank DW Stromberg LMR, McLaughlin MM (1971). The effect of the germ-free state on wound healing. J Surg Res 11: 163.
2. Kurland J, Moore MA (1977). Modulation of hemopoiesis by prostaglandins. Exp Hemaol 5: 357.
3. Ledney GD, Stewart DA, Exum ED (1980). Proliferative responses of lymphomyeloproliferative cells of mice after wound trauma. J Trauma 20: 141.
4. Levenson SM, Kan-Gruber D, Gruber C, Molnar J, Seifter E (1983). Wound healing accelerated by Staphylococcus aureus. Arch Surg 18: 310.
5. Marcelletti JF, Johnson CS, Mortensen RF, Furmanski P (1982). Effect of C-reactive protein on granulocyte-macropahge progenitor cells. J Lab Clin Med 100: 70.
6. Papageorgiou PS, Alqusus Z (1976). Impairment of natural defenses 1. Exogenous cause, mechanisms, and opportunistic infection. Pediatric Annals 5: 440.
7. Philip MA, Standen G, Fletcher J (1980). The effects of surgical trauma on human granulopoiesis. Brit J. Hematol 44: 263.
8. Rowe IF, Worsley AM, Donnelly P, Catovsky D, Goldman JM, Galton DAG, Pepys MB (1984). Measurement of serum C-reactive protein concentration after bone marrow transplantation for leukemia. J Clin Path 37: 263.
9. Walker RI, Porvaznik M (1983). Association of bacteria and endotoxin with post-trauma events. In: Ninneman JL (ed): "Traumatic Injury, Infection and other Immunologic Sequelae," Baltimore: U Park Pres, p. 1.
10. Williams, N (1979). Preferential inhibition of murine macrophage colony formation by prostaglandin E. Blood. 53: 1089.

CARRIER GENERATION, RECOMBINATION, AND TRANSPORT IN ORGANIC CRYSTALS

Martin Pope

New York University, Chemistry Department, New York

Charles E. Swenberg

Armed Forces Radiobiology Research Institute, Bethesda

Various mechanisms of carrier generation in organic crystals are reviewed. These include band-to-band transitions, auto-ionization, and direct charge-pair generation. Geminate recombination is discussed, including the effect of temperature and electric field on the initial charge distribution. Carrier transport is reviewed, using crucial experimental results. An analysis of various transport mechanisms is presented, including one that may be relevant.

Three processes that are of major importance in the phenomenon of photoconductivity are carrier generation, carrier recombination, and carrier transport. These will be discussed in that order, as they relate to homomolecular polycyclic aromatic hydrocarbon (PAH) crystals. It is surprising that the mechanisms of carrier generation and carrier transport in well-characterized crystalline compounds are still subjects for heated dispute.

I. PHOTOGENERATION OF CARRIERS IN THE BULK

Among the homomolecular PAH compounds, anthracene has long been the "hydrogen-atom" for theoretical calculations. It now appears that there are distinct differences not only in the quantitative response of various members of the PAH family to light, but there may be qualitative differences as well. As one proceeds from naphthalene to pentacene for example, the optical absorption spectrum shows a significant increase in the contribution of states that have ionic character (1). This increase in

J. Ladik et al. (eds.), Quantum Chemistry of Polymers - Solid State Aspects, 137–164.

ionic character is paralleled by an increase in the quantum efficiency of photogeneration. However, there is not yet unanimity on the association of this increased ionic character with a specific mode of ionization.

Historically, the first conflicted picture to be resolved was whether the photogeneration of carriers proceeded as a result of a direct transition from the valence band to the conduction band (band-to-band, BB) (2, p. 470). In anthracene, it was known that the absorption spectrum was essentially explicable in terms of transitions to bound, neutral, Frenkel exciton states; the BB transition would thus have to be weak since the final states would be buried in the Frenkel exciton spectrum. An alternative hypothesis was that carrier generation requires the excitation of a Frenkel exciton that could dissociate if its energy was degenerate with that of a pair of uncorrelated carriers. This process is referred to as auto-ionization (AI). It does not follow that all AI transitions lead to completely uncorrelated carrier pairs. Most of the emitted electrons will thermalize within the Coulomb capture radius of the geminate positive ion, forming a transient charge-transfer state that can either decay to the ground state or dissociate by the absorption of ambient energy. Following Jortner (3), the wavefunction of such an AI state can be written as

$$\psi_E = a_E \phi_A + \Sigma_i b_i \phi_i + \int C_{E'} \phi_{E'} dE' \quad (1)$$

where $\phi_{E'}$ are the crystal continuum states, and ϕ_i are the sets of excited vibrational levels of the ground state and of other bound electronic states that are degenerate, or nearly so with the vibrational state localized at ϕ_A. Anticipating the recent work of Bounds and Siebrand (4), an example of another type of bound electronic state that would be degenerate with the ϕ_A would be a charge-transfer (CT) state, in which the hole and electron are on different molecules, but still correlated with one another. These CT states could ionize completely by absorbing thermal energy, or energy from an external electric field or auxiliary light source. The decision as to whether BB transitions or an AI transition was the proper description for the photoconduction process was made on the basis of studies using polarized light, but it is now evident that these experiments would not distinguish between the AI mechanism or that in which a dissociable CT exciton was excited. This may be seen as follows: for the purposes of this argument, assume that all three processes namely AI, BB transitions, and direct CT formation occur. If one classifies bound states as being either Frenkel states or CT states, then the maximum efficiency of carrier production, ϕ^- can be expressed as

$$\phi^- \propto \frac{k_F \{[x(1-y)\ \eta_{AI} + (1-x)]\ \eta_{CT} + \eta_{AI}\ xy\} + \alpha}{k} \qquad (2)$$

where k is the overall optical absorption coefficient, being equal to $k_F + \alpha$, where k_F is the absorption coefficient to a CT state or to a Frenkel state that can autoionize with an efficiency η_{AI}. Here x represents the fraction of states that lead to AI and y represents the fraction of AI states that lead to carriers without passing through an intermediate CT state. The efficiency of ionization of the CT state is given as η_{CT}. In either case, AI or direct CT formation, an intermediate CT state can be formed; this conclusion follows from the observations (5,6) that there is a temperature and field-dependent ion-pair dissociation process that precedes complete ionization. This field and temperature dependent process of dissociation is referred to as the Onsager mechanism (7) which will be discussed shortly. The term α in equation (2) is the absorption coefficient to a plane wave state (BB transitions) in which the ionization efficiency is unity. If BB transitions dominate, then α dominates the numerator and it follows that $\phi^- \propto \alpha/k$. Since ϕ^- is found to be about 10^{-4} in anthracene (it is much higher in tetracene and pentacene, (8)) this implies that $k = k_F + \alpha >> \alpha$ or $k_F >> \alpha$. Thus ϕ^- would vary inversely with the absorption coefficient k_F. It is possible to check this prediction by using polarized light to excite the crystal. In this way, k may be varied by a factor of 7 at a particular wavelength (constant energy), thus providing a technique for changing k without introducing at the same time the additional complication of changing the energy of excitation. This experiment was carried out by Geacintov and Pope (9), and Braun and Hornig (10), and it was found that there was essentially no change in ϕ^- as k was varied. This observation ruled out BB transition in anthracene. This polarization experiment cannot, however, distinguish between the processes of AI and direct CT formation. It is probably the case that both mechanisms are operative in the sense that for some materials and in some energy ranges, one or the other process (or perhaps both) will dominate. Thus, in the subthreshold energy region for photoconduction (i.e. $h\nu < E_g$ where E_g is the band gap and $h\nu$ is the photon energy), the contribution of AI is small, while there is incontrovertible evidence that direct CT exciton formation does take place. This will be discussed shortly. On the other hand for excitation energies exceeding the vacuum level, the observation that electrons can be photoemitted with the maximum kinetic energy (11,12) permitted by the Einstein photoelectric equation is proof that no intermediate CT state need be excited to produce free carriers. Furthermore, it has been found by Chance and Braun (5), that the activation energy E_a for carrier photogeneration in the energy region $5.4 < h\nu < 6.2$ eV is constant at about 0.06 eV and the quantum yield at 6.2 eV is about 4×10^{-4}. This quantum yield should be compared with that of photoemission at 6.2 eV (13), which is about 3×10^{-5}. From geometric consid-

erations, it may be appreciated that roughly one-fourth of the total number of free electrons will emerge from the surface, so the actual AI yield should be at least 10^{-4} at this energy, which is approximately what is observed experimentally in photoconductivity. In addition, the constancy of E_a over the energy region $5.4 < h\nu < 6.2$ eV is consistent with the maintenance of the same mechanism or mechanisms of photogeneration over this energy range and with the position (5) that AI also plays a major role at energies less than the ionization energy of the crystal. It thus appears reasonable to expect that there are excitation energies for which the photoconductivity mechanism in a given PAH crystal changes from direct CT exciton generation to AI.

The CT state in anthracene was first treated theoretically by Hernandez and Choi (14), who concluded that the direct optical transition to this state would have an oscillator strength of 10^{-4}, and that it would be buried in a region of high oscillator strength Frenkel exciton transitions, making its spectroscopic detection difficult. The first indirect evidence for the generation of CT excitons was provided by Pope and Burgos (15), and this was based on photoemission studies, particularly in tetracene. The first optical absorption evidence for the existence of a CT state in a homomolecular PAH crystal was presented by Tanaka (16), who worked with 9,10 dichloroanthracene. These results were substantiated by Abbi and Hanson (17). The proposition that direct CT generation was the primary mechanism for photoconductivity in all PAH crystals was put forth in a series of theoretical papers by Bounds and Siebrand (4,18), and more recently by Bounds, Petelenz and Siebrand (19,20). Experimental evidence for direct excitation of CT exciton states in tetracene and pentacene has been provided by Sebastian, Weiser and Bässler (21). More recently, the CT exciton transition was detected in anthracene by Sebastian, Weiser, Peter, and Bässler (22). All of the experimental studies were based on the electric field modulation of optical absorption.

We will first discuss the theoretical work of Bounds, Petelenz and Siebrand (BPS). The fundamental premise of this study (based on anthracene) is that the direct excitation of the CT exciton is made possible by the coupling of this low oscillator strength state, with that of the high oscillator strength ($f \simeq 1$) S_3 (^1B_u) Frenkel state located at 4.63 eV. The S_3 state thus lies about 0.5 eV above the anthracene band gap $E_g \sim 4.1$ eV, and all optical excitations in the energy region up to 4.63 eV would produce CT states (albeit, vibrationally excited); in other words, there would be an energy of activation for photoconductivity even when the optical energy $h\nu > E_g$. This is in fact observed (5). The energy E_{CT} of CT states of varying separation distance between the charges was calculated by BPS, using the expression

$$E_{CT}(\ell_1 k_1, \ell_2 k_2) = E_g + W_c(\ell_1 k_1, \ell_2 k_2) + \Delta W_{eh}(\ell_1 k_1, \ell_2 k_2) - \Delta W_e - \Delta W_h, \quad (3)$$

where $k_2 \ell_2$ is the molecule and unit cell respectively from which the electron is removed and $k_1 \ell_1$ is the final state of the excess electron; E_g is the band gap, W_c is the Coulomb energy of the two carriers, and ΔW are apparent polarization energies, the subscript eh referring to the electron-hole pair and the separate e and h subscripts to the electron and hole respectively. The apparent polarization energy is defined as

$$\Delta W = P + W_M + W_R \quad , \quad (4)$$

where P is the polarization energy of a charge, which includes charge-induced dipole and induced dipole-induced dipole interactions, W_M is the charge-multipole energy and W_R is the lattice relaxation energy; the P term is the largest in magnitude. The results of these calculations for anthracene are shown in Fig. 1.

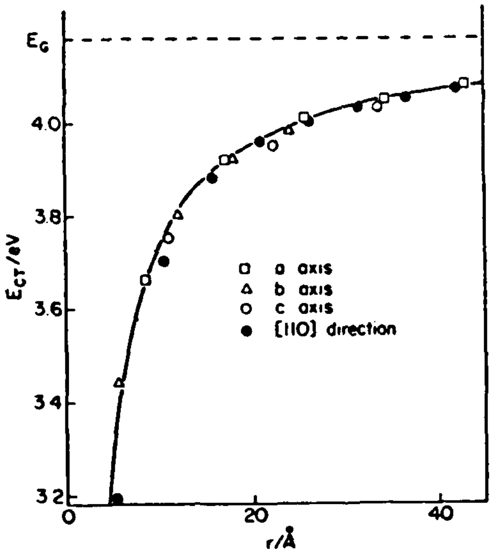

Fig. 1. Energy of an electron-hole pair in anthracene as a function of separation in four crystal directions. The solid line represents the energy the pair would have in an isotropic dielectric with $\varepsilon = 3.23$ for a Coulombic potential. Bounds et al (19).

These data may be described qualitatively but not quantitatively by a Coulomb expression of the form

$$E_n = E_g - \mu e^4/8(h\varepsilon\varepsilon_o n)^2 \quad , \tag{5}$$

where μ is the effective mass of the electron-hole pair, $\varepsilon\varepsilon_o$ the dielectric constant parameters, and n is a principal quantum number, related to the distance r between electron and hole. Equation (5) is overly simple, and when properly corrected, yields the results shown in Table I. The CT state values shown in

Table I. Energy Levels E_n of CT States (in eV) (19)

n	Quasi-Localized Model[a]	Wannier Model[b]
1	3.20	3.46
2	3.70	3.72
3	3.88	3.85
4	3.96	3.93
5	4.00	3.98

[a] Along the [110] direction, calculated using eq. (3).

[b] Calculated using an empirical correction to the Coulomb potential.

Table I can be related to the activation energies E_a found for carrier generation in anthracene by the relationship $E_a = E_g - E_n$; quantum efficiencies of carrier generation $\phi_o(h\nu)$ were also calculated, and the results of these are shown in Fig. 2. The agree-

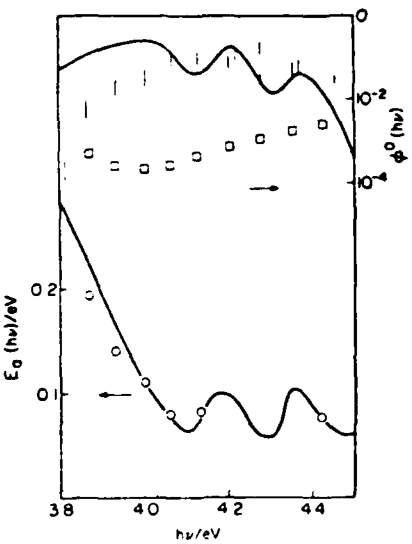

Fig. 2. Calculation (lines) and obsereved activation energies of carrier generation (bottom) and quantum yields of electron-hole pair formation (top). From Bounds et al. (19). Circles and squares taken from (6) and bars from L. E. Lyons and K. A. Milne, J. Chem. Phys., 65 1474 (1976).

ment for the E_a values is good, but not so good for the $\phi_0(h\nu)$ calculations. The explicit assumption is made here that while it is possible to excite vibrational states of CT excitons for each value of E_n, only the 0-0 vibrational state is available for thermal dissociation, the excess energy being dissipated in a time shorter than dissociation or recombination. It was possible for BPS to estimate the contribution of CT states to the overall absorption spectrum; in anthracene, this contribution was small but significant (23), while in tetracene and pentacene, the CT contribution was dominant.

Considerable experimental support for the CT exciton mechanism for carrier generation has been provided by work on electric field modulated absorption spectroscopy. As described Sebastian et al (21), the electric field induced change in absorption coefficient k for excitation of a Frenkel exciton may be given to first order by the expression

$$\Delta k \propto (\Delta \bar{p})\ F^2\ \partial k/\partial E + \ldots + \qquad (6)$$

where $\Delta \bar{p}$ is the average change in molecular polarizability, F is the applied electric field, and $\partial k/\partial E$ is the differential change of absorption coefficient with the optical excitation energy. For the excitation of a pure CT state the change in the absorption coefficient is given by

$$\Delta k \propto (1/3\ qr)^2\ F^2\ \partial^2 k/\partial E^2 + \ldots \qquad (7)$$

where qr is the magnitude of the dipole moment of the CT state. In Fig.3 is shown the absorption and electroabsorption spectra of pentacene; for excitation energies above 1.83 eV it is evident that Δk varies directly with $\partial^2 k/\partial E^2$. Similar studies were made on anthracene by Sebastian et al (22), although it proved to be more difficult to detect the CT states. These authors correlated the energies of these peaks in the CT exciton spectra with the size of the CT exciton using a Coulombic equation similar to that given by equation (8); this is shown in Fig. 4. The extrapolated value of E_g proved to be 4.4 eV, in contrast with the accepted value of about 4.1 eV; they justified this discrepancy by identifying their CT values with the vertical (Franck-Condon) transitions from a Frenkel ground state to vibrationally excited CT states. Furthermore, in opposition to a basic premise of the BPS treatment, they postulated that the excess vibrational energy for any particular CT state could be used to further separate the members of the ion-pair state. This postulate, in a sense, combines the processes of CT exciton absorption and ballistic carrier separation. The identification of the structures found by Sebastian et al (22), in the electroabsorption spectrum with the sequence of CT states of different separations r_{CT} has been

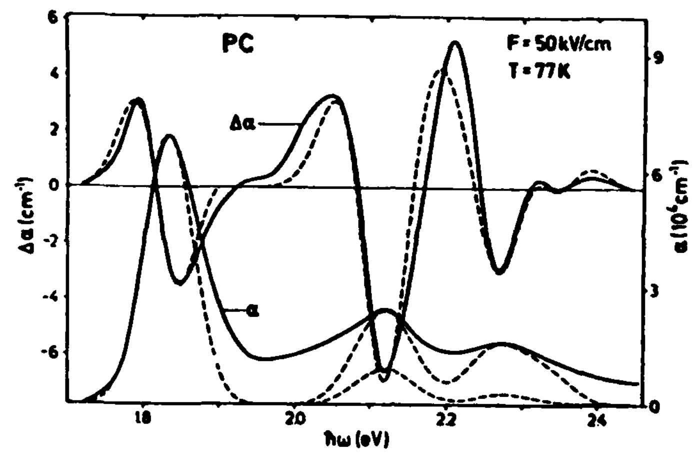

Fig. 3. Absorption and electroabsorption spectra of pentacene films. Solid curves refer to experiment, the dashed curves represent fits on the basis of Stark effect and charge transfer excitons. The lower absorption curves are calculated with the assumption of complete charge transfer. α is denoted by k in text. From Sebastian et al (21).

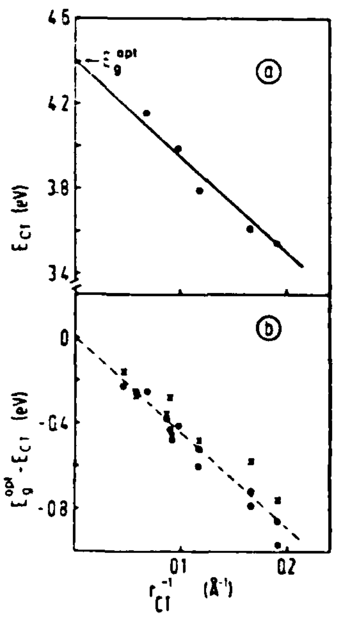

Fig. 4. (a) Charge-transfer energies versus reciprocal CT distance r_{CT}. (b) CT binding energies. Full dots are experimental, crosses and open circles are computed data from ref. 19 (O: point molecule treatment, x: submolecule treatment). From Sebastian et al (22).

questioned by Siebrand and Zgierski (24). These authors calculated the spectrum of CT states in anthracene and attributed the structure observed by SWPB (22), to the vibrational overtones of the nearest-neighbor CT state.

The AI mechanism of ionization coupled with the ballistic model of electron-hole separation has been discussed in detail by Silinsh et al (8), who studied tetracene and pentacene. The essential principles of this model are exposed in Fig. 5. Here,

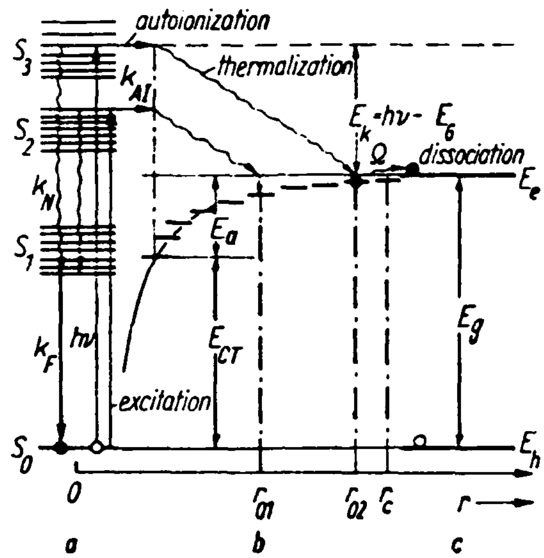

Fig. 5. Photogeneration stages in anthracene-type molecular crystals according to the ballistic model. a) neutral electronic states; b) bounded charge pair (CT) states; c) ionized states of the crystal. From Silinsh et al (8).

AI steps are succeeded by the escape of the hot electrons into the lattice, where they thermalize by acoustic phonon scattering, producing the series of bound CT states. Following the creation of the CT states, the mechanism of dissociation is the same as that of the direct CT exciton generation mechanism. Using a rather simple scattering theory, Silinsh et al (8), calculated the optical energy dependence of the thermalization distances, $r_o(h\nu)$, which in turn, correspond to specific separations of CT states. The agreement between their calculated and experimental values is shown in Fig. 6. The values of the energies of activation E_a were calculated using the expression

$$E_a = E_g - e^2/4\pi\varepsilon\varepsilon_o r_o(h\nu) \quad . \tag{8}$$

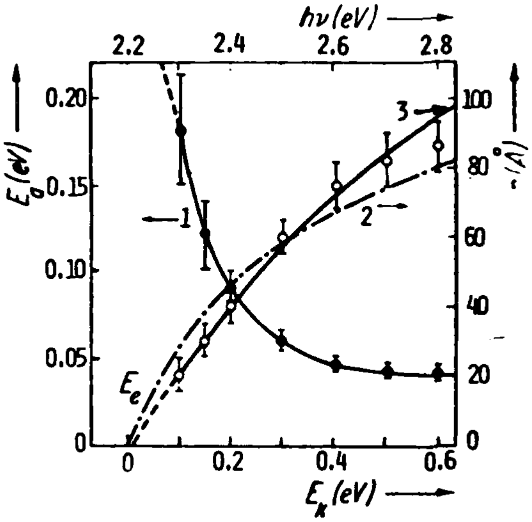

Fig. 6. Experimental zero-field thermalization length $r_o(h\nu)$ (open circles) and corresponding $E_a(h\nu)$ (filled dots) dependences on $h\nu$ in pentacene; (1) $E_a(h\nu)$ curve; (2) $r_o(h\nu)$; calculated using $r_o = (D\tau_{th})^{1/2}$, see text; (3) empirical formula for r_o. From Silinsh et al (8).

As may be seen in Fig. 6 the agreement is satisfactory. Calculations were also made of the photoconductivity quantum efficiency and agreement was found between calculated (using ballistic theory and a modified Onsager theory) and measured values in the energy region $E(h\nu) > E_g$. In the region $E(h\nu) \sim E_g$, they found a discrepancy that they attributed to a contribution from direct CT state absorption. In the higher regions of photon energy, they found another discrepancy that they attributed to excitation to a different AI state.

In the cases considered above, the thermalization distance, or CT exciton size is determined by the energy of the absorbed photon. There is another interesting experimental result in which it appears that the efficiency of photoconduction is independent of photon energy (25). This work was carried out with X-metal-free phthalocyanine crystals embedded in a polymeric matrix. It was found that all the ionization proceeded from the first excited singlet state, S_1. In the direct CT exciton excitation picture, one might explain this result by the proposition that excitation to any state above S_1 results in a rapid internal conversion to S_1, which must have considerable CT character because the application of an external electric field leads to a significant fluorescence quenching from S_1. The quenching would be due to the field-induced dissociation of the CT states, which depletes the concen-

tration of states that could recombine to form singlet-states that could fluoresce. If S_1 lies below the conducting level, as appears to be the case with β-phthalocyanine (2, p. 671) then the AI mechanism with ballistic carrier separation is not plausible, unless the initial state is vibrationally excited.

Summarizing the results presented herein regarding the relative roles of AI and direct CT exciton formation, it appears that there are materials and energy ranges in which one or the other, or both mechanisms prevail. This point has been made by Silinsh et al (8), and we favor this position. The actual determination of the relative roles of AI and direct CT exciton formation might be resolvable if photocurrent rise time measurements could be made. This suggestion was made by Bounds et al (20,23), who presented a theoretical analysis of what the photocurrent rise time should look like in anthracene, as a function of temperature and excitation wavelength. They chose anthracene as a model compound because the calculated values of the absorption coefficient to the CT state seem to be much smaller than the observed absorption coefficient to the Frenkel exciton states. Thus, if the AI plus ballistic model is operative, it should have a much better chance of being seen in anthracene than in pentacene, where the CT transitions appear to dominate Frenkel transitions in the energy region greater than that of S_1. If the ballistic mechanism is operative, Bounds et al (23) assume that only the nearest neighbor CT state will be excited, regardless of photon energy. The rise time of photoconductivity would thus be a constant, independent of photon energy. However, in the case of direct absorption to a CT state there should be an essentially instantaneous population of CT states of all radii. The rise time of conductivity should drop with increasing photon energy, due to the increased population of quickly ionizing large-radius CT exitons. These differences in the rate of formation of the CT state can be incorporated into the overall rate of formation of free carriers. It emerges that by using the parameters required to explain the action spectrum of the energy of activation, it is predicted that the rise time of the photocurrent should be constant at about 55 psec if the ballistic model is correct and should drop to 15 psec with increasing photon energy if the CT mechanism is correct. The assumptions made in deducing this expected behavior are arguable, and it seems that the experiment could be used to rule out direct CT absorption, but not AI.

II. GEMINATE RECOMBINATION

Following the initial step of carrier generation, there evolves a final configuration of a hole and an electron separated from each other by a distance that in some way is a function of the energy of the exciting light (except as indicated above).

These carriers have originated from the same excited molecule and are referred to as geminate pairs. These pair-states can dissociate as a result of a thermally activated diffusive separation of the two carriers and the application of an external field. The quantitative description of this photoionization process was given by Onsager (7). The application of the Onsager theory to organic crystals was carried out by Batt, Braun and Hornig (26,27), and by Chance and Braun (5,28). It was found that the theory was quite successful in explaining the observed results without introducing any parameter other than the dielectric constant of the medium. The Onsager theory gives the probability that a thermalized geminate charge pair will escape recombination, and will dissociate under the influence of an external electric field of strength F. Onsager assumed an isotropic system containing a low concentration of charge pairs (no interaction between charge pairs) in thermal equilibrium with a medium of dielectric constant ε. The relationship for the probability that the charge pair will dissociate is (29)

$$f(r,\theta) = \exp(-A)\exp(-B)\sum_{m=0}^{\infty}\sum_{n=0}^{\infty}\frac{A^m}{m!}\frac{B^{m+n}}{(m+n)!} \qquad (9)$$

which, when only terms linear in B are retained, gives

$$f(r,\theta) = [\exp(-A)](1 + AB) \qquad (10)$$

where $A = 2q/r$, $B = \beta r(1 + \cos\theta)$, $q \equiv e^2/8\pi\varepsilon\varepsilon_0 kT$, $\beta \equiv eF/2kT$, r is an initial separation distance between the oppositely charged carriers and θ is the angle between the radius vector r and the applied field vector F.

The parameter 2q has the dimensions of distance and in the absence of any external field, $f(r,\theta)$ is equal to $\exp(-2q/r)$. The value of 2q is referred to as the Coulombic capture radius r_c, and corresponds to the distance at which the kinetic energy of the diffusing particle is equal to the Coulombic attractive potential energy. For an electron moving with thermal energy kT,

$$e^2/4\pi\varepsilon_0\varepsilon r_c = kT$$

or

$$r_c = e^2/4\pi\,\varepsilon_0\varepsilon kT = 2q \qquad (11)$$

The observed carrier quantum yield Φ can be expressed as the integral of $f(r,\theta)$ over space (28)

$$\Phi = \Phi_0 \int g(r,\theta)\, f(r,\theta)\, d\tau \qquad (12)$$

where Φ_0 is the primary quantum yield in carrier pairs, and $g(r,\theta)$ is the probability per unit volume of finding the ejected electron

ENERGY TRANSFER AND MOLECULAR WEIGHT EFFECTS ON POLYMER LUMINESCENCE

Charles E. Swenberg and Robert T. Devine

Armed Forces Radiobiology Research Institute, Bethesda, USA.

Energy transfer in, and luminescence from polymers in dilute rigid glasses and solid polymer films are subjects of extensive current research. This interest stems partly from the vast differences in optical and electronic properties which polymers exhibit and their usefulness. A microscopic description of how electronic energy is transported and trapped and the various routes of dissipation is essential for understanding inhibition of photodegradation processes in polymers. This chapter will have the limited objectives of (a) reviewing the experimental evidence for intramolecular energy transfer in polymers as demonstrated initially by Fox and Cozzens (1), (b) summarizing experimental evidence for dependence of delayed fluorescence and phosphorescence on the molecular weight of the polymer, (c) developing a simple model which accounts for the enhancement of the delayed fluorescence with increasing degree of polymerization and its saturation for high molecular weight pol, mer, and (d) discussing the time dependence of polymer intramolecular excimer and monomer luminescence using the spectral function formalism for a one-dimensional transport model. The chapter is not intended to be exhaustive in its treatment but rather selective, illustrating the general concepts involved.

I. EVIDENCE FOR ENERGY MIGRATION IN POLYMERS

Singlet and triplet energy transport in polymers with pendent chromophores has been actively studied since the pioneering work of Eisinger and Shulman (2) and Cozzens and Fox (1). Intermolecular transfers of triplet excitation energy in fluid solutions (3) and triplet and singlet exciton migration in crystalline solids such as anthracene (4) were well established prior to conclusive experimental proof of intramolecular energy migration among the chromophores of a polymer. Intramolecular

J. Ladik et al. (eds.), Quantum Chemistry of Polymers - Solid State Aspects, 259–277.

energy transfer in linear organic polymers, such as vinyl polymers, is expected since their adjacent chromophores have separations on the order of 4 Å and favorable relative orientations such that long sequences of closely spaced pendent groups exist. Before presenting experimental and theoretical results of delayed emission dependence on polymer molecular weight we review the classical work of Cozzens and Fox (1) on delayed emission from poly(1-vinylnaphthalene) (P1VN) in tetrahydrofuran-diethyl ether at 77°K. For dilute rigid glasses, where the concentration of the pendent chromophore(s) is generally less than 10^{-3}M, each polymer is spatially well separated from all others thereby precluding intermolecular energy transfer. A property of any dilute polymer glass is that the emission spectrum (at 77°K) exhibits a fluorescence and phosphorescence action spectrum nearly identical to its chromophore analog. For P1VN this implies that 1-ethylnaphthalene and P1VN spectrum are similar although delayed fluorescence is not observed for 1-ethylnaphthalene at equal molar concentrations. Dilute polymer glasses at low temperatures generally do not exhibit excimer fluorescence. Following Stevens (5) we use the term excimer to denote an excited dimer which is dissociative in its ground state. Intramolecular excimer formation occurs when the interaction of an excited chromophore with another chromophore on the same molecule have the proper configurational arrangement; hence excimer fluorescence in solid matrices is sensitive to the temperature at which the matrix is formed as demonstated by the Frank and Harrah (6) study of poly(2-vinylnaphthalene). A typical delayed emission spectrum of P1VN is shown in Fig. 1.

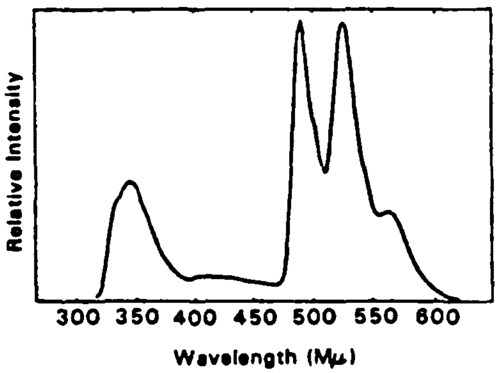

Fig. 1. Delayed emission spectrum of poly(1-vinylnaphthalene) in tetrahydrofuran-diethyl ether at 77°K; excitation wavelength, 290 nm; approximately 10^{-3}M. From Cozzens and Fox (1).

Characteristic of the delayed emission spectrum is the delayed fluorescence band centered at 346 nm and the structured phosphorescence emission between 490 nm and 570 nm. That mobile triplet states and

their mutual annihilation are involved in the origin of the delayed band centered at 346 nm can be shown as follows. Suppose we add to the P1VN-tetrahydrofuran-diethyl ether solution molecules M having the following properties: (1) its lowest singlet absorption band is below that of 1-ethylnaphthalene, (2) its triplet state lies energetically higher than 1-ethylnaphthalene and (3) it has a high intersystem crossing rate so that a large fraction of excited singlet molecules result in triplet excited molecules, then convincing evidence for triplet state involvement is shown if upon excitation of M an identical delayed fluorescence spectra to that resulting from direct excitation of P1VN is observed. Using benzophenone and an exciting at 366 nm, a wavelength at which P1VN does not absorb, Cozzens and Fox (1) observed delayed fluorescence identical to that observed using 290 nm light. Fig. 2 illustrates schematically the energy pathways involved.

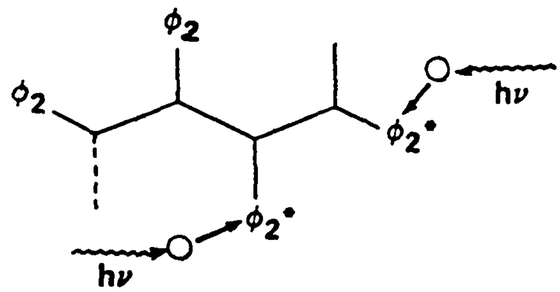

Fig. 2. Schematic model of extended poly(1-vinylnaphthalene) with triplet donor molecules M (O). ϕ_2 denotes a naphthalene moiety and $h\nu$ the incident photon absorbed by M. M* intersystem crosses before transferring its excitation energy to pendent groups.

Observation that I_{DF} varied approximately as the square of the incident intensity suggests the delayed fluorescence arises from triplet (T) - triplet (T) annihilation; symbolized as:

$$T + T \rightarrow S^* + S_0 \rightarrow S_0 + S_0 + h\nu \quad (1)$$

Additional experimental evidence for triplet state involvement is provided by the quenching of both phosphorescence and delayed fluorescence by piperylene, a well known triplet quencher. In fact a study of its quenching effects on the delayed emission demonstrates that at least one of the triplet excitons involved in the fusion process is mobile. This is evident from the phosphoresence quenching curves (Stern-Volmer graphs) of P1VN and 1-ethylnaphthalene illustrated in Fig. 3.

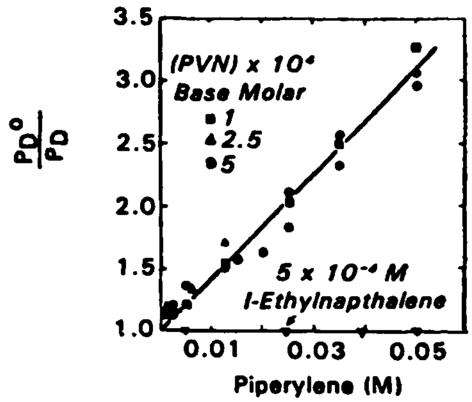

Fig. 3. Quenching poly(1-vinylnaphthalene) and 1-ethyl-naphthalene phosphorescence at 77°K as a function of piperylene molarity. From Cozzens and Fox (1).

Since the probability of quenching is proportional to the concentration of quenchers and the effective quenching volume, the enhanced decrease in P1VN phosphorescence as compared to 1-ethylnaphthalene implies a larger cross-sectional volume; this can only be obtained if some of the pendent triplet excitons are mobile. An alternative experimental technique for proving intramolecular energy transport is offered by studying the luminescence from copolymer glasses. One of the first experiments was Fox and Cozzens (7) study of sensitized phosphorescence from copolymers of styrene and 1-vinylnaphthalene, in which the groups derive from the latter act as energy sinks with respect to chain segment derived from styrene. The delayed emission spectra for a mixture of polystyrene and poly(1-vinylnaphthalene) and the corresponding copolymer is illustrated in Fig. 4. The single broad band centered at 400 nm is attributed to polystyrene whereas the delayed emission from poly-(1-vinylnaphthalene) consists of a group of phosphoresence bands centered about 500 nm and a delayed fluorescence band at 346 nm. Note that in the copolymer, curve A in Fig. 4, no delayed fluorescence is observed, a consequence of the lack of neighboring cluster formation of 1-vinylnaphthalene moieties within the polystyrene chain. Comparison of the spectrum of the copolymer (curve A) relative to an equivalent homopolymer glass mixture (curve B) provides conclusive proof of energy transfer within the host polymer chain since the intensity of the styrene-derived phosphorescence has decreased whereas the 1-vinylnaphthalene-derived phosphorescence band has been correspondingly enhanced.

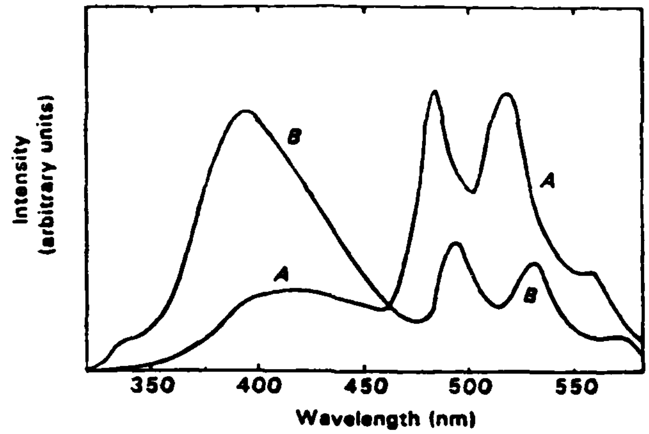

Fig. 4. Delayed emission spectra in 1:1 diethylethertetrahydrofuran glasses. Curve A: Styrene-1-vinylnaphthalene copolymer containing 1 mol percent 1-vinylnaphthalene derived groups. Curve B: Mixture of polystyrene and poly(1-vinylnaphthalene) polymers; 1 mol percent poly(1-vinylnaphthalene). Excitation wavelength 260 nm, 77°K. Modified from Fox and Cozzens (7).

II. MOLECULAR WEIGHT EFFECTS ON DELAYED EMISSION

Low temperature (77°K) emission from isolated polymers in glass matrices, e.g. in 2-methyltetrahydrofuran (MTHF) and tetrahydrofuran: diethyl ether (THF:Et_2O), is characterized by both phosphorescence and delayed fluorescence bands. The intensity of these two emission bands have been shown by a number of investigators (8, 9) to be dependent on the molecular weight of the polymers; the delayed fluorescence intensity (I_{DF}) increasing and the phosphorescence intensity (I_P) decreasing with increasing degree of polymerization. Fig. 5 illustrates this tremendous influence of the average molecular weight of the polymer on the delayed fluorescence and phosphorescence intensity for glasses of poly(N-vinylcarbazole) in MTHF. Similar effects have been reported for poly(2-vinylnaphthalene) in THF:Et_2O (8) and poly(2-naphthylmethacrylate) in matrices of MTHF (10) for luminescence measured at liquid nitrogen temperatures. Although the ratio of I_{DF}/I_P increases with the (average) degree of polymerization ($\bar{P}$) at low molecular weights a saturation in this ratio is observed when $\bar{P} > 100$, where the effective chain length at which saturation occurs depends on the particular polymer. Since this molecular effect on the delayed spectrum is observed in dilute rigid glasses (polymer concentrations less than 10^{-3}M) the fusion process occurs between triplet excited chromophores within a single polymer, ie.

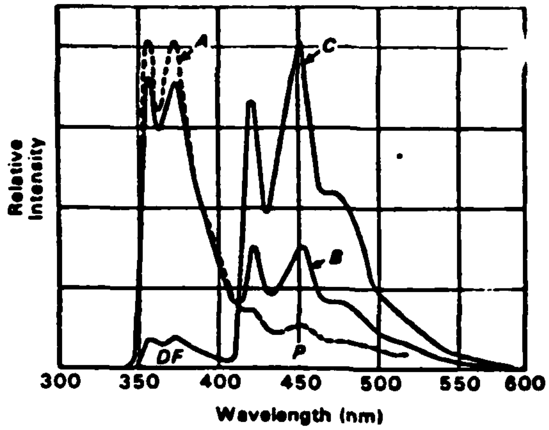

Fig. 5. Delayed emission spectra of three different poly(N-vinylcarbazole) fractions, 6 x 10^{-4} mol basic unit/liter in 2-methyltetrahydrofuran at 77°K. Molecular weights: A) 2 X 10^6; B) 3 X 10^5; C) 9 X 10^4. Excitation wavelength 330 nm. Modified from Klopffer et al (9).

intramolecular exciton fusion as opposed to intermolecular annihilation. A qualitative understanding of enhancement and eventually saturation of I_{DF} with increasing polymer chain length was initially given by Pasch and Webber (8). Their reasoning was as follows. We note first that for a fixed excitation intensity larger polymers have a larger average number of triplet excitons per molecule. If the length (L) of the polymer is comparable to or less than the exciton diffusion length (L_d) and if some of the triplet excitons are mobile, then an increase in L produces a corresponding increase in the delayed fluorescence since a mobile triplet exciton has a nonzero probability of annihilating with either a trapped triplet or another mobile exciton. This increase in I_{DF} with L occurs at the expense of the polymer's phosphorescence. When $L > 2L_d$ no further effects on I_{DF} are expected since excitons separated at distances greater than $2L_d$ do not annihilate. Although this model possesses the essential qualitative feature observed for low temperature polymer glasses a quantitative theory is exceedingly difficult since triplet-triplet annihilation is known to be affected by chromophore separations and intrachain, non-nearest neighbor contacts.

A semiquantitative model of the effects of L on I_{DF} and I_P was given by Webber and Swenberg (11). These authors analyzed the dependence of exciton annihilation on parameters such as lattice size, lattice dimensionality and the exciton fusion rate using a Pauli-Master equation. Their treatment is quite similar to the formalism of Paillotin et al (12) used in modeling the fluorescence quantum yield decreases observed in photosynthetic membranes (13) with increasing excitation

pulse intensity. Let $P_n(t)$ denote the probability that a lattice contains n excitons at time t. The (Ansatz) master equation obeyed by the components $P_n(t)$ for a lattice of size L is

$$\frac{dP_n}{dt} = S(t) + D(t) + A(t) \tag{2}$$

where

$$S(t) = \beta\left(\frac{L}{L_o}\right)P_{n+1}(t) - \beta\left(\frac{L}{L_o}\right)P_n(t) \tag{3}$$

is the excitation rate,

$$D(t) = (n+1)\beta P_{n+1}(t) - n\beta P_n(t) \tag{4}$$

denotes the net monomolecuar decay and

$$A(t) = G_{n+1}\frac{L_c\beta}{L^2}P_{n+1}(t) - G_n\frac{L_c\beta}{L^2}P_n(t) \tag{5}$$

is the decrease in the n^{th} state caused by exciton annihilation. L_o is the parameter describing the excitation intensity, L_o is inversely proportional to the excitation intensity, β is the unimolecular exciton decay rate, L_c is the second order dimensionless rate constant for exciton fusion and G_n describes the dependence of the annihilation on the occupation number, n, of the lattice. Previous formulations of exciton annihilation (12) assumed that $G_n = n(n-1)$ which corresponds to twice the number of exciton pairs on the lattice. In Webber and Swenberg (11) formulation, however, the general form, namely

$$G_n = \left[n(n-1)\right]^{\alpha} \tag{6}$$

was assumed. The constant α was taken to differ from unity and a value of 1.5 was adapted on the basis of computer simulations. This is discussed later in the text. The addition of the double annihilation events, events where both excitons disappear simultaneously upon annihilation, are already included in equation (2) since Paillotin et al (12) have shown that inclusion of level transitions, n → n-2 simply alter the scaling factors of the final equations; their explicit inclusion is therefore unimportant in semiquantitative modeling of I_{DF} dependence on chain length, L, discussed herein.

In the absence of annihilation, the occupation distribution, P_n, obeys Poisson statistics,

$$P_n = (L/L_o)^n \frac{1}{n!} \exp(-L/L_o) \tag{7}$$

For $L_c \setminus 0$

$$P_n = \frac{(L/L_o)^n \prod_{m=1}^{n}(m + G_m L_c/L^2)^{-1}}{\sum_{k=1}^{\infty}(L/L_o)^k \prod_{m=1}^{k}(m+G_m L_c/L^2)^{-1}} \tag{8}$$

and the value of n for which P_n is maximal decreases as L_C increases; the density of excitons on a polymer diminishes relative to the Poisson limit ($L_C = 0$). The effects of bimolecular annihilation on the steady-state distribution is illustrated in Fig. 6. Experiments displaying the increase in I_{DF} and decrease in I_P with increasing molecular weight reported by Webber and coworkers (8, 10) and Klöpffer et al (9) were performed under steady-state conditions, hence the experimental measureables in terms of the distribution functions P_n are

$$I_P \propto \frac{\langle n \rangle}{L} = \frac{1}{L}\sum n P_n \tag{9}$$

and

$$I_{DF} \propto \frac{\langle n(n-1) \rangle}{L^3} = \frac{1}{L^3}\sum n(n-1)P_n \tag{10}$$

The additional L^{-1} dependence in equation (10) arises because under the experimental conditions polymers in low temperature glasses had constant chromophore densities. For simplicity we have neglected in equations (9) and (10) the weighted sum over the polydispersiveness of the sample and assume that L in the above equations corresponds to an average degree of polymerization, $\bar{P}$. How I_{DF} behaves for L large can

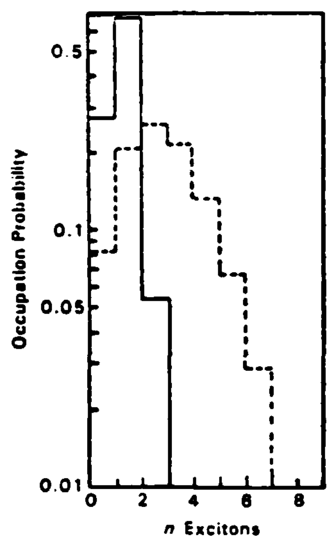

Fig. 6. Comparison of normal Poisson distribution (---) and modified Poisson distribution (—) for $L_C = 10^5$, $\alpha = 1$. Both are for L = 250, L_o = 100. From Webber and Swenberg (11).

be seen by noting that for large L_c and large L the second order term, G_n, dominates. In this limit P_n exhibits a maximum at

$$\bar{n} = \left(L^3 / L_c L_0 \right)^{1/2\alpha} \tag{11}$$

Hence the asymptotic limit of Ip depends on the numerical value of the parameter α . For

$$\alpha > 3/2, \; I_p \to 0 \quad \text{as } L \to \infty \tag{12}$$

$$\alpha = 3/2, \; I_p \to (L_c L_0)^{-1/3} \quad \text{as } L \to \infty \tag{13}$$

$$\alpha < 3/2, \; I_p \to \infty \quad \text{as } L \to \infty \tag{14}$$

In contrast to I_p, the delayed fluorescence is relatively insensitive to α for large L_c and α values near unity. Fig. 7(A) illustrates the theoretical dependence of I_{DF} and Ip on chain length L as calculated by Webber and Swenberg (11). It is evident that the predictions of the model are qualitatively similar to the delayed emission data from poly(2-vinylnaphthalene) reported in Fig. 7(B).

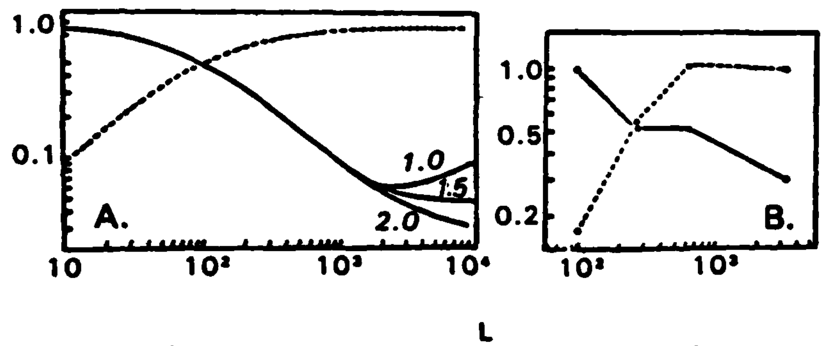

Fig. 7. (A) Theoretical plot of triplet density ($L_0 I_p$), for α = 1.0, 1.5, and 2.0 (——), and annihilation density ($L_0 I_{DF}$) (---), where Ip and I_{DF} are given by eqs. (9) and (10) respectively. The latter curve is essentially independent of α for L_c large. $L_c = 10^8$ for these plots. (B) Plots of experimental phosphorescence and delayed fluorescence intensity for poly(2-vinylnaphthalene) versus L. From Webber and Swenberg (11).

It is important to emphasize that the fusion model described by Eq. (2) explicitly neglects the spatial variables of the excitons, an assumption which is strictly valid only when the randomization time is rapid compared to the annihilation rate (12, 14). For singlet migration

within the photosynthetic membrane where the hopping rate is greater than $10^{11}sec^{-1}$ this assumption is known to be valid (12), however triplet transport among the pendent groups of a polymer is quite slow, less than $10^{10}sec^{-1}$, and suggest the inapplicability of the randomization approximation. Inclusion of non-randomized events unfortunately necessitates extensive computer simulations. A further difficulty with the formalism is that the effects of a finite diffusion length (L_d) of the exciton has not been properly incorporated into the theory. Although α not equal to unity decreases the importance of bimolecular annihilation when $L_d < L$ by shifting the peak in the distribution ν_n to smaller n values there are nevertheless annihilating events contributing to I_{DF} for separations (on the average) greater than $2L_d$.

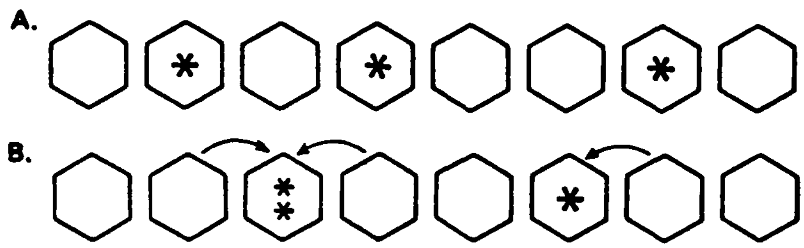

Fig. 8. Schematic of model used to derive rate constant k_n^x · A) At t = 0 there are 3 excitons. B) At t = τ (one hopping time unit) there is a collision which is indicated by double asterisk on single molecule.

A rationalization for α = 1.5 was based on an effective decay constant determined from numerical simulations of the probability distribution of first collision time, $\Psi_n(t)$ for lattices containing L sites and n excitons. A collision was defined as either two excitons arriving at the same site or neighboring sites at the same time. The function $\Psi_n(t)$ was constructed by repeated simulations for a fixed number of excitons. Fig. 8 illustrates the case where n = 3. In this case a collision occurred after only a single hopping time unit. In terms of the simulated distribution function and in the absence of unimolecular decay, the occupation distribution is given by

$$P_n(t) = 1 - \int_0^t \Psi_n(t)\,dt \qquad (15)$$

The effects of annihilation on $P_n(t)$ is apparent in Fig. 9 and illustrates the highly nonexponential behavior expected for the delayed fluorescence. The effective annihilation rate was defined by Webber and Swenberg (11) as

$$k_n^x = -\ln(x)/t_x^n \qquad (16)$$

where $P_n(t_x^n) = x$. The dependence of k_n^x for x = 0.5 illustrated in Fig. 10 is suggestive of a nonintegral value for α. An α somewhat smaller than the simulated value might be expected because of near intrachain crossings; the parameter α includes crudely the effects of nonintegral dimensionality effects. Disregarding the enhancement in excimer emission α is expected to be lower in solvents where chain contraction occurs.

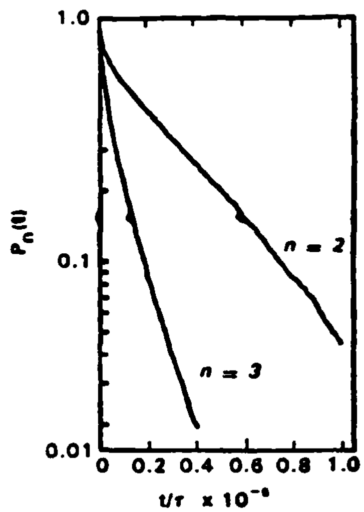

Fig. 9. Semilogarithmic plot of $P_n(t)$ for n = 2 and 3 for a one dimensional lattice with L = 400 constructed from 4000 trials. From Webber and Swenberg (11).

A comparison of simulated decays for lattices with 100 and 500 sites under steady state initial conditions with experimental decay profiles of P2VN is shown in Fig. 11. It is evident that the quality features of $I_{DF}(t)$ are consistent with experimental data in the sense that (1) there is a strong L dependence, (2) decays are nonexponential, and (3) first order processes do not dominate the kinetics. Only when first order kinetics dominate is $I_{DF}(t)$ exponential with a decay time (T_{DF}) one-half the phosphorescence lifetime (T_p). Unfortunately a direct comparison of lifetime data is difficult since polymer phosphorescence usually arises from shallow traps, e.g. in P1VN T_{DF} = 80 msec whereas T_p = 1.9 sec (1).

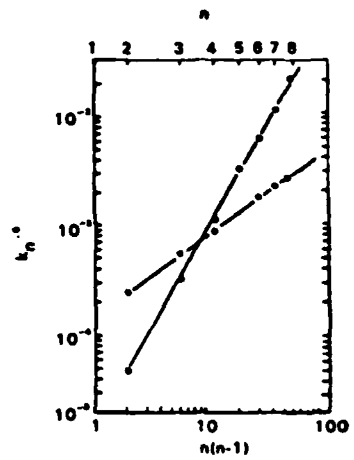

Fig. 10. Cor uter calculated decay constants for one dime..sional (O) and two-dimensional lattices (●). See text equation (16). The slopes are 1.8 and 0.7, respectively. From Webber and Swenberg (11).

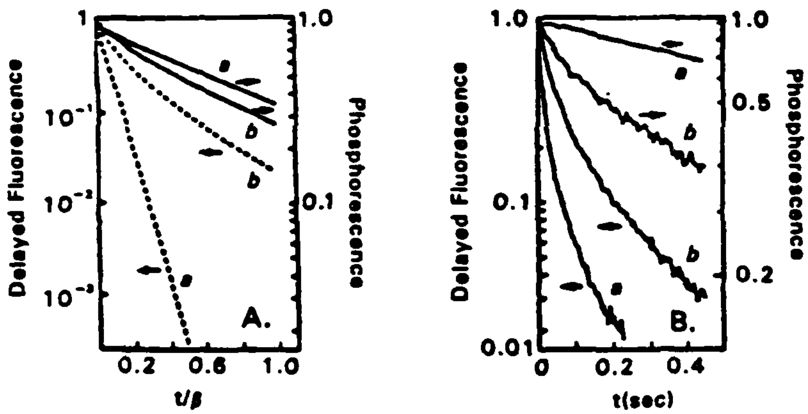

Fig. 11. (A) Semilogarithmic plot of Ip (—) and LI_{DF} (---) versus t/β. For L = 100 (a curves) and L = 500 (b curves) with L_C = 5 X 10^4, α = 1.5. (B) Experimental decay curves for poly(2-vinylnaphthalene) phosphorescence and delayed fluorescence. The a-curve corresponds to L = 100 and the b-curve corresponds to L = 3250. Date reported in Webber and Swenberg (11).

Kim and Webber (16) have shown that even films and powders of P2VN at 77°K exhibit molecular weight effects on the delayed emission spectrum similar to its manifestation in dilute polymer glasses. In solid matrices, however, both the delayed fluorescence and phosphorescence are broad, structureless, and red shifted (~700 cm^{-1} for I_P and ~1800 cm^{-1} for I_{DF} in P2VN) relative to their positions in glasses. Thus the delayed emission, as Fig. 12 illustrates, is chiefly excimer in nature (17). Presumably the steric arrangement of neighboring polymer chains inhibit interpolymer excitonic migration. This could arise either from unfavorable chromophore distances, thereby lessening the likelihood of interchain Forster transfer or points of contact are excimer-forming sites (18). The assignment of the phosphorescence to intra- or inter-molecular excimers is not easy in solid vinyl polymers although the delayed excimer fluorescence necessitates both mobile and trapped triplet excitons.

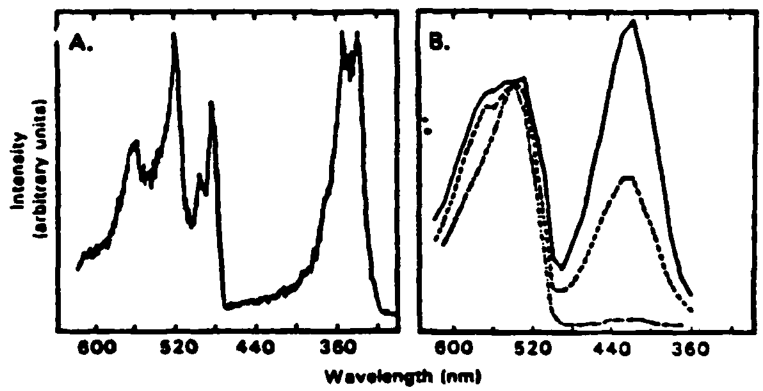

Fig. 12. (A) Delayed emission spectrum of poly(2-vinyl-naphthalene) in 2-methyltetrahydrofuran at 77°K. (B) Delayed emission spectra for powdered poly(2-vinyl-naphthalene) of different molecular weights: (——) 505,000; (- - -) 100,000; (-·-·-) 49,000. Spectra scaled to equal phosphorescence intensity maxima. From Kim and Webber (16).

III. Fluorescence Decay Profiles

A quantitative analysis and microscopic assignments of the time resolved fluorescence emission components from polymers in the solid or solution phase to specific physical entities is generally exceedingly difficult. This stems partly from (1) the intrinsic heterogeneity of the emission which in some cases arises from the preponderance of shallow traps, (2) the formation of intramolecular and in solid films or powders intramolecular excimers and (3) the effects of dimensionality and size.

The monomer fluorescence intensity decay for many polymers, such as poly(N-vinylcarbazole) (19), P1VN and P2VN (20), but not polystyrene in CH_2Cl_2 solution at room temperature (21), is highly nonexponential. Although it is tempting to associate components in any decay profile as originating from separate distinquishable molecular species it is important to know that any identification need not be unique. A point well illustrated by the fact that recent theoretical studies of excitation energy transport (among monomer units) and trapping have demonstrated that size and dimensionality of a physical system can result in nonexponentiality in the monomer emission (23, 24). This is apparent for one dimensional systems, an appropriate model for dilute polymers solutions in a good solvent where the polymer is primarily extended with few intramolecular neighbor contacts.

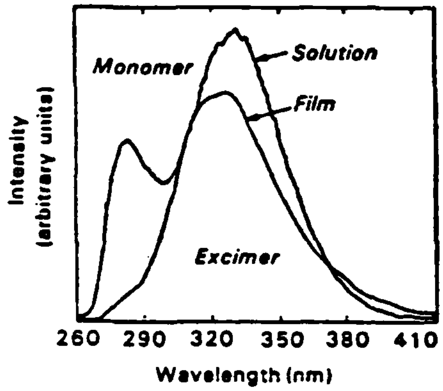

Fig. 13. Room temperature fluorescence spectra of polystyrene in CH_2Cl_2 solution and of film cast from CH_2Cl_2 solution. Excitation wavelength 250 nm. From Gupta et al (21).

For a dilute solution of vinyl polymers the prompt fluorescence spectra exhibits both excimer and monomer emission. For films emission is primarily excimer in character. Fig. 13 illustrates these general features for polystyrene. The temporal characteristics of these emission bands provide information on the formation process of the excimer band and the intramolecular singlet exciton migration rate. This can be seen as follows. Neglecting chain crossings, excimers results either (1) from rotation of a pendent group into a favorable position for excimer formation with its neighbor while in its excited singlet state or (2) from the trapping of monomer excitation energy at excimer forming sites (EFS), i.e.: properly performed chromophore pairs. The routes available for monomer decay and excimer formation are illustrated in Fig. 14. Two limiting cases can be distinquished: (1) rotational alignment in the excited state is fast compared to the rate of excited singlet energy migration, i.e.: $K_R > K_E$ and (2) where $K_E > K_R$. In the first case the

excimer rise time provides an estimate of the rotation rate of the pendent groups. In case (2), EFS can be considered as partitioning the extended polymer into finite disjoint monomer segments bounded by absorbing excimer forming sites. We restrict our discussion to case (2) as this will illustrate how nonexponential monomer decays can occur in the absence of special moieties. Consider a chain segment N monomer units in length as illustrated in Fig. 15.

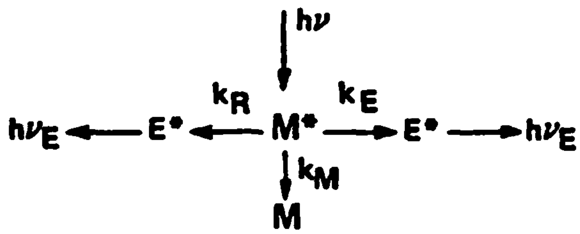

Fig. 14. Excited state kinetic scheme for a single monomer (M) and excimer (E) species. K_R denotes the rate constant for direct formation of excimers, k_E is the trapping rate function for monomer excitation energy at excimer-forming sites. See text for details.

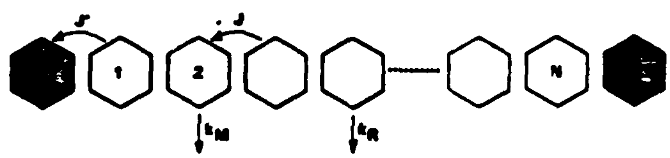

Fig. 15. One dimensional model employed in calculating effective exciton trapping function, k_E, at excimer forming sites. J denotes the monomer nearest neighbor intermolecular transfer energy, J′ is the transfer energy from a neighboring monomer to an excimer forming site, K_R is the rate constant for direct formation of excimers.

Let $Q_i(t)$ denote the probability excitation energy resides at site $i(1 \leq i \leq N)$ at time t, then in the incoherent limit, a valid approximation since both phase and spatial coherence time is considerably less than 10^{-11} sec for disordered systems (4), the equations describing the evolution of $Q_i(t)$ are:

$$\frac{dQ_i}{dt} = J(Q_{i+1} - 2Q_i + Q_{i-1}) - Q_i/\tau \tag{17}$$

$$\frac{dQ_1}{dt} = J(Q_2 - Q_1) - J'Q_1 - Q_1/\tau \tag{18}$$

$$\frac{dQ_N}{dt} = J(Q_{N-1} - Q_N) - J'Q_N - Q_N/\tau \tag{19}$$

in the absence of biomolecular annihilation. The definition of the parameters are evident from Figs. 14 and 15 and $\tau = (k_M + k_R)^{-1}$. In the limit where $J = J'$ and for uniform initial conditions the solution (25) to eqs. (17) - (19) gives the monomer fluorescence for an N site system as

$$FM(t) = C \exp(-t/\tau)\, G_N(t) \tag{20}$$

where C is an appropriate construct and $G_N(t)$ is the spectral response function for an N sites;

$$G_N(t) = \frac{2}{N(N+1)} \sum_{k=1}^{[(N+1)/2]} \cot^2\beta_k \exp\left[-4Jt \sin^2\beta_k\right] \tag{21}$$

and

$$2\beta_k = (2k-1)\pi/(N-1) \tag{22}$$

The monomer fluorescence measured is given by an appropriate average of the spectral function times $\exp(-t/\tau)$. It is apparent from equation (21) that decay profiles are non-exponential. Under thermodynamic equilibrium conditions, Fredrickson and Frank (26) have shown in the average t matrix approximation (27) and for small dyad trap concentrations, $q \ll 1$, and long times, $tJ \gg 1$,

$$FM(t) \propto \exp\left[4q^2Jt - t/\tau\right] \operatorname{erfc}\left[2q(Jt)^{1/2}\right] \tag{23}$$

Although the one-dimensional diffusion problems with randomly distributed deep traps solved exactly by Movaghar et al (28) predicts a long time decay proportional to $\exp(-\alpha t^{1/3})$ the above solution is sufficient in illustrating the nonexponentiality of the decay profiles. Fig. 16.(A) shows that the effects of increasing the intramolecular transfer rate J or decreasing the rotational rate, k_R, enhances the nonexponential character of the decay profiles. Furthermore it is evident from the kinetic scheme in Fig. 14 that the trapping rate function is given by

$$k_E = -\frac{d}{dt} \ln G(t) \tag{24}$$

where G(t) denotes the ensemble average spectral function. At low

excimer concentrations it follows from eq. (23) that $k_E \propto t^{-1/2}$. This particular functional form has been utilized by Smith et al (29) to analyze the transient luminescence properties in isotopically doped 1,4-dibromonaphthalene. The excimer fluorescence, FE(t), can also be formulated (26) in terms of the spectral function, namely

$$FE(t) \propto \mathcal{L}^{-1}\{[1-(s+k_m)\tilde{G}(s+1/\tau)]/(s+k)\} \qquad (25)$$

where $\mathcal{L}^{-1}$ denotes the inverse Laplace transform and $\tilde{G}$ is the Laplace transform of G(t). Model calculations by Fredrickson and Frank (26) are shown in Fig. 16. The important point to note about Fig. 16.(B) is that the excimer risetime decreases as the energy transfer rate is increased and an enhancement in the excimer intensity is expected. A similar increase in intensity is predicted for increases in k_R; Fig. 16. (C) illustrates this point.

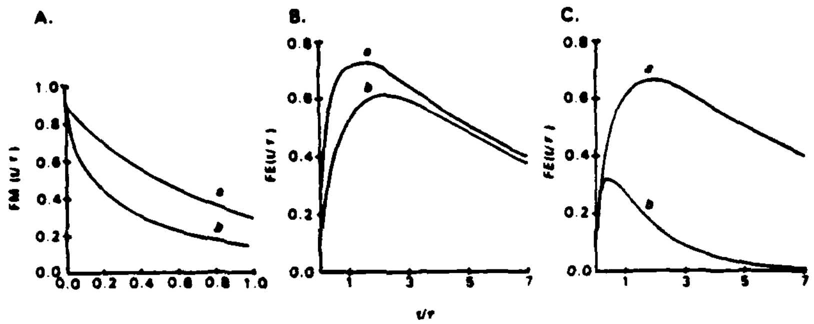

Fig. 16. Time dependence of monomer and excimer fluorescence using eqs. (23) and (25) at a fixed dyad trap fraction q = 0.05. A) Monomer fluorescence; a) $\tau J = 10$, b) $\tau J = 100$; B) Excimer fluorescence with monomer (τ_m) and excimer (τ_E) lifetimes 50 nsec and 80 nsec, respectively, $\tau = 10$ nsec; a) $J = 10^{10} s^{-1}$, b) $J = 10^7 s^{-1}$; C) Excimer fluorescence, $\tau_m J = 50$, $\tau_E J = 80$, a) $\tau J = 10$, b) $\tau J = 50$. Modified from Fredrickson and Frank (26).

The Aspler et al (30) study of time resolved fluorescence from copolymers poly(1-naphthylmethacrylate)-9-vinylanthracene provides an illustration of how an estimate of the transfer rate within the naphthyl chromophores can be inferred from the risetime of 9-vinylanthracene (9-VA) moieties. In this case intramolecular excimers are replaced by traps

and $K_R = 0$. This can be seen as follows. The main observation is that 9-VA emission at 425 nm is within experimental error the same whether the copolymer is excited in the naphthyl absorption band, 280 nm, or at 380 nm where only 9-VA absorbs. To be consistent with the rapid risetime in trap emission, $k^{-1} < 10^{-9}$ sec, where $k^{-1} = k_E^{-1} + \tau_M$. Since $\tau_M = 1.5 \times 10^{-9}$ sec, it follows that $k_E > 3 \times 10^9 \text{sec}^{-1}$, a value which should be viewed as a lower limit.

For generalization of the time dependence luminescence properties for more complex donor and acceptor configurations and higher dimensionality effects, the papers by Fayer and coworkers (22 to 24) should be consulted.

REFERENCES

1. Cozzens, R.F., and Fox, R.B., J. Chem. Phys., 50, 1532 (1969).

2. Eisinger, J., and Shulman, R.G., Proc. Natl. Acad. Sci. USA, 55, 1387 (1969).

3. See e.g., Photophysics of Aromatic Molecules, Birk, J.B. (John Wiley and Sons, Inc., London, 1970).

4. See e.g., Electronic Processes in Organic Crystals, Pope, M., and Swenberg, C.E., (Clarendon Press, Oxford University Press, New York, 1982).

5. Stevens, B., Spectrochim. Acta, 18, 439 (1962).

6. Frank, C.W., and Harrah, L.A., J. Chem. Phys., 61, 1526 (1974).

7. Fox, R.B., and Cozzens, R.F., Macromolecules, 2, 181 (1969).

8. Pasch, N.F., and Webber, S.E., Chem. Phys., 16, 361 (1976).

9. Klöpffer, W., Fischer, D., and Naundorf, G., Macromolecules, 10, 450 (1977).

10. Pasch, N.F., and Webber, S.E., Macromolecules, 11, 727 (1978).

11. Webber, S.E., and Swenberg, C.E., Chem. Phys., 49, 231 (1980).

12. Paillotin, G., Swenberg, C.E., Breton, J., and Geacintov, N.E., Biophys. J., 25, 513 (1979).

13. Geacintov, N.E., Breton, J., Swenberg, C.E., and Paillotin, G., Photochem. Photobiol., 26, 629 (1979).

14. Paillotin, G., J. Theor. Biol. 58, 219 (1976).

15. Paillotin, G., J. Theor. Biol. 58, 237 (1976).

16. Kim, N., and Webber, S.E., Macromolecules, 13, 1233 (1980).

17. Klöpffer, W., in Organic Molecular Photophysics, Vol. 1 pp. 357 to 400, ed. J.B. Birks (John Wiley and Sons, Inc. London, 1973).

18. Klöpffer, W., J. Chem. Phys., 50, 2337 (1969).

19. Roberts, A.J., Cureton, C.G., and Phillips, D., Chem. Phys. Lett., 72, 554 (1980).

20. Phillips, D., Roberts, A.J., and Soutar, I., Polymer, 22, 293 (1981).

21. Gupta, M.C., Gupta, A., Horwitz, J., and Kliger, D., Macromolecules, 15, 1372 (1982).

22. Gochanour, C.R., Andersen, H.C., and Fayer, M.D., J. Chem. Phys., 70, 4254 (1979).

23. Ediger, M.D., and Fayer, M.D., J. Chem. Phys. 78, 2518 (1983).

24. Loring, R.F., Andersen, H.C., and Fayer, M.D., J. Chem. Phys. 76, 2015 (1982).

25. Pearlstein, R.M., J. Chem. Phys., 56, 2431 (1972).

26. Fredrickson, G.H., and Frank, C.W., Macromolecules, 16, 572 (1983).

27. Richards, P.M., Phys. Rev., B20, 2964 (1979).

28. Movaghar, B., Sauer, G.W., and Wurtz, D., J. Stat. Phys., 27, 473 (1982).

29. Smith, D.D., Powell, R.C., and Zewarl, A.H., Chem. Phys. Lett., 68, 309 (1979).

30. Aspler, J.S., Hoyle, C.E., and Guillet, J.E., Macromolecules, 11, 925 (1978).

END

FILMED

3-86

DTIC